SUPRAMOLECULAR ASSEMBLY OF NANOSTUCTURED MATERIALS FOR FABRICATION OF FUNCTIONAL INTERFACES

By

Ankush Ashok Gokhale

A DISSERTATION

Submitted to
Michigan State University
in partial fulfillment of the requirements
for the degree of

Chemical Engineering-Doctor of Philosophy

2014

ABSTRACT

SUPRAMOLECULAR ASSEMBLY OF NANOSTRUCTURED MATERIALS FOR FABRICATION OF FUNCTIONAL INTERFACES

By

Ankush Ashok Gokhale

In recent years, there has been increased focus towards miniaturization to build sustainable devices by harnessing the power of synergistic nanoarchitectures. Drawing upon the strength of the intermolecular forces, supramolecular assembly techniques have enabled the inclusion of a host of inhomogeneous nanomaterials to give form and structure to macroscopic objects. Supramolecular techniques are well suited to customize and improvise the assembly of nanomaterials to allow full translation of their nanoscale properties to macroscopic structures. In our work, we have primarily focused on developing novel supramolecular multifunctional architectures for fabrication of nanostructured interfaces.

Firstly, we designed a unique recyclable two-tier carbonaceous biocatalyst consisting of a polyelectrolyte modified iron-oxide doped graphene support and a biocatalytic component in the form of cellulase, an enzyme capable of hydrolyzing lignocelluloses to reducing sugars. A combination of strong and weak polyelectrolytes enabled long-term stabilization of hydrophobic graphene platelets in aqueous medium and provided an effective means to control the biocatalytic activity of the immobilized cellulase as a function of pH and temperature. We also show how the effect of the dissociation of weak polyelectrolytes can overcome the geometric disadvantage imposed by flat 2D supports. A combination of polyelectrolyte swelling, improved colloidal stability and enhanced enzyme mobility contributed to preservation of the biocatalytic activity.

Secondly, we also designed a novel supramolecular conductive interface consisting of multilayered thin films of functionalized graphene platelets in conjunction with anionic polyelectrolytes. The interplay of hydrogen bonding and electrostatic forces was studied and its effect on film thickness and morphology was evaluated. Films developed in this work show impressive gas shielding capabilities comparable to commercial grade silicon oxide coatings and almost a five orders of magnitude reduction in sheet resistance.

Lastly, a bioelectronic interface to detect and quantify the presence of anionic nitrate species was assembled from a surfactant stabilized supramolecular matrix. Nitrate based fertilizers pose major health hazards when they combine with sources of drinking water. In this work, we developed a novel 1D nanoarray of polyethylenedioxythiophene based nitrate biosensor capable of detecting and quantifying minute concentrations of nitrate species. Low detection limit (0.1 ppm), high signal to noise ratio and improved affinity towards nitrate species as compared to other interfering ions are significant features of this sensor.

Dedicated to my beloved parents for their love, motivation and unconditional support.

ACKNOWLEDGMENTS

First and foremost, I would like to thank the Department of Chemical Engineering at Michigan State University for placing faith in my abilities as a researcher and inducting me in the graduate program. I am thankful to the department for its continued support in the form of fellowships, assistantships, travel awards and easy access to research facilities that created a conductive environment for scholarship and learning.

My advisor, Prof. Ilsoon Lee has been the most influential guiding force in my PhD years. I wholeheartedly thank him for his tutelage and wonderful inputs. A special thanks to Dr. Jue Lu and Ranjith Weerasiri from Technova Corporation for their guidance and feedback on my projects. I would also like to thank my PhD committee members Prof. Wei Liao, Prof. David Hodge and Prof. Robert Ofoli for their invaluable suggestions and comments during the PhD program.

I would also like to thank Prof. Daina Briedis and Prof. Charles Petty in the Chemical Engineering department for their help, support and advice especially during the first few years of my PhD. Having served as a teaching assistant for Prof. Briedis for three semesters gave me a chance to witness and appreciate the effort it takes to produce fifty minutes of quality lecture.

I would like to thank all the past and present members of our research group including Dr. Sumit Mehrotra, Dr. Shaowen Ji, Dr. Wei Wang, Oishi Sanyal, Jing Yu and Anna Song for their help and co-operation. I greatly appreciate the undergraduate students Nathan Parker and Andrew Izbicki for their assistance in my research experiments. I would also like to thank all my office-mates in 2522 EB : Dr. Xiangfeng Ma, Dr. Rui Lin, Ying Liu, Bhushan Awate and Yangmu Liu for their friendship and companionship. It was great to have met and in some cases worked with some interesting people : Ryan Stoklosa, Dan Williams, Tongjun Liu, Zhenglun Li, Muyang Li,

Rohit Nehe, Apoorav Shaligram and Ezhiylmurugan Rangaswamy. I thank them all for the technical and non-technical discussions we had over the past five years. A special thanks to Lee Alexander for all the water-cooler conversions we used to have. After my graduation, that is one thing I am sure to miss.

Last but not the least; I thank my parents for their unconditional love and support. Back in the day while I was still deciding the right grad school to go to, I distinctly recall my late father's words of encouragement to take up the offer to study at Michigan State University. Now on the verge of completion, I do have a sense of satisfaction of a job well done. To have a part of your family with you in new place is always a blessing. It was a great relief knowing that I always had my brother Amit and my sister-in-law Swarupa to turn to if I needed help. Watching my niece Aditi grow up from a baby into a toddler and now a preschooler has always brought me a sense of joy.

TABLE OF CONTENTS

LIST OF TABLES

LIST OF FIGURES

Chapter 1: Introduction

1.1 Overview of Supramolecular chemistry

Supramolecular assembly is a branch of chemistry that studies the interplay of noncovalent interactions and its effect on organization of an ensemble of discrete atoms, ions and molecules. While molecular chemistry is dominated by covalent forces, supramolecular chemistry relies on subtle intermolecular forces that exist freely in nature[1]. While initially confined to host-guest systems, the definition of supramolecular chemistry has now been expanded to explain a whole range of phenomena. Biological systems starting from natural molecules such as proteins, oligonuclueotides and lipids to larger complex applications such as targeted drug release, enzyme-substrate interactions, self-assembly and interactions between cells, tissues and pathogens (also known as polyvalency) are reported to rely on the supramolecular forces[2, 3]. Most biological systems are complex crowded biochemical environments which require information to flow to specific interactive species[4]. Through supramolecular interactions, molecular information can be easily transferred between the interacting species with minimum signal dilution due to other interfering species. As a result, specialized molecular receptors with high degree of specificity to recognize the pattern of flow of information can be utilized for supramolecular catalysis and selective transport processes[5]. In recent years, several examples of supramolecular catalysis ranging from biocatalytic conversions[6, 7] to metal-complex transformations[8-10] have been reported. Similarly examples of transport processes as a result of supramolecular interactions are also reported[11, 12].

The intermolecular interactions as a result of the supramolecular arrangement of the species are roughly classified into two types depending on the strength of the forces. Isotropic forces are medium range interactions that give shape, size and structural packing to the material while anisotropic interactions are long range directional interactions that can exist in charged species[13]. Supramolecular interactions cover wide spectra of weak noncovalent interactions. Table 1 lists the different types of interactive forces and provides a comparative analysis of their respective bond energies.

Table 1.1 Bond energies of different types of interactions. Reproduced partially with permission from [14]

Type of interaction	**Bond energy (kJ/mole)**	**Character**
Covalent bond	350	Irreversible
Hydrogen bond	10-65	Selective, directional
Vander Waal forces	<5[15]	Non-selective, non-directional
Co-ordination binding	50-200	Directional
'fit interaction'*	10-100	Very selective
'amphiphilic'**	5-50	Non-selective
ionic	50-250 (depends on solvent and ions)	Non-selective
Hydrophobic effects	Difficult to access accurately	-
π-π stacking forces	0-50[15]	Weakly directional

*: precise fitting of surfaces based on geometric limitations (lock-key principle)

**: observed in surfactant micelles

Among the different supramolecular forces, a few have been highlighted here due to their versatility and unique applications. Hydrogen bonds display a wide window of bond energies. The formation of the hydrogen bond is a result of interaction between a donor containing an acidic hydrogen atom and an acceptor containing lone pair of electrons[15]. In some cases, hydrogen bonds assume the proportion of a quasi-covalent bonds with bond energies rivaling those of covalent interactions whereas sometimes they can be as weak as Vander Waal

forces[16]. These forces are an example of powerful selective interactions that can be assembled using appropriate solvents and are completely reversible at room temperature. Similarly, though inherently weak, nature bears testimony to the collective effect of a large number of Vander Waal forces of interaction. Examples such as a house-lizard adhering to a wall or ceiling as a result a Vander Waal forces of attraction acting through the fine hair-like structures located on its footpad abound in nature[13, 17]. π-π stacking forces (aromatic-aromatic) are another example of secondary interactions. These interactions include face-to-face, edge-to-face and offset,slipped interactions[18]. Aromatic interactions are hypothesized to be a combination of a variety of noncovalent forces such as Vander Waal, hydrophobic and electrostatic. The hydrophobic element in these interactions makes them strong in water whereas the electrostatic component makes it selective[19]. In recent years, there has been increased focus on using supramolecular techniques for stabilization and functionalization of a number of nanomaterials. These techniques can provide robust bottom-up strategies to assemble a broad spectrum of nanostructures on the host substrates. Multifunctional tailor-made substrates fabricated using this route, have found applications in catalysis, sensing, and drug delivery.

1.2 Supramolecular nanostructured assemblies and nanobiocatalysis

The synergistic combination of supramolecular nanostructures and biocatalysis provides a unique opportunity to combine specificity (due to biocatalysis) and ‘smart’ materials (due to supramolecular assembly techniques). Higher ordered structures can be easily built by tweaking the biocatalytic component. It has been reported that the supramolecular assembly of amphiphilic molecules can be manipulated by a biocatalytic process induced by different concentrations of enzyme resulting in structurally diverse nanoassemblies[20]. In other words, supramolecular structures of lowest free energy configurations can be obtained by manipulating the biocatalytic

process. Figure 1 shows an example of the biocatalytic modification of a supramolecular assembly process. The left part of the image shows the assembly of peptides through self-assembly. The image on the right shows cleavage of the methyl group as a result of enzymatic hydrolysis and the resultant self-assembled peptide structure. Another example where biocatalysis has proven to be of great utility is formation of supramolecular hydrogels. Unlike chemically cross-linked polymeric hydrogels, supramolecular hydrogels are formed when self-assembly of small molecules result in formation of nanofiber networks[21]. Gao and co-workers[22] used an enzymatic reaction to trigger the self-assembly of a taxol derivative to form a nanofiber structure.

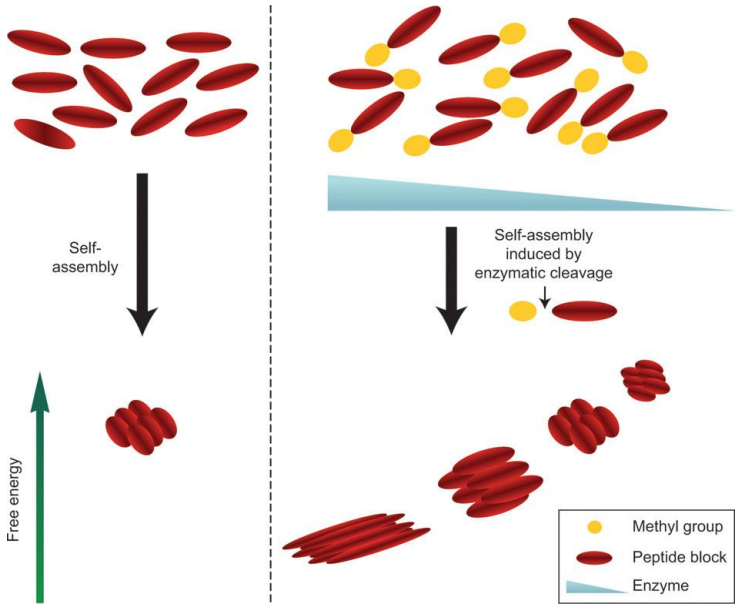

Figure 1.1 Biocatalytic manipulation of supramolecular nanostructures. (reproduced with permission from: [23])

Just as biocatalysis can assist in formation of supramolecular assemblies, supramolecular nanostructures can also aid in facilitating biocatalytic conversions. Freeman *et. al.*[24] reported the formation of supramolecular cocaine-aptamer complexes that stimulated the biocatalyzed oxidation of ethanol. Similarly, the supramolecular assembly of nucleic acid-hemin complex can

act as a biocatalyst producing chemiluminescence[25]. Another example of a supramolecular arrangement to facilitate biocatalytic conversion is provided by Gonzales-Campo et. al.[26] The authors have shown an interesting site-specific enzyme immobilization method to construct a supramolecular microfluidic chip for biocatalytic transformations.

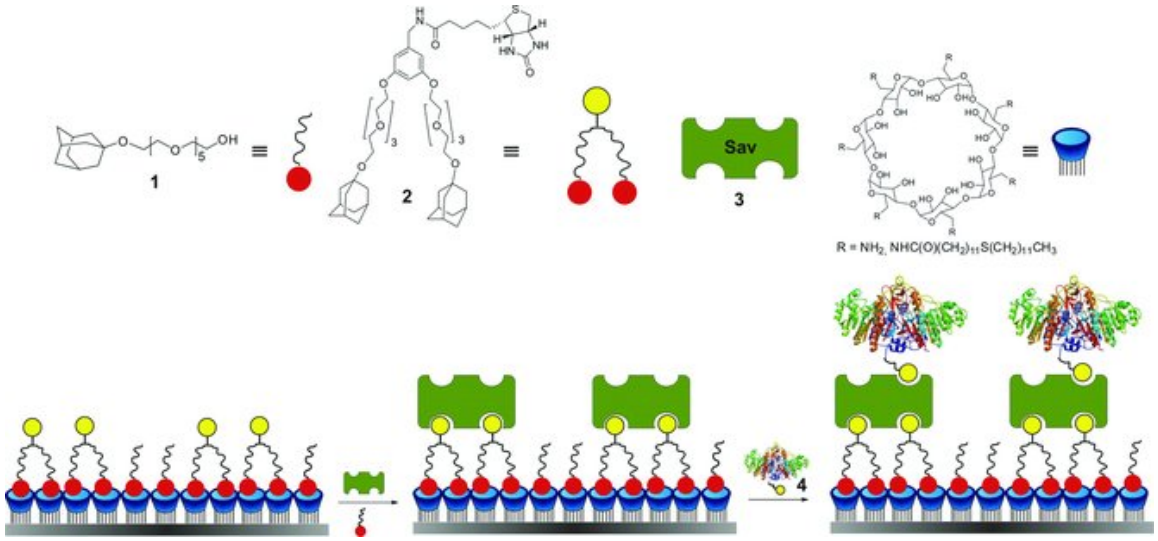

Figure 1.2 Site-specific enzyme immobilization for construction of supramolecular microfluidic chip. (Reproduced with permission from [26]) Note: Sav: biotin-Streptavidin

Similarly, supramolecularly assembled amphiphiles for the formation of biocompatible membranes for filtration, immobilization and biocatalytic utilization of proteins/enzymes has been recently reported[27]. Here, the authors have illustrated a good example of fabricating immobilization supports that can be easily recycled and reused over multiple cycles. Figure 3 shows a schematic diagram for the formation of these supramolecularly assembled membranes.

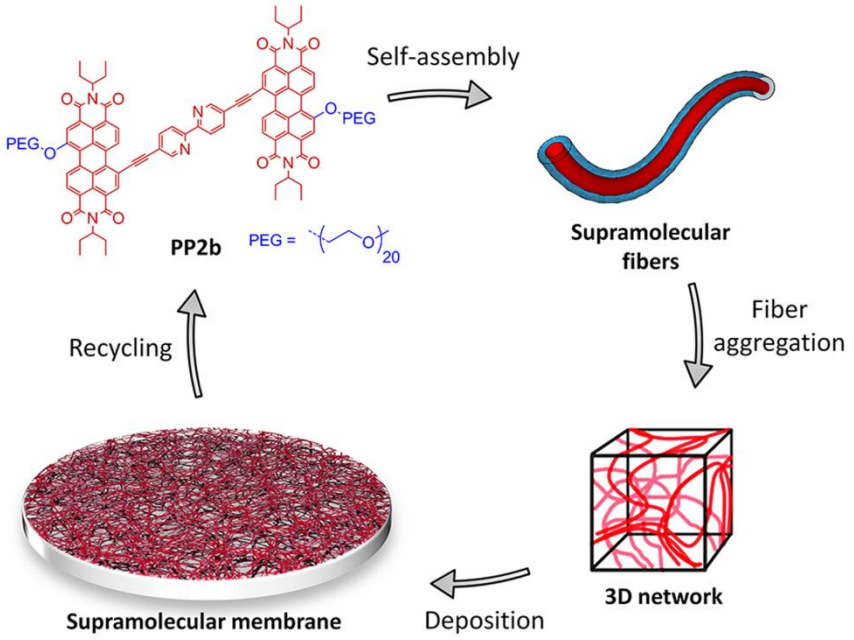

Figure 1.3 Supramolecularly assembled amphiphile (PP2b) for separation, immobilization and biocatalytic utilization of enzymes/proteins. Reproduced from: [27]

1.3 Fabrication of nanostructured interfaces using supramolecular techniques

The use of supramolecular techniques for fabrication of nanostructured interfaces has enjoyed tremendous success due to versatility, flexible nature of the noncovalent interfaces and precise control that these techniques offer. Supramolecular nanostructured interfaces have carved a place for themselves in almost every application such as thin films, sensors and semiconductor/electronics industry. Two approaches commonly used for fabrication of nanostructured interfaces include the 'top-down' approach and the 'bottom-up' approach. A schematic diagram shown in Figure 4 shows the difference in the two approaches. Top down approach which includes techniques such as photolithography or electron lithography has shown a remarkable ability to commercially produce nanointerfaces with great precision. However, in the sub-100 nm region this approach faces several challenges [28, 29]. Bottom-up approach on the other hand utilizes smaller building blocks such as atoms, molecules to produce larger

structures. Hence this approach is well-suited to produce nanostructures in nanoscale regimes where top-down approach fails or faces technological challenges.

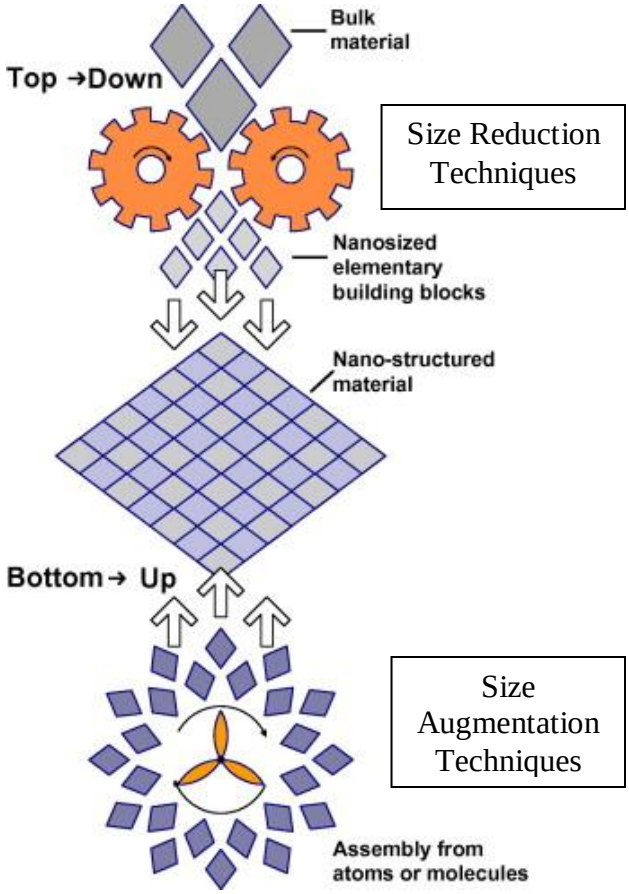

Figure 1.4 Schematic diagram illustrating the difference between top-down and bottom-up approaches. Top down approach relies on controlled dismembering of larger blocks to get nanosized materials. Bottom-up methods utilize controlled assembly of atoms, molecules as for producing nanoscale interfaces. Reproduced with permission from: [30]

The application of supramolecular chemistry to bottom-up approach presents exciting opportunities to fabricate multifunctional interfaces. Though it is not possible to introduce all such applications, keeping in mind the scope of this dissertation a few examples pertaining to thin film fabrication and development of nanostructured interfaces for biosensor applications are provided here.

Controlled deposition of different types and sizes of nanoparticles in the form of thin films can find wide range of applications due to difference in fluorescence, absorption and other properties arising out of contributions from individual components[31]. Aggregation is a common problem in such systems. To overcome the same, Kao and co-workers[31] recently developed block co-polymer (BCP) supramolecular approach. The authors used the rigid comb-blocks in the BCP polymer to orient multi-dimensional (1D chains, 2D lattice and 3D arrays) of a mixture of nanoparticles by spatial arrangement of these particles in the supramolecular network. Similarly, Tang and co-workers[32] reported the formation of block-copolymer assemblies with tunable supramolecular interactions depending on stoichiometry and the number of hydrogen bonds and studied their effect on film morphology. Several other examples including layer-by-layer assembly (LbL)[33-40], Langmuir-Blodgett[41, 42], hot-wall process[43], molecular beam deposition process[44] involving supramolecular interactions for effective growth of thin films are available in literature. An interesting review on fabrication of thin films using supramolecular polymers is presented by Tsukruk[45]. Figure 5 shows the growth of supramolecular thin films using the sequential LbL approach. More details about this process will be covered in the subsequent chapters.

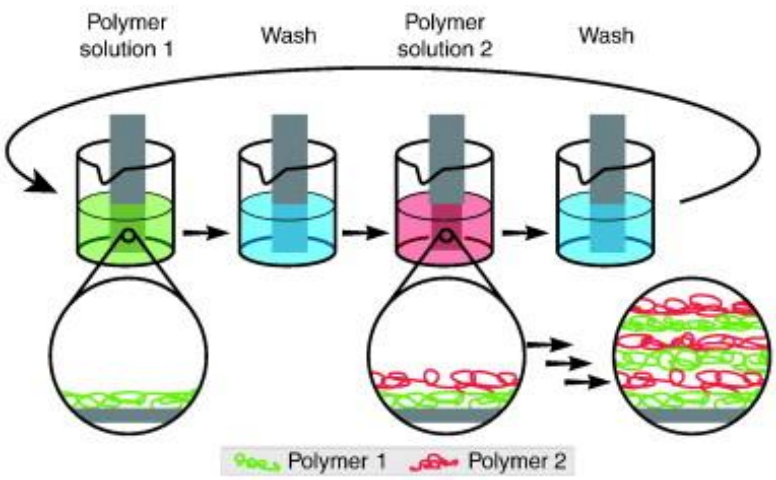

Figure 1.5 Supramolecular layer-by-layer assembly of polyelectrolytes for formation of thin films on substrates (Reproduced with permission from [46]).

Just like thin films, the application of supramolecular assemblies for biosensor technology also holds great promise. Most sensors comprise of two critical elements: the sensing element for the detection of the signal and a transducer to convert the signal into desired output. Supramolecular techniques provide excellent opportunities to integrate these two elements. One of the most common techniques involve guest-host supramolecular interactions for the immobilization of enzymes, cells, nanoparticles on desired substrates to fabricate stable biosensors. Villalonga and co-workers[47] used the same strategy to immobilize xanthine oxidase on a hybrid electrochemical platform consisting of gold nanoparticles and carbon nanotubes. Miranda and co-workers[48] exploited the electrostatic interactions between cationic gold nanoparticles and negatively charge β-galactosidase to design a biosensor for detection of colorimetric bacteria. In another example Alarcon-Angeles and co-workers[49] used a hybrid supramolecular matrix consisting of carbon nanotubes and electropolymerized β-cyclodextrin (CD)-glucose oxidase that suited the microenvironment for effective operation of the enzyme. Figure 6 shows the inclusion of various components in biosensor design.

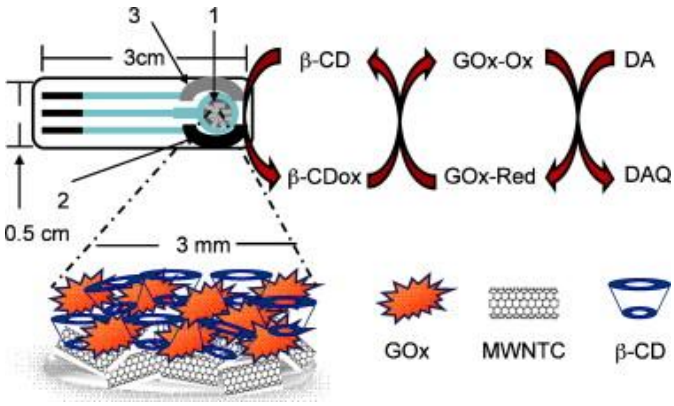

Figure 1.6 Entrapment of glucose oxidase (GOx) in a supramolecular matrix of multiwall carbon nanotubes (MWCNT) and β-cyclodextrin (CD). (Reproduced with permission from [49]).

REFERENCES

REFERENCES

1. Lehn, J.-M., *Toward complex matter: Supramolecular chemistry and self-organization.* Proceedings of the National Academy of Sciences, 2002. **99**(8): p. 4763-4768.

2. Uhlenheuer, D.A., K. Petkau, and L. Brunsveld, *Combining supramolecular chemistry with biology.* Chemical Society Reviews, 2010. **39**(8): p. 2817-2826.

3. Badjic, J.D., et al., *Multivalency and cooperativity in supramolecular chemistry.* Accounts of chemical research, 2005. **38**(9): p. 723-732.

4. Savir, Y. and T. Tlusty. *Molecular recognition as an information channel: The role of conformational changes*. in *Information Sciences and Systems, 2009. CISS 2009. 43rd Annual Conference on*. 2009. IEEE.

5. Lehn, J.-M., *From supramolecular chemistry towards constitutional dynamic chemistry and adaptive chemistry.* Chem. Soc. Rev., 2007. **36**(2): p. 151-160.

6. Elemans, J.A., et al., *Bio-Inspired Supramolecular Catalysis.* Supramolecular Catalysis, 2009: p. 143-164.

7. Wiester, M.J., P.A. Ulmann, and C.A. Mirkin, *Enzyme mimics based upon supramolecular coordination chemistry.* Angewandte Chemie International Edition, 2011. **50**(1): p. 114-137.

8. Brown, C.J., et al., *High-turnover supramolecular catalysis by a protected ruthenium (II) complex in aqueous solution.* Journal of the American Chemical Society, 2011. **133**(31): p. 11964-11966.

9. Wang, Z.J., et al., *Hydroalkoxylation catalyzed by a gold (I) complex encapsulated in a supramolecular host.* Journal of the American Chemical Society, 2011. **133**(19): p. 7358-7360.

10. Yoon, H.J., et al., *Allosteric supramolecular triple-layer catalysts.* Science, 2010. **330**(6000): p. 66-69.

11. Sakai, N., et al., *Supramolecular n/p-heterojunction photosystems with antiparallel redox gradients in electron-and hole-transporting pathways.* Journal of the American Chemical Society, 2010. **132**(20): p. 6923-6925.

12. Huettner, S., et al., *Tunable charge transport using supramolecular self-assembly of nanostructured crystalline block copolymers.* ACS nano, 2011. **5**(5): p. 3506-3515.
13. Desiraju, G.R., *Chemistry beyond the molecule.* Nature, 2001. **412**(6845): p. 397-400.

14. Faul, C.F.J. and M. Antonietti, *Ionic Self-Assembly: Facile Synthesis of Supramolecular Materials.* Advanced Materials, 2003. **15**(9): p. 673-683.

15. Hoeben, F.J.M., et al., *About Supramolecular Assemblies of π-Conjugated Systems.* Chemical Reviews, 2005. **105**(4): p. 1491-1546.

16. Jeffrey, G.A., *An introduction to hydrogen bonding*. Vol. 12. 1997: Oxford University Press New York.

17. Santos, D., et al., *Directional adhesion for climbing: theoretical and practical considerations.* Journal of Adhesion Science and Technology, 2007. **21**(12-13): p. 1317-1341.

18. Roesky, H.W. and M. Andruh, *The interplay of coordinative, hydrogen bonding and π–π stacking interactions in sustaining supramolecular solid-state architectures.: A study case of bis(4-pyridyl)- and bis(4-pyridyl-N-oxide) tectons.* Coordination Chemistry Reviews, 2003. **236**(1–2): p. 91-119.

19. Waters, M.L., *Aromatic interactions in model systems.* Current opinion in chemical biology, 2002. **6**(6): p. 736-741.

20. Hirst, A.R., et al., *Biocatalytic induction of supramolecular order.* Nat Chem, 2010. **2**(12): p. 1089-1094.

21. Yang, Z. and B. Xu, *Supramolecular hydrogels based on biofunctional nanofibers of self-assembled small molecules.* Journal of Materials Chemistry, 2007. **17**(23): p. 2385-2393.

22. Gao, Y., et al., *Enzyme-Instructed Molecular Self-assembly Confers Nanofibers and a Supramolecular Hydrogel of Taxol Derivative.* Journal of the American Chemical Society, 2009. **131**(38): p. 13576-13577.

23. Gazit, E., *Bioinspired chemistry: Diversity for self-assembly.* Nature Chemistry, 2010. **2**(12): p. 1010-1011.

24. Freeman, R., et al., *Supramolecular cocaine− aptamer complexes activate biocatalytic cascades.* Journal of the American Chemical Society, 2009. **131**(14): p. 5028-5029.

25. Xiao, Y., et al., *Lighting Up Biochemiluminescence by the Surface Self-Assembly of DNA–Hemin Complexes.* ChemBioChem, 2004. **5**(3): p. 374-379.

26. González-Campo, A., et al., *A Supramolecular Approach to Enzyme Immobilization in Micro-Channels.* Small, 2012. **8**(22): p. 3531-3537.
27. Krieg, E., et al., *Separation, Immobilization, and Biocatalytic Utilization of Proteins by a Supramolecular Membrane.* PLoS ONE, 2013. **8**(5): p. e63188.

28. Teo, B. and X.H. Sun, *From Top-Down to Bottom-Up to Hybrid Nanotechnologies: Road to Nanodevices.* Journal of Cluster Science, 2006. **17**(4): p. 529-540.

29. Balzani, V., A. Credi, and M. Venturi, *The Bottom-Up Approach to Molecular-Level Devices and Machines.* Chemistry – A European Journal, 2002. **8**(24): p. 5524-5532.

30. Sanchez, F. and K. Sobolev, *Nanotechnology in concrete – A review.* Construction and Building Materials, 2010. **24**(11): p. 2060-2071.

31. Kao, J., et al., *Size-Dependent Assemblies of Nanoparticle Mixtures in Thin Films.* Journal of the American Chemical Society, 2013. **135**(5): p. 1680-1683.

32. Tang, C., et al., *Thin film morphology of block copolymer blends with tunable supramolecular interactions for lithographic applications.* Macromolecules, 2010. **43**(6): p. 2880-2889.

33. Crespo-Biel, O., et al., *Supramolecular Layer-by-Layer Assembly: Alternating Adsorptions of Guest- and Host-Functionalized Molecules and Particles Using Multivalent Supramolecular Interactions.* Journal of the American Chemical Society, 2005. **127**(20): p. 7594-7600.

34. Decher, G., *Fuzzy nanoassemblies: toward layered polymeric multicomposites.* Science, 1997. **277**(5330): p. 1232-1237.

35. Decher, G. and J. Hong, *Buildup of ultrathin multilayer films by a self-assembly process: II. Consecutive adsorption of anionic and cationic bipolar amphiphiles and polyelectrolytes on charged surfaces.* Berichte der Bunsengesellschaft für physikalische Chemie, 1991. **95**(11): p. 1430-1434.

36. Gokhale, A.A., et al., *Conductive oxygen barrier films using supramolecular assembly of graphene embedded polyelectrolyte multilayers.* Journal of colloid and interface science, 2013.

37. Gokhale, A.A., J. Lu, and I. Lee, *Immobilization of cellulase on magnetoresponsive graphene nano-supports.* Journal of Molecular Catalysis B: Enzymatic, 2013. **90**(0): p. 76-86.

38. Zheng, H., et al., *Two component particle arrays on patterned polyelectrolyte multilayer templates.* Advanced Materials, 2002. **14**(8): p. 569.

39. Kidambi, S., I. Lee, and C. Chan, *Controlling primary hepatocyte adhesion and spreading on protein-free polyelectrolyte multilayer films.* Journal of the American Chemical Society, 2004. **126**(50): p. 16286-16287.

40. Hendricks, T.R., et al., *Intact pattern transfer of conductive exfoliated graphite nanoplatelet composite films to polyelectrolyte multilayer platforms.* Advanced Materials, 2008. **20**(10).

41. Ni, Y., R.R. Puthenkovilakom, and Q. Huo, *Synthesis and Supramolecular Self-Assembly Study of a Novel Porphyrin Molecule in Langmuir and Langmuir–Blodgett Films.* Langmuir, 2004. **20**(7): p. 2765-2771.

42. Bjørnholm, T., T. Hassenkam, and N. Reitzel, *Supramolecular organization of highly conducting organic thin films by the Langmuir-Blodgett technique.* Journal of Materials Chemistry, 1999. **9**(9): p. 1975-1990.

43. Khan, R.U.A., et al., *Supramolecular Ordered Organic Thin Films for Nonlinear Optical and Optoelectronic Applications.* Advanced Functional Materials, 2006. **16**(2): p. 180-188.

44. Esembeson, B., et al., *A High-Optical Quality Supramolecular Assembly for Third-Order Integrated Nonlinear Optics.* Advanced Materials, 2008. **20**(23): p. 4584-4587.

45. Tsukruk, V.V., *Assembly of supramolecular polymers in ultrathin films.* Progress in Polymer Science, 1997. **22**(2): p. 247-311.

46. Wohl, B.M. and J.F.J. Engbersen, *Responsive layer-by-layer materials for drug delivery.* Journal of Controlled Release, 2012. **158**(1): p. 2-14.

47. Villalonga, R., et al., *Supramolecular Immobilization of Xanthine Oxidase on Electropolymerized Matrix of Functionalized Hybrid Gold Nanoparticles/Single-Walled Carbon Nanotubes for the Preparation of Electrochemical Biosensors.* ACS Applied Materials & Interfaces, 2012. **4**(8): p. 4312-4319.

48. Miranda, O.R., et al., *Colorimetric bacteria sensing using a supramolecular enzyme–nanoparticle biosensor.* Journal of the American Chemical Society, 2011. **133**(25): p. 9650-9653.

49. Alarcón-Ángeles, G., et al., *Enzyme entrapment by β-cyclodextrin electropolymerization onto a carbon nanotubes-modified screen-printed electrode.* Biosensors and Bioelectronics, 2010. **26**(4): p. 1768-1773.

Chapter 2: Scope of the dissertation

2.1 Overview of the dissertation

The emergence of nanotechnology tools has made it possible to readily synthesize and characterize nanostructured materials. The application of supramolecular chemistry has provided the means to organize these nanostructures in an orderly manner by fine-tuning the intermolecular forces needed for effective binding of the different nanoscale components[1]. This dissertation is an effort in that direction. By exploring different supramolecular interactions, novel architectures for three different types of applications are presented here. The first application deals with bringing about novel structural changes in the design of a supramolecular carbonaceous enzymatic nanobiocatalyst so that it tunes well with the microenvironment it operates. The second application deals with development of synergistic supramolecular thin films with potential applications in electronics/packaging industry. The third project shows the electropolymerization of 1D polymer/enzyme nanowires from a supramolecularly assembled surfactant-stabilized matrix to serve as an amperometric sensor for detection and quantification of anionic species. A brief description of each of these applications is provided here.

2.2 Supramolecular modification of graphene platelets for the biocatalytic saccharification of biomass

There has been growing interest in cellulosic ethanol as the next generation fuel in recent years[2, 3]. Depleting fossil fuels, concerns about energy security as well as magnanimous government incentives in the form of subsidies and tax-breaks have positioned cellulosic ethanol to be a strong contender as an alternative energy source[4, 5]. With several governments around the world recommending the use of bioethanol blended fuel to meet the ever increasing energy

demands, there has been considerable effort to find a practical and economically feasible solution to production of ethanol from renewable resources. The enzymatic conversion of lignocelluloses to reducing sugars by cellulase is the key step in the production of bioethanol. According to some studies, in a typical hydrolysis process cellulases and β-glucosidases account for as much as 50% of the total costs[6, 7]. A truly cost efficient process would therefore demand evolving sustainable routes to ensure recovery of cellulase followed by its reuse. Immobilization of enzymes on solids supports is one such route. Functional nanomaterials are promising candidates for enzyme immobilization with a view to developing efficient industrial biocatalysts with tailor-made catalytic properties. In the first project (Chapter 3), the preparation of pH tunable, temperature sensitive magnetoresponsive graphene-based nano-bio carriers for cellulase immobilization is reported. A simple route to overcome the geometric disadvantage imposed by most 2D immobilization supports and make them capable of closely mimicking free enzymes (FE) operating under similar reaction conditions is discussed. The supramolecular assembly of oppositely charged quenched polyelectrolytes and maghemite-magnetite nanoparticles on 2D graphene supports followed by immobilization of cellulase shows a marked improvement in the biocatalytic activity of the graphene supports. The incorporation of magnetic nanoparticles opens up the possibility of recovery and reuse of the enzyme over multiple cycles. Cellulase immobilization is achieved by a combination of weak polyelectrolyte brushes and zero-length spacer molecules. The swelling behavior of annealed polyelectrolyte brushes is a strong function of the environmental conditions. The degree of polyelectrolyte swelling can be easily tweaked by manipulating the pH and temperature, providing us an effective tool to control the activity of immobilized enzymes. Activity of immobilized cellulase is evaluated using both soluble as well as insoluble substrates like 2% w/v CMC and avicel respectively.

2.3 Conductive graphene-embedded films using a supramolecular layer-by-layer approach

In recent years, with a view to move up in the value-chain, there has been a growing trend towards integrating functionalized nanostructures in packaging films. Packaging films are projected to constitute nearly 42% of the 100 million ton polymer market[8]. Inclusion of nanomaterials in during the fabrication of packaging films is expected to add synergy as well improve the economics of the process. Nano-enabled packaging materials especially food and beverage packaging materials grew significantly to reach US $4.13 billion in 2008 and are expected to reach US $7.3 billion in 2014[8]. Besides, food packaging, the use of nano-enabled barrier films in the electronics industry is also gaining ground. Siemens has been developing nanotechnology enabled color displays on packaging films for the past few years[9]. Another area where barrier films play a significant role is in fabrication of OLEDs. Active matrix organic light emitting devices (AMOLED) currently occupy 2.3% of the mobile phone display market[10]. But OLEDs can operate on lower battery power as compared to its traditional rivals. It is estimated that by 2015, AMOLEDs would occupy as much as 40% of the market share[10]. This presents a huge market for gas barrier packaging films.

The supramolecular self-assembly of polyelectrolyte multilayers (PEMs) provides robust bottom-up strategies to assemble a broad spectrum of nanostructures on the host substrates. The idea of using suramolecularly assembled polyelectrolytes for graphene modification suggested in the first project was further expanded to bring other types of applications under its ambit. In the second project (chapter 4) the formation of graphene nanoplatelet (GNP) embedded polyelectrolyte films to enhance the oxygen barrier properties of poly (ethylene terephthalate) (PET) films is discussed. Despite cheaper costs and high mechanical strength, the diffusion of small gas molecules such as oxygen through PET films remains a matter of great concern. The

simple yet robust supramolecular deposition of GNP/polyelectrolyte on PET substrates significantly increases the tortuous path the oxygen molecule has to travel making it harder to diffuse through the PET film. With permeability coefficients in the range of 10^{-18} cc.cm/cm^2.s.Pa, the coatings developed in this study show three orders of magnitude reduction as compared to the permeability coefficient of the bare PET film, significantly lower than that of ethylene vinyl alcohol (EVOH) and comparable to silicon oxide thin films used in commercial gas barrier foils. The use of GNPs in the multilayered films also helped reduce the electrical sheet resistance to about 1 MΩ which is five orders of magnitude lower than the original PET substrate opening up promising opportunities for future use in semiconductor and electronics industry. Making suitable modifications in the deposition process, three configurations of GNP embedded PEM multilayers namely hydrogen bonded, electrostatic and composite films were developed and their effect on oxygen barrier property and sheet resistance was monitored. Oxygen permeability of films was tested in accordance with ASTM D-3985 using a MOCON 2/21 ML instrument whereas electrical sheet resistance was quantified using a Gamry Femtostat Electrochemical Impedance station.

2.4 Nanostructured biosensor for nitrate detection and quantification

Nanostructured biosensors provide a unique amalgamation of high aspect ratio nanomaterials and substrate specific biological components. The use of nanostructured enzymatic biosensors in environmental monitoring is fast emerging as an important tool to provide valuable inputs on the presence of contaminants in the ecosystem. In the past few decades, there has been a steady rise in the release of nitrate (NO_3^-), a prominent water soluble contaminant associated with the increasing use of nitrate based fertilizers. The first step in environmental remediation is assessing the threat by accurate quantification of the contaminant.

The use of nanostructured enzymatic biosensors in environmental monitoring is fast emerging as an important tool to provide valuable inputs on the presence of contaminants in the ecosystem. In this study, we suggest the use of a highly sensitive, enzymatic biosensor capable of detecting and quantifying minute concentrations of nitrate. The nitrate biosensor consists of a sensing element in the form of nitrate reductase, a class of enzyme capable of reducing nitrate to nitrite immobilized within a conductive polymer matrix responsible for generating a quantifiable amperometric response. In our work, nanoarrays of co-immobilized nitrate reductase and poly(3,4-alkylenedioxypyrrole) (PEDOT), a conducting polymer resistant to nuclueophilic attack at the β-position were grown from a supramolecular surfactant stabilized matrix using a template assisted electropolymerization route. The performance of the biosensor is a strong function of electropolymerization conditions and the morphology of the PEDOT nanostructures. The electropolymerized biosensor displays excellent specificity w.r.t other interfering ions as evidenced from the initial rate kinetics. With a response time of a few seconds, limit of detection (LOD) as low as 108 ppb and sensitivity of about 2.6 μA/μM cm^2, the one-step electropolymerized nanostructured nitrate biosensor developed in this study shows improved performance compared to other electrochemical biosensors. As per our knowledge this is the first attempt to grow single-step enzyme co-immobilized PEDOT nanostructured biosensor while still retaining the upright nanowire structure. This combined with easy and fast fabrication technique (polymerization time is just 300 seconds) opens up exciting opportunities for developing high accuracy PEDOT based nanobiosensors for on-field testing of nitrate contaminants in the future.

REFERENCES

REFERENCES

1. Ling, X.Y., D.N. Reinhoudt, and J. Huskens, *From supramolecular chemistry to nanotechnology: assembly of 3D nanostructures.* Pure and Applied Chemistry, 2009. **81**(12): p. 2225-2233.

2. Goldemberg, J., *Ethanol for a sustainable energy future.* science, 2007. **315**(5813): p. 808-810.

3. Zhang, Y.-H.P., *Reviving the carbohydrate economy via multi-product lignocellulose biorefineries.* Journal of industrial microbiology & biotechnology, 2008. **35**(5): p. 367-375.

4. Luo, L., E. van der Voet, and G. Huppes, *An energy analysis of ethanol from cellulosic feedstock–Corn stover.* Renewable and Sustainable Energy Reviews, 2009. **13**(8): p. 2003-2011.

5. Prasad, S., A. Singh, and H. Joshi, *Ethanol as an alternative fuel from agricultural, industrial and urban residues.* Resources, Conservation and Recycling, 2007. **50**(1): p. 1-39.

6. Galbe, M. and G. Zacchi, *A review of the production of ethanol from softwood.* Applied microbiology and biotechnology, 2002. **59**(6): p. 618-628.

7. Tu, M., R.P. Chandra, and J.N. Saddler, *Evaluating the distribution of cellulases and the recycling of free cellulases during the hydrolysis of lignocellulosic substrates.* Biotechnology progress, 2007. **23**(2): p. 398-406.

8. Silvestre, C., D. Duraccio, and S. Cimmino, *Food packaging based on polymer nanomaterials.* Progress in Polymer Science, 2011. **36**(12): p. 1766-1782.

9. Yam, K.L., *The Wiley encyclopedia of packaging technology*2009, Hoboken, N.J.: John Wiley & Sons.

10. Laaperi, A., *Disruptive factors in the OLED business ecosystem.* Information Display, 2009. **9**(09): p. 09.

Chapter 3: Supramolecular modification of graphene platelets for biocatalytic saccharification of biomass

(This chapter is reproduced with permission from Journal of Molecular Catalysis B: Enzymatic 90 (2013): 76-86.)

3.0 Abstract

In this study, we show an effective way to immobilize cellulase enzyme on solid nanographene supports using supramolecular assembly techniques. Using a bottom-up assembly approach we show the hydrophilic stabilization of graphene supports using a combination of polyelectrolytes. The inclusion of iron-oxide nanoparticles in the assembly allows facile magnetic separation allowing recycle and reuse of the immobilized enzyme. Weak polyacrylic acid brushes act as spacers between the magnetic graphene supports and cellulase. We show the effect of dissociation of weak polyacid on the enzyme activity. Compared to free enzymes, as much as 80% of the activity is preserved. The resilience of the immobilized enzymes was tested by repeated magnetic separation, recycle and reuse. As much as 55% of the activity was retained after four cycles of reuse.

3. 1. Introduction

There has been a growing interest in graphene and graphene based nanomaterials ever since the facile method for its isolation was first reported in 2004.[1] Because of its unique physical and electronic properties, graphene, a 2D one atom thick allotrope of carbon, has been canvassed as a potential replacement for silicon in the near future.[2] Besides the obvious applications in electronics and semiconductor industry, graphene with its high surface area and large aspect ratio, can provide ample opportunities to anchor a host of biomolecules on its surface. Recently some groups used graphene oxide (GO) based carriers for loading biomacromolecules such as

enzymes and anti-cancer therapeutics followed by their targeted release[3-6]. Unlike its oxide, the solubility of graphene in water is poor making its dispersion in aqueous medium difficult. Hence, the complete biological potential has not been realized because of the hydrophobic nature of pristine graphene. In the past, studies have suggested that the shape and degree of curvature of the support used for enzyme immobilization can have a significant effect on enzyme activity[7, 8]. Davison *et.al.* [9] hypothesized that curved nanostructures especially concave structures can provide ample opportunities for protein binding and help in enzyme stabilization. Soybean peroxidase immobilization studies carried out by Asuri *et. al.* [10] on curved single walled-carbon nanotubes (SWNT) and flat 2-D graphite flakes indicated that deactivation constants for 2-D graphite supports tend to be higher as compared to curved SWNT supports. Conformational changes induced in the structure of the enzyme as it binds to solid supports can inhibit its bioactivity. Zhang and co-workers[6] reported lower enzymatic activity due to conformational changes occurring during the immobilization of horseradish peroxidase on flat GO supports. While shape and size of the supports along with the conformational changes as a result of immobilization would continue to play an important role in enzymatic activities, in this work we address both these concerns by making suitable modifications in the biocatalyst architecture. Graphene nanoplatelets (GNP) are new generation carbon nanomaterials prepared by exfoliation of natural graphite. Because of their planar morphology, they act as flat 2-D supports when used for immobilization of biomolecules. Carbon nanostructures have been used in the past for biomolecule immobilization because of their ability to stabilize biological structures at elevated temperatures[11-14]. Ji and co-workers[15] showed that the lipase immobilized on multiwalled carbon nanotubes show improved hydrolytic activity. It has been hypothesized that carbon nanotubes because of their higher thermal conductivity ensure efficient heat transfer to the

immobilized enzyme. In carbon chemistry, graphene is the 2-D analog of carbon nanotubes and should share similar heat conduction properties. Another type of 2-D nanomaterial is clay platelets. However, the sorption and immobilization of biomolecules on clay depends on several factors such as pH and type of cation present in the platelets making it difficult to isolate the effect of shape of the carrier[16, 17].

Graphene nanoplatelet composed of a few layers of graphene sheets stacked together is one of the most common types of nanostructured graphene.[18, 19]The surface of these platelets is composed of sp^2 hybridized pure graphene. Platelets with BET surface areas up to 900 m^2/gm can be produced by exfoliation. Such exfoliated cost-effective GNPs with a projected price of $5/lb can be produced at Michigan State University using a process described elsewhere[20]. High surface area and low cost of production make graphene an ideal candidate for enzyme immobilization. In the past, surface modification using wet chemistry techniques has been used to address the issue of hydrophobicity of carbon nanostructures. These methods generally require using strong inorganic acids and physical processes such as ultrasonication, and high shear homogenization in presence of surface active reagents[21-24]. However, not all methods are suited for biological modification. Use of toxic chemicals or harsh process conditions can instead have a deleterious effect on the biological viability of carbon nanostructures.

Originally conceived by Iler[25] and further developed by Decher and coworkers[26, 27], the layer-by-layer assembly (LbL) has become an important tool to produce nanoscopically structured novel materials. Initially used for building polyelectrolyte multilayers, this versatile technique is now also used to incorporate a plethora of nanoscopic, polymeric and bioactive components within the film structure[28]. Using extremely simple apparatus such as beakers and tweezers, the LbL technique allows us to prepare nanoscopic synergistic functional films by

combining various components within the same unit. The ability to blend together various functional materials by creating supramolecular multilayered assemblies makes LbL a very good example of 'bottom-up' approach. Smuleau *et. al.*[29] and Dotzauer *et. al.*[30] showed the immobilization of enzymes and gold nanoparticles respectively on polyelectrolyte films assembled on membrane filters. Smuleau and co-workers reported that the interaction between the oppositely charged polyelectrolyte layers and the protein molecules enables a 25 fold increase in immobilization. Very small conformation changes were noticed in the biomolecule configuration after the polyelectrolyte modification. Dotzauer and co-workers showed that gold nanoparticles immobilized on porous supports using the LbL approach can efficiently reduce almost 99% of the 4-nitrophenol. Wang and Caruso[31] applied the electrostatic LbL assembly to 3D macroporous membranes for the immobilization of catalase. The polyelectrolyte multilayers accomplish two outcomes. Firstly they allow attachment of the catalase enzyme on the membrane. Secondly they also prevent the leakage of the enzymes facilitating improved biocatalytic performance. Siqueira Jr. *et. al.*[32] review the various strategies used for immobilization of biomolecules on LbL and Langmuir-Blodgett nanofilms. Lee and co-workers at Michigan State University incorporated proteins, dendrimers, nanoparticles, lipids, cells, and metals onto or into the LbL layers for a variety of applications such as biosensing, biocatalysis, and biomedical applications[33-37]. The molecular-level design of interfacial bonding at the interface via self-assembly is the key to fabricating stable and functional interface[38, 39]. This affects the adhesion and functions of the resulting nanostructured interfaces.

Cellulose, a major component of the lignocellulosic biomass, is hydrolyzed by cellulase to yield reducing sugars[40]. Cellulase, a class of saccharifying enzymes, has gained attention in recent years due to the significant role it plays in the production of ethanol from cellulosic

substrates. Cellulase is not just one enzyme system According to the widely accepted view, efficient saccharification of cellulosic biomass is achieved by the cooperative action of a number of enzymes including endo-glucanase and exo-glucanase[41, 42]. The endo-exo synergism disrupts the cellulosic matrix to ultimately release reducing sugars[41]. The cost of cellulase accounts for a significant portion of the hydrolysis costs, which according to some estimates, is as high as 50%[43, 44]. In recent years, a combination of genetic engineering and cheaper downstream processes has helped bring about several improvements in enzyme production as well as cellulase performance[43, 45]. However, further reduction in the cost of cellulase enzymes by genetically modifying the cellulolytic microorganisms would be challenging[43]. Cellulase recovery and reuse is another potential approach that can be used to offset the high costs associated with enzyme use. Unfortunately, during a typical hydrolysis reaction, cellulases tend to get distributed over two heterogeneous phases: the solid substrate and the liquid supernatant thus making recovery of the enzymes difficult[43, 46].

Immobilization of cellulase on solid supports has been suggested as a viable alternative[47]. Immobilization of enzymes on supports helps to improve the overall operational stability of enzymes by increasing their resilience towards changes in external factors like temperature and pH[48-50]. Moreover, it prevents cellulase redistribution over two heterogeneous phases facilitating easy separation, providing a facile route to recycle and reuse the enzyme over multiple cycles. In this work, the presence of iron oxide nanoparticles on graphene supports allows for the magnetic separation of the immobilized cellulase. The recovered cellulase is then reused over multiple cycles thus reducing the overall cost of using fresh enzymes. With cellulase poised to capture the second largest segment in the enzyme market [51], improved

immobilization strategies with a recovery mechanism to save costs are necessary to ensure its optimum use.

In our recent graphene studies, we used different cationic and anionic polyelectrolytes like poly(diallydimethylammonium chloride) (PDAC) and sulfated poly(styrene) (SPS) respectively to disperse GNPs in aqueous medium [18, 52, 53]. The nanoplatelets develop cationic or anionic surface charge depending on the type of polyelectrolyte used. Electrostatic assembly of oppositely charged nanoplatelets is possible using the LbL technique. In this work, we utilize a similar approach to prepare novel magnetoresponsive biocompatible graphene supports for cellulase immobilization. These supports will be hence forth called magnetic nanoparticle incorporated graphene nanoplatelets. (MNP-GNP). Maghemite-magnetite decoration followed by cellulase immobilization is carried out by using a combination of quenched and annealed polyelectrolytes. Strong polyelectrolytes mentioned above are used for efficient electrostatic binding of anionic iron oxide nanoparticles (8-10 nm in size). Polyacrylic acid, a weak polyelectrolyte, makes the surface of MNP-GNP biocompatible. Cellulase is then attached to the supports using covalent chemistry. Weak polyacid brushes such as PAA are pH and heat sensitive[54-56]. The swelling behavior of pH, heat tunable polyacrylic acid brushes gives us an opportunity to control cellulase mobility. The presence of nanoparticles and polyelectrolytes between the graphene support and the enzyme provides a ‘cushioning effect’. Increased freedom of movement, enhanced enzyme mobility and reduced steric hindrance due to the underlying support help fine-tune the microenvironment of the immobilized enzymes to closely resemble that of free enzymes[57]. Thus, the limitations imposed by the 2D morphology of graphene supports can be effectively addressed by making suitable changes in the design of the immobilized biocatalyst.

3.2. Experimental procedures

3.2.1 Materials

Poly(diallydimethylammonium chloride) (PDAC), sulfated poly(styrene) (SPS), and polyacrylic acid (PAA) sodium salt (35 wt% solution in water) were purchased from Sigma Aldrich. Average molecular weights of PDAC, SPS and PAA were ~100,000-200,000, 70,000, and 15,000 respectively. Carboxymethyl cellulose (CMC) sodium salt, 2-(*N*-morpholino)ethanesulfonic acid (MES) and citric acid monohydrate were purchased from Fisher Scientific Co. Avicel PH- 101, 50 μm in size was obtained from Fluka. 1-Ethyl-3-(3′-dimethylaminopropyl) carbodiimide, Hydrochloride (EDAC, HCl) was purchased from EMD Chemicals. Accellerase-1000, a commercial cellulase enzyme was a kind gift from Genencor Division, Danisco US Inc., Rochester, NY, USA. Exfoliated graphene nanoplatelets (GNP) (BET surface are 327 m^2/gm and size $\leq$ 1μm) were provided by Dr. Drzal's research group at MSU. All aqueous solutions were prepared using deionized (DI) water (>18.1 MΩ) supplied by a Barnstead Nanopure Diamond-UV purification unit equipped with a UV source and final 0.2 μm filter. Unless specified otherwise, all procedures were carried out at room temperature.

3.2.2 Preparation of polyelectrolyte solutions

Aqueous polyelectrolyte solutions were prepared containing either 20 mM PDAC or 2 mg/ml SPS. Sodium chloride concentration was adjusted to 0.1 M. The concentration of PAA solution was 1 mg/ml with no addition of salt. The solutions were filtered through 0.22 μm cellulose-acetate membrane-filter system from Nalgene to remove particulates. The aqueous polyelectrolyte solutions were used without pH adjustment.

3.2.3 Preparation of polyelectrolyte-multilayered graphene scaffolds

Around 200 mg of GNP were added to 50 ml of SPS solution. The resultant suspension was stirred for 30 minutes. This was followed by ultrasonication for 90 minutes. The SPS modified graphenic suspension was then centrifuged at 4000 rpm followed by three washes of deionized water to remove the excess SPS. To deposit a PDAC layer, the SPS-coated GNP is added to 50 ml of PDAC. A similar procedure as described above is repeated. In order to achieve uniform surface coverage of polyelectrolytes, we deposited in all four layers of SPS and PDAC (i.e. two bilayers). Positively charged PDAC layer occupies the uppermost layer in the quad-layer assembly.

3.2.4 Alkaline co-precipitation of maghemite-magnetite nanoparticles (8-10 nm)

Detailed description of preparation of aqueous suspension of magnetic nanoparticles is available elsewhere[58, 59]. Briefly speaking, Fe^{3+} and Fe^{2+} ions are mixed in the molar ratio of 2:1. 5 ml of ammonium hydroxide is added drop-wise. The mixture is heated to 80^0C under nitrogen purging. 1 ml of citric acid (2.38 M) is added to the above mixture and the temperature is raised to 95^0C. Heating is continued for 90 minutes. The colloidal solution is then separated by centrifugation (9000 rpm) and washed thrice with a mixture of acetone and water to get a stable dispersion. The nanoparticles are then dispersed in 30 ml of deionized water and stored at room temperature.

3.2.5 Maghemite-Magnetite decoration of polyelectrolyte-modified graphene scaffolds

The maghemite-magnetite nanoparticles solution is diluted to 0.53 mg/ml by adding DI water. Around 50 ml of this solution is combined with polyelectrolyte-coated graphene as synthesized above and sonicated for 90 minutes. The maghemite-magnetite decorated graphene

is then centrifuged and washed with copious quantity of DI water to remove the unattached nanoparticles. With each successive wash, the color of the supernatant changes from pale brownish-yellow to that of clear liquid. Finally the precipitate is dried in an oven at 65°C for two days and stored in a vacuum desiccator for future use.

3.2.6 Immobilization of cellulase on maghemite-magnetite graphene scaffolds

Depending on the substrate used for hydrolysis, a predetermined quantity of maghemite-magnetite decorated graphene is added to 1 mg/ml PAA solution. Ultrasonication for 60 minutes helps in efficient dispersion of MNP-GNP in PAA. The PAA grafted graphene scaffolds are then centrifuged and washed twice with copious quantities of DI water. Terminal carboxylic acid groups of PAA are activated by immersing the PAA grafted MNP-GNP in 0.1 M/0.5 M MES/NaCl buffer containing 100 mg. of EDAC, HCl. The pH of the buffer solution prior to addition of EDAC, HCl was adjusted to 5.5. The carboxylic group activation continues for 1 hour on a tube rotator at room temperature. The EDAC activated PAA modified MNP-GNP is centrifuged at 4000 rpm and washed twice with DI water to remove unattached EDAC, HCl. Accelerase-1000, a commercial cellulase enzyme containing both endo and exo glucanase is centrifuged at 2000 rpm. The supernatant solution is separated, diluted to 1.375 mg/ml and used for further experiments. 2 ml of this diluted enzyme solution is added to EDAC activated graphene supports as prepared above. Incubation continues for 15 hours on a tube rotator at 4^0C. After the incubation time, the immobilized enzymes are centrifuged at 4000 rpm, washed thrice with DI water. The washings are pooled together for protein estimation. The PAA modified immobilized enzymes (now called IMC-PAA) are then suspended in appropriate buffer solution of desired pH. A separate set of immobilized enzymes are prepared by following the exact

procedure except without using PAA and EDAC, HCl. These immobilized enzymes will be henceforth called IMC.

3.2.7 Characterization of polyelectrolyte coated graphene supports

The zeta potential of graphene particles after polyelectrolyte and enzyme modification was measured by ZetaPALS instrument (Brookhaven Instruments Corp., Holtsville, NY). To determine the ζ-potential, 100 µl of the sample was added to 1.4 ml 1 mM KCl solution. The KCl solution was filtered through 0.22 µm cellulose acetate membrane filter prior to use. Phase analysis light scattering studies typically determine the electrophoretic mobility of charged particles from measurable parameters such as velocity of the particles and the magnitude of the applied electric field. This data is then fitted to the Smoluchowski equation by the ZetaPALS software to obtain the zeta potential value.

3.2.8 Characterization of GNPs and MNP-GNPs

The scanning electron microscopy (SEM) investigation for high-resolution imaging was carried out using a JEOL 7500F with field emission. Transmission electron microscopy (TEM) studies were carried out using a JEOL 100CX and JEOL 2200FS. Both SEM and TEM analyses help us to determine the morphology of graphene before and after nanoparticle decoration. To determine the extent of nanoparticles doping, MNP-GNP samples were digested in HCl/HNO_3 (3:1 volume ratio) mixture and the samples were analyzed using inductively couple plasma optical emission spectroscopy (ICP-OES).

3.2.9 Protein assay

Protein concentration of the enzyme solution before and after immobilization is determined using the Bradford method[60]. Protein loaded on MNP-GNPs was estimated by doing a simple

mass balance before and after immobilization. The protein loading was found to be 2.5 ± 0.75 mg/gm MNP-GNP. Covalent immobilization helps prevent enzyme leaching. However, a very small quantity of protein may still desorb from the immobilized enzyme if subjected to repeated use. The protein desorbed during the recyclability studies is quantified using the micro-bicinchoninic acid (mBCA) assay, a technique typically used for measuring small quantities of protein (0.5-20µg/ml). Since glucose can interfere with mBCA results, two separate sets of experiments, one for measuring glucose and other for measuring desorbed protein were performed. For the later set of experiments, no substrate was added.

3.2.10 Measurement of cellulase activities

Cellulase activities are traditionally measured by quantifying the end-products of the hydrolysis reaction[61]. These end-products are in the form of reducing sugars. For CMC experiments, 10 mg. MNP-GNPs were used. For avicel based experiments, 5 mg. were used. The amount of protein immobilized on MNP-GNPs was estimated as described in the previous section. Free enzyme solution having the same protein content as the immobilized enzymes was prepared by diluting with appropriate buffer solution. The biocatalytic activity of free and immobilized enzymes was measured under similar reaction conditions using 2% w/v CMC and avicel. Hydrolysis was run for 90 minutes. Samples were subjected to 5 minutes of boiling to stop the reaction. The amount of generated glucose was measured using high-performance liquid chromatography (HPLC). One activity unit is defined as the amount of cellulase that catalyzes CMC or avicel to release 1 µmole glucose/min/mg. of protein under specified hydrolysis conditions. We define two terms here, relative activity and mimicking ability of immobilized enzymes. Thus, while relative activity normalizes the enzyme activity on the basis of specific hydrolysis parameters most frequently used in cellulase assay procedures (50 $^{\circ}$C and pH 4.8),

mimicking ability is a measure of the biocatalytic potential of immobilized enzymes when compared to free enzymes at the same pH and temperature.

$$Relative\ activity(\%) = \frac{Immobilized\ enzyme\ activity\ under\ specified\ hydrolysis\ condition}{Free\ enzyme\ activity\ at\ a\ pH\ of\ 4.8\ and\ 50^0C} \times 100 \quad \text{.....(1)}$$

$$Mimicking\ ability(\%) = \frac{Immobilized\ enzyme\ activity\ under\ specified\ hydrolysis\ condition}{Free\ enzyme\ activity\ at\ same\ pH\ and\ temperature} \times 100$$

.....(2)

For recyclability studies, 50 mg. of MNP-GNP were used. Each hydrolysis cycle was run for 60 minutes at a temperature of 50 $^{\circ}$C and pH 5.2. The immobilized enzymes were magnetically separated after every cycle. Four hydrolysis cycles were repeated using the same set of conditions, each time adding a fresh batch of substrate.

3.3. Results and Discussions

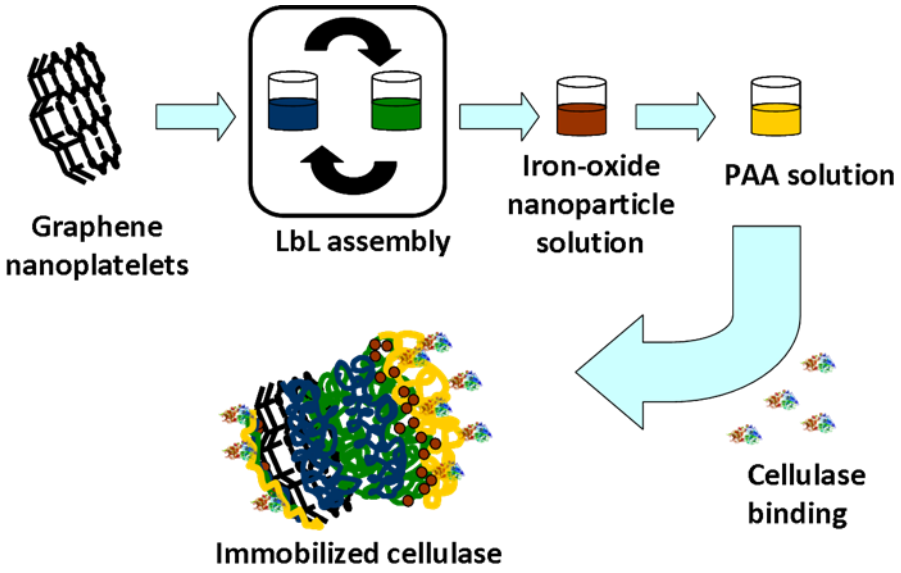

Figure 3.1 Schematic illustration of the design of the proposed biocatalyst: Assembly of polyelectrolytes, nanoparticles and cellulase on graphene nanoplatelets. (Figure not drawn to scale)

Figure 3.1 illustrates a schematic diagram showing the 'bottom-up' assembly of quenched polyelectrolytes, iron-oxide nanoparticles, annealed polyelectrolyte and finally cellulase. As seen from the figure, because of the presence of polyelectrolytes and nanoparticles, we anticipate that most of the cellulase immobilization occurs on the outer surface of modified GNPs as opposed to between the individual nanoplatelets The proposed design is particularly attractive because it helps minimize internal diffusion limitation which otherwise is a major impediment in enzyme biocatalysis.

Based on key steps involved in the preparation of the biocatalyst, we broadly discuss the theory and results under three headings: Maghemite-magnetite decoration of GNPs, chemisorption of PAA brushes, and lastly its proposed effect on enzyme activity.

3.3.1 Maghemite-Magnetite decoration of graphene nanoplatelets

One of the very first steps in the design of graphene based biocatalyst is to improve its long term stability in aqueous medium. Stable aqueous dispersion can be obtained by subjecting graphene to polyelectrolyte modification, as shown in our previous work [18, 52, 53]. Table 3.1 shows the cyclic nature of charge overcompensation as each bilayer of SPS and PDAC is sequentially adsorbed on the surface of GNPs. Table 1 also shows the effect of adsorption of magnetic nanoparticles (zeta potential turns negative) and PAA (degree of negative charge increases further) on the polyelectrolyte modified graphene supports.

Table 3.1 ζ-potential (mV) of modified GNP dispersions. The last component in each line represents the terminal (topmost) layer in the multilayer assembly. Error bars represent the standard deviation of 3 replicate samples.

Type of terminal layer	**Zeta potential (mV)**
GNP-SPS	-51.50 ± 0.75
GNP-SPS-PDAC	43.25 ± 1.23
GNP-SPS-PDAC-SPS	-49.25 ± 1.22
GNP-$(SPS-PDAC)_2$	46.91 ± 0.95
GNP-$(SPS-PDAC)_2$-MNP	-26.36 ± 2.92
GNP-$(SPS-PDAC)_2$-MNP-PAA	-41.78 ± 3.15

In case of pristine GNPs, the Vander-Waals force of attraction primarily caused by polarized π-electrons along with the hydrophobic interactions between individual graphene sheets cause the nanoplatelets to aggregate, rendering them insoluble in water[62]. High molecular weight polyions (in this case SPS and PDAC) possess a remarkable ability to cover substrate irregularities through multipoint attachment[63]. As compared to small molecules and charged colloids, they provide a more consistent and uniform coating[64]. Depending on the functional groups, different polyelectrolytes can disperse GNPs upto varying degree of stability[18]. The ability of negatively charged SPS, the first polyelectrolyte in the quad-layer assembly, to solubilize GNPs can be explained by the concept of 'polymer wrapping'. The concept of

'polymer-wrapping' followed by LbL assembly has been used in the past to add functionality to different types of carbon nanostructures including carbon nanotubes[65, 66]. SPS is an amphiphile. While its backbone is highly hydrophobic, the sulfonate groups impart hydrophilic and anionic character to the molecule. Limited scale interaction calculations reveal that the robust adsorption of SPS on GNPs is primarily because of edge-to-face interactions between the graphene surface and aromatic rings of SPS[67]. Thus, while the hydrophobic areas of the GNPs are screened by the hydrophobic part of SPS, the anionic sulfonate groups project themselves in the aqueous medium and stabilize the suspension through mutual repulsion. The polyelectrolyte multilayer formation is a thermodynamic driven process in which both electrostatic as well as hydrophobic interactions play an important role. The incoming polyelectrolyte solution also produces a change in the ionic environment as well as the hydration shell around both the polyelectrolytes[68]. A simple free energy model developed by Kotov[68] to explain the polyelectrolyte adsorption process accounts for all individual contributions mentioned above.

The presence of two bilayers of oppositely charged polyelectrolytes serves two purposes. Firstly, it gives rise to tightly coiled intertwined polyelectrolyte conformations around the GNPs. The polyelectrolytes stabilize the GNPs promoting their effective dispersion in aqueous medium. It has been suggested that multilayers of strong polyelectrolytes (in this case SPS and PDAC) can disperse colloidal particles more effectively as opposed to weak polyelectrolytes because of their stability over wide range of conditions[69]. Secondly, they also serve as precursor films for the subsequent adsorption of iron oxide nanoparticles. It is a widely accepted view that the presence of precursor films help in eliminating substrate effects generating surfaces with almost uniform configurations[63]. In our case, we observed that precursor film composed of two bilayers was sufficient to enable reasonably uniform adsorption of iron-oxide nanoparticles. The

incorporation of iron oxide nanoparticles on the surface of graphene nanoplatelets makes these supports magnetic. Thus, rather than using the cumbersome energy intensive process of centrifugation, facile separation of these supports can be achieved by using small bar/disc magnets. Cellulase immobilization on magnetic supports offers attractive opportunities to lower the enzyme requirement of the process by recovery and reuse over multiple cycles.

Alkaline co-precipitation of maghemite-magnetite nanoparticles is a long established method for preparation of monodisperse iron oxide nanoparticles. According to Massart,[59] surfactantless iron oxide colloids may aggregate due to neutralization of charges when used between pH 5 to pH 9. α-hydroxy acids such as tartaric, oleic and gluconic acid have been used in the past to stabilize the colloids[70]. In our case, we used citric acid, another α-hydroxy acid known for bearing tridentate carboxylate ligands. The presence of three negatively charged acidic groups not only helps in stabilizing the magnetic nanoparticles over a wide range of pH but also provides sufficient interaction sites when the citric acid capped iron oxide nanoparticles are adsorbed on the positively charged PDAC layer. The nanoparticle decoration as estimated by ICP-OES is about 47 mg iron/gm of MNP-GNP. It has been shown that the isoelectric point of citric acid coated magnetic nanoparticles is lesser than pH 3 [71] which is lower than the lower-bound of the pH range we use for our enzyme activity tests. Thus, the chances of iron oxide nanoparticles reversing their surface charge and getting desorbed from the surface of graphene are minimal. The SEM and TEM micrographs (Figure 3.2) show the adsorption of iron oxide nanoparticles roughly of size 8-10 nm on the surface of polyelectrolyte-coated GNPs.

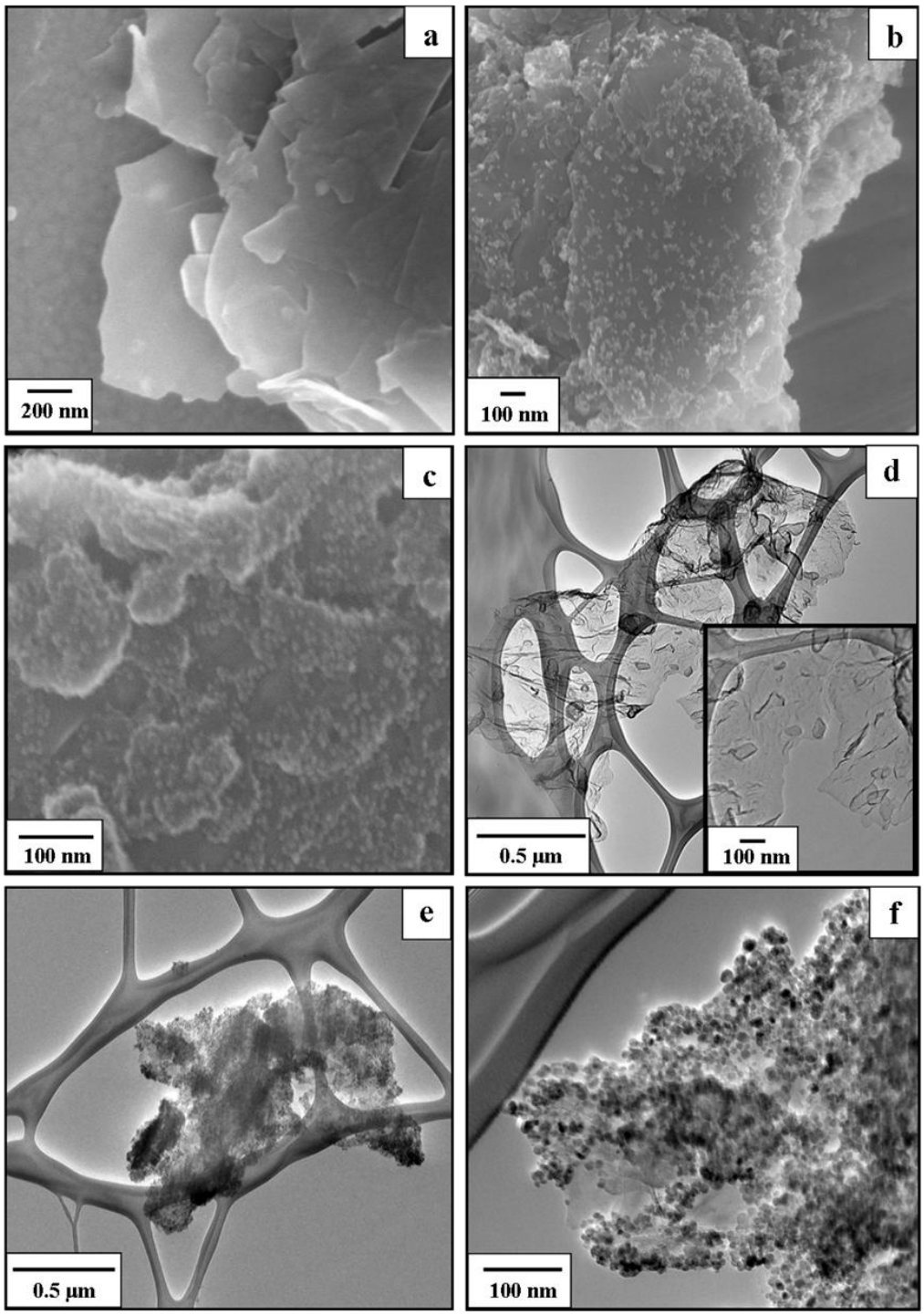

Figure 3.2 SEM micrographs of (a) GNP, (b) MNP-GNP (low magnification), and (c) MNP-GNP (high magnification): Average size of iron oxide nanoparticles around 8-10 nm. (d) TEM micrograph of GNP. The inset shows high magnification image of a selected portion of the same platelet. Scale bar for the inset is 100 nm. TEM micrographs of (e) MNP-GNP (low magnification) and (f) TEM micrograph of MNP-GNP (high magnification): Almost uniform coating of iron-oxide nanoparticles (8-10 nm) is observed on the surface of the graphene nanoplatelet.

The size of the iron-oxide nanoparticles has a significant bearing on the superparamagnetic property with the saturation magnetization decreasing with increasing particle size[72]. Besides our current strategy of using polyelectrolyte precursor films to fixate nanoparticles, another promising approach suggested in literature is embedding metal precursors in the graphene matrix[19]. These precursors act as 'seeds' for the subsequent growth of nanoparticles. The 'seeding' approach has been shown to produce dense uniform films of nanoparticles. However, with higher loading of nanoparticles, there are greater chances of aggregation[73]. Also, the nanoparticles grown from precursors show a high degree of polydispersity. Though methods have been suggested to monitor the growth of nanoparticles and ensure the monodispersity,[19, 73] they usually require careful process control, or additional steps such as developing a method to embed the precursor in the support matrix followed by its chemical reduction. The layer-by-layer method, on the other hand, involves separate preparation of nanoparticles of desired size to suit our needs. The nanoparticles can then be adsorbed on the surface of graphene by merely contacting the supports with the nanoparticle solution. The incorporation of iron-oxide nanoparticles on GNPs provides these supports with a new functionality. The magnetoresponsive behavior of GNPs after nanoparticle decoration is evident from Figure 3.3.

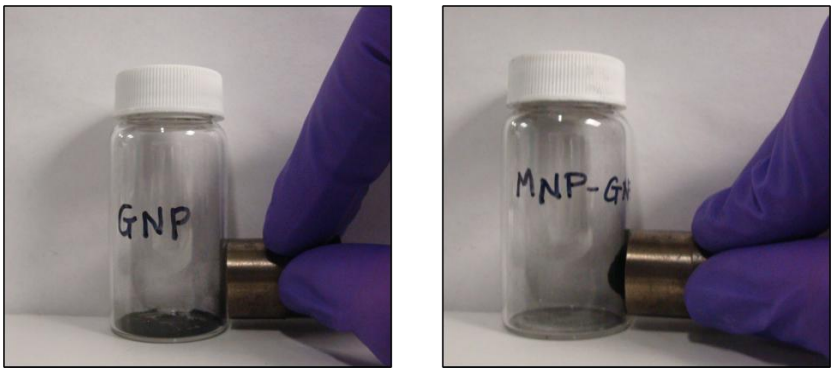

Figure 3.3 Effect of external magnetic field on graphene nanoplatelets (a) before iron oxide nanoparticle decoration: No change observed (b) after iron-oxide nanoparticle decoration: GNPs driven towards the magnetic source.

3.3.2 Chemisorption of polyacrylic acid brushes on MNP-GNP

Maghemite-magnetite decorated graphene supports offer an attractive opportunity to immobilize a number of bioactive components. Biological molecules have often shown subdued activity when subjected to direct immobilization on supports[74]. So in this case, we use polyacrylic acid, a well-known biocompatible material, to serve as a bridge between the cellulase enzyme and the MNP-GNPs. Many studies have shown that PAA can be used as an effective biomaterial in several applications such as muco-adhesion, drug delivery, etc.[75, 76]. PAA also serves as a good dispersing agent. Going back to Table 1, we observe that the use of PAA helps in increasing the magnitude of negative zeta potential, thus improving stability of the dispersion. PAA has multiple hydrophilic carboxylic groups, some of which are used up when PAA interacts with the iron oxide layer of MNP-GNPs while the rest can be utilized for cellulase immobilization. Sugama *et. al.* [77] has proposed two possible mechanisms for chemisorption of PAA on metal oxide surfaces. One of the proposed mechanisms suggests that the acid base interaction between the –COOH groups of PAA and the polar groups –OH of the oxide allow for strong chemisorption of PAA on the metal oxide surface. The other mechanism involves formation of a salt bridge between the carboxylic groups of PAA and the free metal ions of the metal oxide. The formation of a hydrophilic PAA layer on the surface of MNP-GNP helps to improve its dispersibility in aqueous medium. As mentioned earlier, the remaining –COOH groups are then utilized for cellulase binding. EDAC- HCl, a commonly used zero-length spacer molecule, helps to covalently bind the amine groups of cellulase to the –COOH groups of PAA.

Besides being a biocompatible material capable of anchoring proteins through covalent linkage, PAA is also a weak polyelectrolyte. Unlike strong polyelectrolytes, which regardless of the pH, dissociate completely when in solution, weak polyelectrolytes are heavily influenced by

salt content and acidity/alkalinity of the contacting solution[78]. In order to eliminate one of the interfering factors, no salt was added while preparing the PAA solution. When the PAA is chemisorbed on the surface of MNP-GNP, it gives rise to coiled conformations with some of the segments stretching out into the solution because of electrostatic repulsion. Studies have shown that the benign nature of the 'brush-like' polyelectrolyte assembly helps in preserving most of the activity of the enzymes or other bioactive molecules immobilized within the assembly[79, 80].

There are many examples in literature that focus on 'smart' polyelectrolyte-protein bioconjugates[81-84]. Wang and Caruso[85] used PAA to infiltrate into protein loaded silica mesoporous spheres. PAA binds to most proteins electrostatically and covalently and thus acts as a 'bridging agent'.In some cases, even a small change in the environmental condition can trigger a large response in the structure and properties of the bioconjugate. Imanishi and Ito[82] used glucose oxidase immobilized weak PAA brushes to build a 'chemical valve' that would permit the transport of insulin under low pH condition.

An important criterion in case of weak polyelectrolyte brushes is the pK_a value. Based on values available in literature, the pK_a value of polyacrylic acid brushes occurs between 4.2-4.8[86-88]. An important fact worth noting at this juncture is that the pH optimum of cellulase is also in that range, the relevance of which should become clear later. It has been well-established[56] that when the $pH < pK_a$, the protonation of weak polyelectrolyte brushes leads to collapse of the chain segments. When the $pH > pK_a$, more and more –COOH groups become charged producing swollen brushes with chain segments extending all the way into the contacting buffer solution. This pH-induced swelling of the PAA brushes can have a significant bearing on the enzyme activity. Similar examples of pH-responding polymer brushes for

biological applications can be found in literature[89-91]. While Zhou *et. al.* [91] discuss reversible immobilization of a protein Cytochrome c made possible because of the pH induced protonation-deprotonation of PAA brushes, Tam and co-workers[89] demonstrated the successful use of a modified Poly(4-vinyl pyridine), (P4VP) polybase brush for bioelectronic applications. The electrochemical activity is enhanced at low pH when the brushes are in a swollen state. A collapsed P4VP brush at higher pH restricts the flow of electrons between the redox species and the conductive support thus reducing the electrochemical activity. Likewise, neutron reflectometry (NR) experiments have also confirmed that certain polymer brushes such PAA brushes show a remarkable swelling behavior when subjected to moderate heat treatment[92].

3.3 Effect of PAA brushes on activity of immobilized enzymes

Figure 3.4 illustrates how environmental conditions such as pH and temperature affect the PAA brushes.

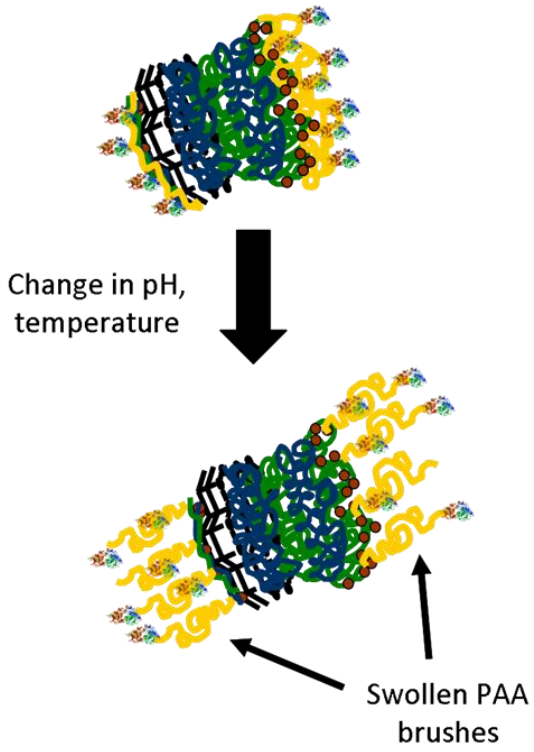

Figure 3.4 Effect of swollen PAA brushes on cellulase mobility. (a) Higher steric hindrance due to collapsed PAA brushes. (b) Higher cellulase mobility and increased substrate-enzyme interaction due to swollen PAA brushes. (Figure not drawn to scale)

Before examining how these conditions typically affect the immobilized enzyme activity, it is important to note that cellulases consist of a complex mixture of various enzymes and this includes endoglucanase and exoglucanse. Endo- and exo glucanases usually produce a synergistic effect making it difficult to demarcate the contribution of each enzyme. However, some studies claim that certain substrates because of their internal structure can help isolate endo and exoglucanse activities from each other[93]. Carboxymethyl cellulose (CMC), a soluble form of cellulose, is a model substrate used to evaluate the cleavage of internal glycosidic bonds, an action which is typical endoglucanase. Henceforth, activity determined using CMC as substrate would be referred to as CMCase activity. Exoglucanase activity, a measure of the efficiency with which the terminal glycosidic bonds are cleaved, can be evaluated using avicel, a crystalline form of cellulose. For the enzyme recovery experiments, we continued to use avicel since it

resembles the real biomass samples more closely as compared to CMC. Henceforth, activity determined by using avicel as the substrate would be referred to as avicelase activity.

3.3.3.1 Effect of pH on enzyme activity

Data obtained from hydrolysis of avicel and CMC by three sets of enzymes (FE, IMC-PAA and IMC) is shown in Figures 3.5. Relative enzyme activity was evaluated at six different values of pH starting with a pH of 3.0.. Subsequent points are 0.7 pH units apart. These pH values were selected keeping in mind the pK_a value of the PAA brushes (4.2-4.8). pH 3.0 and 6.5 are far off from the pKa value of PAA. They form the two extremities of the data set. Our data (not included here) showed that the trend exhibited by the enzymes at these two data-points continues likewise beyond these points. Data obtained at pH 3.7, 4.4 5.1 and 5.8 is critical in understanding the effect of PAA brushes on immobilized cellulase activity. pH 3.7 is slightly below the lower bound of the pKa value. At this pH, the brushes are protonated and are in a collapsed state. pH 4.4 is in the transition range as the brushes undergo a transformation from a collapsed state to swollen state. pH 5.1 is slightly higher than the upper bound of the pK_a value. At this pH, the brushes are swollen and extend all the way into the buffer solution. At a pH of 5.8, other concerns such as higher agglomeration due to lower zeta potential and lower enzymatic activity, start dominating. Two different types of buffer solution were used. 0.05 M citrate buffer was used in experiments where the pH was adjusted to 3 and 3.7 and 4.4. 0.05 M MES buffer solution was used for adjusting the pH to 5.1, 5.8 and 6.5.

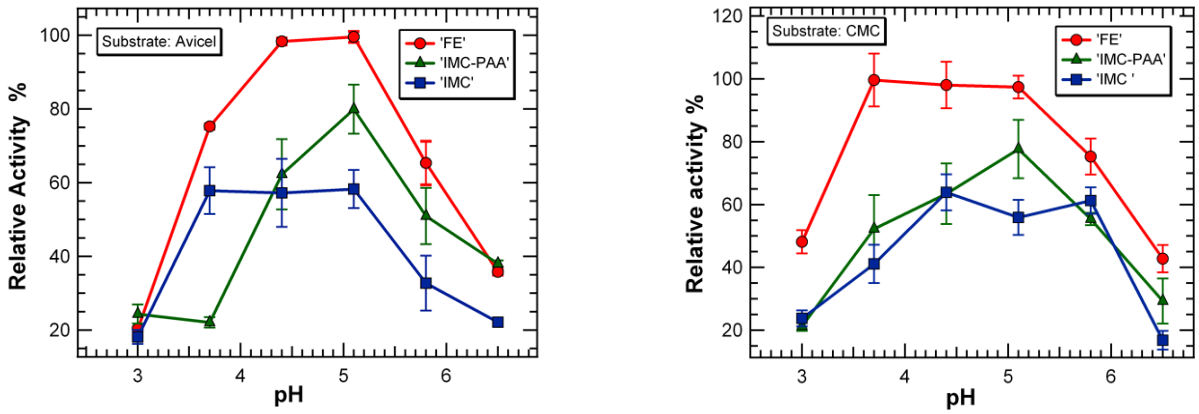

Figure 3.5 Relative activity of free and immobilized enzymes as a function of pH (a) Avicelase activity (b) CMCase activity. Conditions: 2%w/v avicel/CMC, Hydrolysis time: 90 minutes, Temperature 50 ^{0}C. Error bar represent standard deviation of three replicate samples.

Refer Figure 3.5(a). The free enzyme activity is about 20% at a pH of 3.0 reaches 75% at a pH of 3.7. At a pH 4.4 and 5.1 it is almost 100% and finally tapers off to 65% and 35% at pH of 5.8 and 6.5 respectively. IMC follows a similar trend, though the activity is much lower at the same pH. Enzyme activity reaches an optimum value of around 57% around pH 3.7 and stays in a similar range upto pH 5.1. On the other hand, in case of IMC-PAA, there is a steep rise from 22% to almost 80% as the pH is raised from 3.7 to 5.1. The endo-glucanase data obtained by substituting avicel with CMC (Figure 5(b)) mirrors the same trend. IMC-PAA activity increases from 52% to 78% in the pH range 3.7-5.1. On the other hand, the avicelase and CMCase activitites for IMC remain low (upto 62% at the most) in the pH interval 3.7-5.1.

We attribute the sudden spike in enzyme activity from pH 3.7 to 5.1 as fallout of the swelling behavior exhibited by the PAA brushes. At lower pH, the brushes are in collapsed state pulling the enzymes closer to the graphene support. The steric hindrance caused by the proximity of the enzyme to the underlying support could explain the reduced enzyme activity. As the pH is raised above the pK_a value, the brushes elongate and push the enzymes away from the graphene support. Greater interaction between the catalytic sites of the enzyme and the substrate enhances

the activity. This proposed theory is further supported by the IMC data. Without the PAA brushes, both avicelase as well as CMCase activities show lower activity in the pH range 3.7-5.1.

We carried out a zeta potential analysis (please refer Table 3.2) of both IMC-PAA and IMC over the entire pH range starting 3.0 to 6.5. Zeta potential being an indication of the stability of colloidal particles can provide valuable insight into the behavior of enzyme modified particles at different pH conditions. Table 3.2 clearly shows how the PAA modification impacts the charge structure of the immobilized enzymes. The difference in charge structure can influence the microenvironment of the immobilized enzymes producing variations in the enzyme activity. For IMC, the particles display a positive charge at lower pH (3.0 and 3.7). The zeta potential is negative at other pH values. This implies that the isoelectric point for IMC lies somewhere between 3.7 and 4.4. On the other hand, IMC-PAA shows a negative zeta potential over the corresponding pH range. An interesting observation can be made from this analysis. The zeta potential data for IMC shows that the magnitude of surface charge for this set of immobilized enzymes is low. In other words, IMC enzymes are not very stable and must be agglomerating during the hydrolysis process thus reducing their effectiveness. On the other hand, IMC-PAA becomes much more stable as the pH is raised from 3.0 to 5.1. At 4.4 and 5.1, it shows identical surface charge of almost similar magnitude within the margin of error. Thereafter at pH 5.8 and 6.5, the magnitude of zeta potential reduces, thereby reducing its stability and hence its effectiveness.

Table 3.2 ζ-potential (mV) of IMC and IMC-PAA as a function of pH. Error bars represent the standard deviation of 3 replicate samples.

pH	IMC	IMC-PAA
3.0	7.23 ± 0.63	-19.28 ± 1.38
3.7	7.51 ± 0.79	-25.61 ± 2.27
4.4	-11.85 ± 0.54	-31.72 ± 2.32
5.1	-13.18 ± 0.57	-29.13 ± 1.25
5.8	-10.29 ± 0.95	-18.97 ± 0.98
6.5	-10.78 ± 0.69	-17.94 ± 1.23

Depending on the source from which it is derived and the ingredients that make up the enzyme broth, the pH optimum for cellulase ranges from 4.2-5.0 with most studies using the value 4.8 for experimental purposes. As mentioned before, the choice of the weak polyelectrolyte and the conditions under which it is used in the immobilization process are very important. PAA has a pK_a value which almost coincides with the optimum pH for free enzymes. Consider poly(methacrylic acid), another example of a weak polyelectrolyte. AFM studies haves confirmed that densely grafted poly(methacrylic) acid brushes show a remarkable swelling behavior at a pH of about 9[94]. Swelling starts at around 7.0 and continues till 10.5. The biocatalytic potential of cellulase at this pH is highly doubtful rendering the whole exercise of using pH tunable annealed brushes ineffective.

3.3.3.2 Effect of temperature on cellulase activity

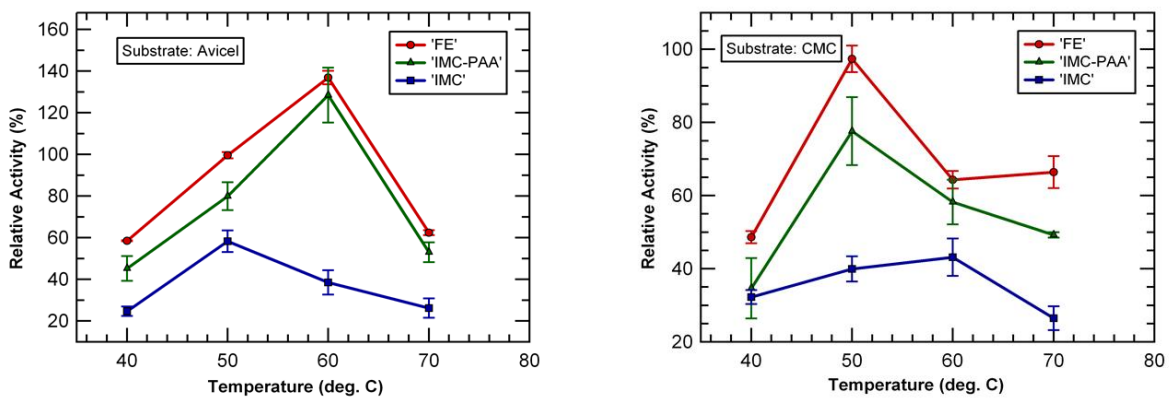

(a) **(b)**

Figure 3.6 Relative activity of free and immobilized enzymes as a function of temperature (a) Avicelase activity (b) CMCase activity. Conditions: (a)2 %w/v avicel (b)2%w/v CMC, Hydrolysis time: 90 minutes, solution pH: 5.1. Error bars represent standard deviation of three replicate samples.

Data for three systems: FE, IMC-PAA and IMC is presented in Figure 3.6(a) and (b). Our results show that immobilized enzymes with PAA brushes closely follow the trend shown by free enzymes. It has been shown previously that PAA adopt a swollen conformation at higher temperatures[95, 96]. In another example involving formation of a mixed hydrogel of poly(vinyl) alcohol (PVA) and PAA, Lee and co-workers[97] have argued that at higher temperature the dissociation of hydrogen bonding between the –OH group of (PVA) and –COOH of PAA produces excess carboxylate ions which can lead to swollen configuration. We hypothesize that in our case as the temperature is raised from 40^0C through 70^0C, the PAA brushes continue to undergo incremental swelling as a result of interactions between the –OH groups of the iron-oxide and –COOH groups of PAA. We believe that just like pH variation, increase in temperature also facilitates formation of swollen brushes ensuring greater mobility and better substrate-enzyme interaction. Thus, IMC-PAA can closely mimic the free enzymes. At 60^0C, avicelase activity for IMC-PAA reaches its optimum value. Likewise, the CMCase activity for IMC-PAA reaches its optimum of 78% at 50^0C. On the other hand, IMC show subdued avicelase

as well as CMCase activity (57% or less) over the entire temperature range. Thus the swollen conformation of PAA brushes provided a favorable micro-environment for cellulase. After reaching a maximum at 60^0C for avicel and 50^0C for CMC, cellulase activity showed a decline. However this decrease in cellulase activity also corresponds to decrease in activity of free enzymes as seen from Figure 3.6 and could be attributed because of partial deactivation of the active centers at higher temperatures.

3.3.3.3 Mimicking ability of Immobilized enzymes

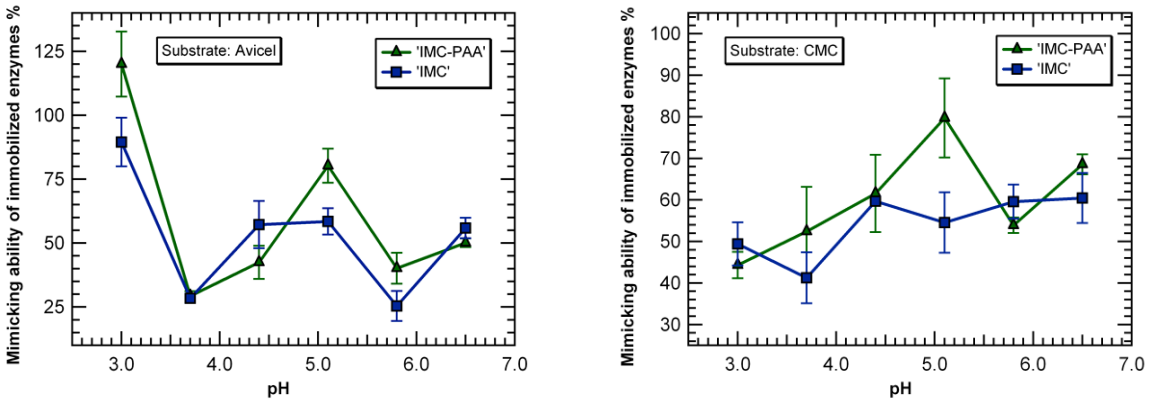

(a) **(b)**

Figure 3.7 Mimicking ability of immobilized enzymes as a function of (a) Avicelase activity at variable pH (b) CMCase activity at variable pH (c) Avicelase activity at variable temperature (d) CMCase activity at variable temperature. Conditions: (a) 2%w/v avicel (b) 2%w/v CMC, Hydrolysis time: 90 minutes, Temperature 50 ^{0}C. Data was collected at pH 3.0, 3.7, 4.4 ,5.1, 5.8 and 6.5. (c) 2 %w/v avicel (d) 2%w/v CMC, Hydrolysis time: 90 minutes, solution pH: 5.1. Data collected at 40^0C, 50^0C, 60^0C and 70^0C. Error bars represent standard deviation of three replicate samples.

Figure 3.7 (cont'd)

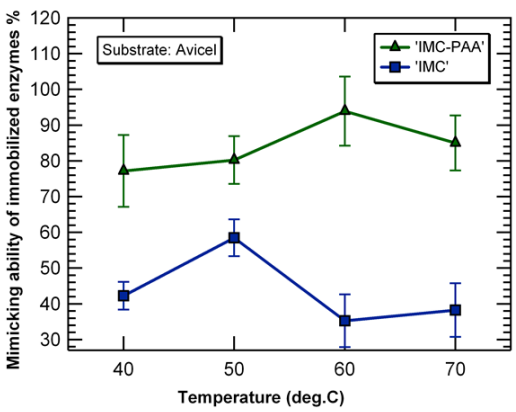

(c)

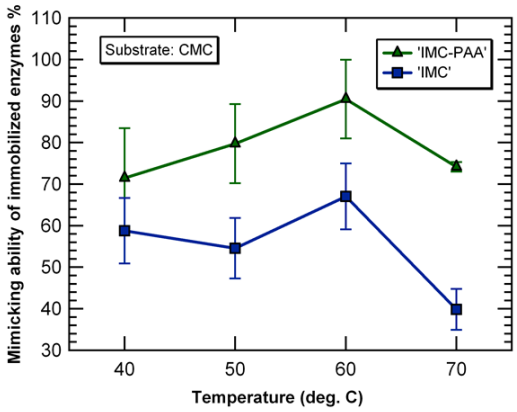

(d)

The mimicking ability of immobilized enzymes (IMC-PAA and IMC) is shown in Figure 3.7. The superiority of IMC-PAA over IMC is evident in this figure. In Figure 3.7(a) and (b) we see a marked improvement in the mimicking ability of IMC-PAA as the pH is raised to 5.1. We observe higher than expected enzymatic activities for both IMC-PAA and IMC at extreme pH conditions of 3.0 and 6.5. This can be attributed to lower free enzyme activity at those pH values. In Figure 3.7 (c) and (d), we observe that IMC-PAA closely mimic free enzymes at a temperature of 60^0C almost to the extent of 90-95%. Both avicelase and CMCase activities for IMC-PAA consistently register 70% or more mimicking ability over the entire temperature range.

3.3.4 Magnetic separation, recovery and reuse of immobilized enzymes

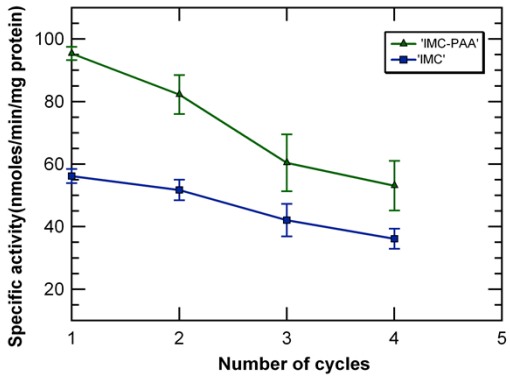

Figure 3.8. Specific activity of immobilized enzymes with and without PAA brushes vs. number of cycles of hydrolysis.

Immobilized enzymes were subjected to four cycles of hydrolysis to test their efficiency after repeated use. Data provided in Figure 3.8 shows that immobilized enzyme activity decreases after every hydrolysis cycle. The decrease in enzymatic activity is not uncommon and is routinely observed in most immobilized enzyme systems that are used multiple times. The decrease could be because of protein desorption as well as denaturation. However, our results (not shown here) indicated that in case of IMC-PAA, using covalent chemistry helped minimize protein loss due to desorption. Compared to IMC, IMC-PAA displays higher resilience to activity loss. As much as 55% of the original activity is retained after four cycles of use.

3.4. Conclusion

In summary, we demonstrated a polyelectrolyte based, ‘bottom-up’ approach for preparation of maghemite-magnetite decorated graphene supports followed by successful immobilization of cellulase using a combination of annealed polyacid brushes and zero-length spacer molecules. The method proposed here is simple and can be easily repeated with other proteins/enzyme systems. The cellulase hydrolysis results from the initial-rate experiments confirm considerably high endo and exo-glucanase activities for soluble as well as insoluble substrates respectively. Immobilized enzyme activity was studied as a function of both pH and temperature. Annealed

polyacid brushes being pH and heat sensitive, play a very crucial role in biocatalysis. The lower enzymatic activity reported for most flat 2-D carriers can be overcome with the use of swollen PAA brushes.The immobilized enzymes with PAA brushes closely mimic free enzymes (as much as 90-95%) at 60^0C and a pH of 5.1. This is, by far, the highest cellulase activity reported for two-dimensional flat carriers.

Three factors namely protein loading, activity of the loaded enzyme and more importantly, the activity of loaded enzyme after several cycles of recycle should be taken into consideration while evaluating the overall operational efficiency of immobilized enzymes. The proposed immobilized enzyme design addresses the three key issues raised above. Firstly, a fair amount of protein loading up to 2.5 ± 0.91 mg/gm was observed when PAA modified magnetoresponsive graphene supports were used for immobilization. There is still some scope to increase the protein loading by (a) using the 'grafting-from' approach to grow PAA brushes which is suggested as a more efficient way to ensure dense coverage of PAA. However, this comes at the cost of increased pK_a value. Its effect on enzyme activity remains to be seen. (b) Immobilizing cellulase at a pH close to its isoelectric point (pI). However, one should note that since cellulase is a combination of several enzymes, an exact value for pI may not be available. Secondly, the pH and heat tunable flexible polyacid brushes provide better mobility to the enzyme enhancing its interaction with the substrate under consideration. Lastly, the covalent binding helps minimize enzyme leeching, thus allowing multiple cycles of reuse. As much as 55% of the specific activity of immobilized enzymes is retained after four cycles of use.

REFERENCES

REFERENCES

1. Novoselov, K.S., et al., *Two-dimensional atomic crystals.* Proceedings of the National Academy of Sciences of the United States of America, 2005. **102**(30): p. 10451-10453.

2. Van Noorden, R., *Moving towards a graphene world.* Nature, 2006. **442**(7100): p. 228-229.

3. Zhang, L.M., et al., *Functional Graphene Oxide as a Nanocarrier for Controlled Loading and Targeted Delivery of Mixed Anticancer Drugs.* Small, 2010. **6**(4): p. 537-544.

4. Liu, Z., et al., *PEGylated nanographene oxide for delivery of water-insoluble cancer drugs.* Journal of the American Chemical Society, 2008. **130**(33): p. 10876-+.

5. Sun, X.M., et al., *Nano-Graphene Oxide for Cellular Imaging and Drug Delivery.* Nano Research, 2008. **1**(3): p. 203-212.

6. Zhang, J.L., et al., *Graphene Oxide as a Matrix for Enzyme Immobilization.* Langmuir, 2010. **26**(9): p. 6083-6085.

7. Kim, J., J.W. Grate, and P. Wang, *Nanostructures for enzyme stabilization.* Chemical Engineering Science, 2006. **61**(3): p. 1017-1026.

8. Kim, J., H.F. Jia, and P. Wang, *Challenges in biocatalysis for enzyme-based biofuel cells.* Biotechnology Advances, 2006. **24**(3): p. 296-308.

9. Davison, B.H., et al., *Enzyme stabilization by covalent binding in nanoporous sol-gel glass for nonaqueous biocatalysis.* Biotechnology and Bioengineering, 2001. **74**(3): p. 249-255.

10. Asuri, P., et al., *Increasing protein stability through control of the nanoscale environment.* Langmuir, 2006. **22**(13): p. 5833-5836.

11. Asuri, P., et al., *Water-soluble carbon nanotube-enzyme conjugates as functional biocatalytic formulations.* Biotechnology and Bioengineering, 2006. **95**(5): p. 804-811.

12. Pavlidis, I.V., et al., *Development of effective nanobiocatalytic systems through the immobilization of hydrolases on functionalized carbon-based nanomaterials.* Bioresource Technology, 2012. **115**: p. 164-171.

13. Feng, W. and P.J. Ji, *Enzymes immobilized on carbon nanotubes.* Biotechnology Advances, 2011. **29**(6): p. 889-895.

14. Lu, J., R.R. Weerasiri, and I. Lee, *Carbon nanotubes tuned foam structures as novel nanostructured biocarriers for lignocellulose hydrolysis.* Biotechnology Letters, 2013. **35**(2): p. 181-188.

15. Ji, P.J., et al., *Lipase Covalently Attached to Multiwalled Carbon Nanotubes as an Efficient Catalyst in Organic Solvent.* Aiche Journal, 2010. **56**(11): p. 3005-3011.

16. Staunton, S. and H. Quiquampoix, *Adsorption and Conformation of Bovine Serum-Albumin on Montmorillonite - Modification of the Balance between Hydrophobic and Electrostatic Interactions by Protein Methylation and Ph Variation.* Journal of Colloid and Interface Science, 1994. **166**(1): p. 89-94.

17. Sinegani, A.A.S., G. Emtiazi, and H. Shariatmadari, *Sorption and immobilization of cellulase on silicate clay minerals.* Journal of Colloid and Interface Science, 2005. **290**(1): p. 39-44.

18. Lu, J., et al., *Stable Aqueous Suspension and Self-Assembly of Graphite Nanoplatelets Coated with Various Polyelectrolytes.* Journal of Nanomaterials, 2010. **18**: p. 64-86.

19. Lee, I., et al., *Nanometal-decorated exfoliated graphite nanoplatelet based glucose biosensors with high sensitivity and fast response.* Acs Nano, 2008. **2**(9): p. 1825-1832.

20. Drzal, L.T. and H. Fukushima, *Expanded graphite and products produced therefrom,* , in *U.S. Patent Application 11/361, 255*2006.

21. Rao, C.N.R., A. Govindaraj, and B.C. Satishkumar, *Functionalised carbon nanotubes from solutions.* Chemical Communications, 1996(13): p. 1525-1526.

22. Zhao, W., C.H. Song, and P.E. Pehrsson, *Water-soluble and optically pH-sensitive single-walled carbon nanotubes from surface modification.* Journal of the American Chemical Society, 2002. **124**(42): p. 12418-12419.

23. Niyogi, S., et al., *Ultrasonic dispersions of single-walled carbon nanotubes.* Journal of Physical Chemistry B, 2003. **107**(34): p. 8799-8804.

24. Badaire, S., et al., *In situ measurements of nanotube dimensions in suspensions by depolarized dynamic light scattering.* Langmuir, 2004. **20**(24): p. 10367-10370.

25. Iler, R.K., *Multilayers of Colloidal Particles.* Journal of Colloid and Interface Science, 1966. **21**(6): p. 569-&.

26. Decher, G. and J.D. Hong, *Buildup of Ultrathin Multilayer Films by a Self-Assembly Process .1. Consecutive Adsorption of Anionic and Cationic Bipolar Amphiphiles on Charged Surfaces.* Makromolekulare Chemie-Macromolecular Symposia, 1991. **46**: p. 321-327.

27. Decher, G., and J. D. Hong, *Buildup of ultrathin multilayer films by a self-assembly process: II. Consecutive adsorption of anionic and cationic bipolar amphiphiles and*

polyelectrolytes on charged surfaces. Berichte der Bunsengesellschaft für physikalische Chemie,1991. **95**(11): 1430-1434.

28. Ariga, K., J.P. Hill, and Q.M. Ji, *Layer-by-layer assembly as a versatile bottom-up nanofabrication technique for exploratory research and realistic application.* Physical Chemistry Chemical Physics, 2007. **9**(19): p. 2319-2340.

29. Smuleac, V., D.A. Butterfield, and D. Bhattacharyya, *Layer-by-layer-assembled microfiltration membranes for biomolecule immobilization and enzymatic catalysis.* Langmuir, 2006. **22**(24): p. 10118-10124.

30. Dotzauer, D.M., et al., *Catalytic membranes prepared using layer-by-layer adsorption of polyelectrolyte/metal nanoparticle films in porous supports.* Nano Letters, 2006. **6**(10): p. 2268-2272.

31. Wang, Y.J. and F. Caruso, *Macroporous zeolitic membrane bioreactors.* Advanced Functional Materials, 2004. **14**(10): p. 1012-1018.

32. Siqueira, J.R., et al., *Immobilization of biomolecules on nanostructured films for biosensing.* Biosensors & Bioelectronics, 2010. **25**(6): p. 1254-1263.

33. Kidambi, S., I. Lee, and C. Chan, *Primary neuron/astrocyte co-culture on polyelectrolyte multilayer films: A template for studying astrocyte-mediated oxidative stress in neurons.* Advanced Functional Materials, 2008. **18**(2): p. 294-301.

34. Hassler, B.L., et al., *Renewable dehydrogenase-based interfaces for bioelectronic applications.* Langmuir, 2007. **23**(13): p. 7127-7133.

35. Hendricks, T.R., et al., *Intact pattern transfer of conductive exfoliated graphite nanoplatelet composite films to polyelectrolyte multilayer platforms.* Advanced Materials, 2008. **20**(10): p. 2008-2012.

36. Kidambi, S., et al., *Cell adhesion on polyelectrolyte multilayer coated polydimethylsiloxane surfaces with varying topographies.* Tissue Engineering, 2007. **13**(8): p. 2105-2117.

37. Sambanthamoorthy, K., et al., *Identification of a novel benzimidazole that inhibits bacterial biofilm formation in a broad-spectrum manner.* Antimicrobial agents and chemotherapy, 2011. **55**(9): p. 4369-4378.

38. Lee, I. and R.P. Wool, *Polymer adhesion vs substrate receptor group density.* Macromolecules, 2000. **33**(7): p. 2680-2687.

39. Lee, I. and R.P. Wool, *Controlling amine receptor group density on aluminum oxide surfaces by mixed silane self assembly.* Thin Solid Films, 2000. **379**(1-2): p. 94-100.

40. Lee, I., W. Wang, and S. Ji. *DEVICE AND METHOD FOR PRETREATMENT OF BIOMASS* 2011.

41. Medve, J., et al., *Hydrolysis of microcrystalline cellulose by cellobiohydrolase I and endoglucanase II from Trichoderma reesei: Adsorption, sugar production pattern, and synergism of the enzymes.* Biotechnology and Bioengineering, 1998. **59**(5): p. 621-634.

42. Woodward, J., *Synergism in Cellulase Systems.* Bioresource Technology, 1991. **36**(1): p. 67-75.

43. Tu, M.B., R.P. Chandra, and J.N. Saddler, *Evaluating the distribution of cellulases and the recycling of free cellulases during the hydrolysis of lignocellulosic substrates.* Biotechnology Progress, 2007. **23**(2): p. 398-406.

44. Galbe, M. and G. Zacchi, *A review of the production of ethanol from softwood.* Applied Microbiology and Biotechnology, 2002. **59**(6): p. 618-628.

45. Tu, M.B., R.P. Chandra, and J.N. Saddler, *Recycling cellulases during the hydrolysis of steam exploded and ethanol pretreated lodgepole pine.* Biotechnology Progress, 2007. **23**(5): p. 1130-1137.

46. Lee, D., A.H.C. Yu, and J.N. Saddler, *Evaluation of Cellulase Recycling Strategies for the Hydrolysis of Lignocellulosic Substrates.* Biotechnology and Bioengineering, 1995. **45**(4): p. 328-336.

47. Taherzadeh, M.J. and K. Karimi, *Enzyme-Based Hydrolysis Processes for Ethanol from Lignocellulosic Materials: A Review.* Bioresources, 2007. **2**(4): p. 707-738.

48. Tran, D.N. and K.J. Balkus, *Perspective of Recent Progress in Immobilization of Enzymes.* Acs Catalysis, 2011. **1**(8): p. 956-968.

49. Sheldon, R.A., *Enzyme immobilization: The quest for optimum performance.* Advanced Synthesis & Catalysis, 2007. **349**(8-9): p. 1289-1307.

50. Gokhale, A.A. and I. Lee, *Cellulase Immobilized Nanostructured Supports for Efficient Saccharification of Cellulosic Substrates.* Topics in Catalysis, 2012: p. 1-16.

51. van Beilen, J.B. and Z. Li, *Enzyme technology: an overview.* Current Opinion in Biotechnology, 2002. **13**(4): p. 338-344.

52. Worden, R.M., et al., *Simple fabrication of a highly sensitive glucose biosensor using enzymes immobilized in exfoliated graphite nanoplatelets Nafion membrane.* Chemistry of Materials, 2007. **19**(25): p. 6240-6246.

53. Lee, I., et al., *Intact pattern transfer of conductive exfoliated graphite nanoplatelet composite films to polyelectrolyte multilayer platforms.* Advanced Materials, 2008. **20**(10): p. 2008-+.

54. Ruhe, J., et al., *Polyelectrolyte brushes.* Polyelectrolytes with Defined Molecular Architecture I, 2004. **165**: p. 79-150.

55. Biesalski, M., D. Johannsmann, and J. Ruhe, *Synthesis and swelling behavior of a weak polyacid brush.* Journal of Chemical Physics, 2002. **117**(10): p. 4988-4994.

56. Dong, R., M. Lindau, and C.K. Ober, *Dissociation Behavior of Weak Polyelectrolyte Brushes on a Planar Surface.* Langmuir, 2009. **25**(8): p. 4774-4779.

57. Wan, L.S., et al., *Enzyme immobilization on electrospun polymer nanofibers: An overview.* Journal of Molecular Catalysis B-Enzymatic, 2009. **56**(4): p. 189-195.

58. Liu, Z.L., et al., *Synthesis and characterization of ultrafine well-dispersed magnetic nanoparticles.* Journal of Magnetism and Magnetic Materials, 2004. **283**(2-3): p. 258-262.

59. Massart, R., *Preparation of Aqueous Magnetic Liquids in Alkaline and Acidic Media.* Ieee Transactions on Magnetics, 1981. **17**(2): p. 1247-1248.

60. Bradford, M.M., *Rapid and Sensitive Method for Quantitation of Microgram Quantities of Protein Utilizing Principle of Protein-Dye Binding.* Analytical Biochemistry, 1976. **72**(1-2): p. 248-254.

61. Ghose, T.K., *Measurement of Cellulase Activities.* Pure and Applied Chemistry, 1987. **59**(2): p. 257-268.

62. Kotov, N.A., et al., *Aqueous dispersions of single-wall and multiwall carbon nanotubes with designed amphiphilic polycations.* Journal of the American Chemical Society, 2005. **127**(10): p. 3463-3472.

63. Kotov, N.A., J.W. Ostrander, and A.A. Mamedov, *Two modes of linear layer-by-layer growth of nanoparticle-polylectrolyte multilayers and different interactions in the layer-by-layer deposition.* Journal of the American Chemical Society, 2001. **123**(6): p. 1101-1110.

64. Decher, G., *Fuzzy nanoassemblies: Toward layered polymeric multicomposites.* Science, 1997. **277**(5330): p. 1232-1237.

65. Correa-Duarte, M.A., et al., *Alignment of carbon nanotubes under low magnetic fields through attachment of magnetic nanoparticles.* Journal of Physical Chemistry B, 2005. **109**(41): p. 19060-19063.

66. Liz-Marzan, L.M. and M.A. Correa-Duarte, *Carbon nanotubes as templates for one-dimensional nanoparticle assemblies.* Journal of Materials Chemistry, 2006. **16**(1): p. 22-25.
67. Nguyen, S.T., et al., *Stable aqueous dispersions of graphitic nanoplatelets via the reduction of exfoliated graphite oxide in the presence of poly(sodium 4-styrenesulfonate).* Journal of Materials Chemistry, 2006. **16**(2): p. 155-158.

68. Kotov, N.A., *Layer-by-layer self-assembly: The contribution of hydrophobic interactions.* Nanostructured Materials, 1999. **12**(5-8): p. 789-796.

69. Kato, N., et al., *Thin multilayer films of weak polyelectrolytes on colloid particles.* Macromolecules, 2002. **35**(26): p. 9780-9787.

70. Corot, C., et al., *Recent advances in iron oxide nanocrystal technology for medical imaging.* Advanced Drug Delivery Reviews, 2006. **58**(14): p. 1471-1504.

71. Nigam, S., K.C. Barick, and D. Bahadur, *Development of citrate-stabilized Fe(3)O(4) nanoparticles: Conjugation and release of doxorubicin for therapeutic applications.* Journal of Magnetism and Magnetic Materials, 2011. **323**(2): p. 237-243.

72. Mukadam, M.D., et al., *Particle size-dependent magnetic properties of gamma-Fe2O3 nanoparticles.* Journal of Magnetism and Magnetic Materials, 2004. **272**: p. 1401-1403.

73. Xing, Y.C., *Synthesis and electrochemical characterization of uniformly-dispersed high loading Pt nanoparticles on sonochemically-treated carbon nanotubes.* Journal of Physical Chemistry B, 2004. **108**(50): p. 19255-19259.

74. Chimanage, P., et al., *Properties of Cellulase Immobilized on Agarose-Gel with Spacer.* Biotechnology and Bioengineering, 1986. **28**(12): p. 1876-1878.

75. Park, H. and J.R. Robinson, *Mechanisms of Mucoadhesion of Poly(Acrylic Acid) Hydrogels.* Pharmaceutical Research, 1987. **4**(6): p. 457-464.

76. Ma, Y.H., et al., *Magnetically targeted thrombolysis with recombinant tissue plasminogen activator bound to polyacrylic acid-coated nanoparticles.* Biomaterials, 2009. **30**(19): p. 3343-3351.

77. Sugama, T., L.E. Kukacka, and N. Carciello, *Nature of Interfacial Interaction Mechanisms between Polyacrylic-Acid Macromolecules and Oxide Metal-Surfaces.* Journal of Materials Science, 1984. **19**(12): p. 4045-4056.

78. Zhang, H.N. and J. Ruhe, *Polyelectrolyte complexes and multilayers at solid surface via polymer brushes.* Abstracts of Papers of the American Chemical Society, 2003. **225**: p. U621-U621.

79. Ballauff, M., T. Neumann, and B. Haupt, *High activity of enzymes immobilized in colloidal nanoreactors.* Macromolecular Bioscience, 2004. **4**(1): p. 13-16.

80. Caruso, F. and C. Schuler, *Enzyme multilayers on colloid particles: Assembly, stability, and enzymatic activity.* Langmuir, 2000. **16**(24): p. 9595-9603.

81. Galaev, I.Y. and B. Mattiasson, *'Smart' polymers and what they could do in biotechnology and medicine.* Trends in Biotechnology, 1999. **17**(8): p. 335-340.

82. Imanishi, Y. and Y. Ito, *Glucose-sensitive insulin-releasing molecular systems.* Pure and Applied Chemistry, 1995. **67**(12): p. 2015-2021.

83. Uhlmann, P., et al., *In-situ investigation of the adsorption of globular model proteins on stimuli-responsive binary polyelectrolyte brushes.* Langmuir, 2007. **23**(1): p. 57-64.

84. Cole, M.A., et al., *Stimuli-responsive interfaces and systems for the control of proteinâ€“surface and cellâ€“surface interactions.* Biomaterials, 2009. **30**(9): p. 1827-1850.

85. Wang, Y.J. and F. Caruso, *Nanoporous protein particles through templating mesoporous silica spheres.* Advanced Materials, 2006. **18**(6): p. 795-+.

86. Choi, H.K., M.K. Chun, and C.S. Cho, *Mucoadhesive drug carrier based on interpolymer complex of poly(vinyl pyrrolidone) and poly(acrylic acid) prepared by template polymerization.* Journal of Controlled Release, 2002. **81**(3): p. 327-334.

87. Ding, B., et al., *Layer-by-layer structured films of TiO2 nanoparticles and poly(acrylic acid) on electrospun nanofibres.* Nanotechnology, 2004. **15**(8): p. 913-917.

88. Leaist, D.G., *Coupled Diffusion of Weakly Ionized Poly-Electrolytes - Polyacrylic Acids in Water.* Journal of Solution Chemistry, 1989. **18**(5): p. 421-435.

89. Tam, T.K., et al., *Polymer brush-modified electrode with switchable and tunable redox activity for bioelectronic applications.* Journal of Physical Chemistry C, 2008. **112**(22): p. 8438-8445.

90. Gil, E.S. and S.M. Hudson, *Stimuli-reponsive polymers and their bioconjugates.* Progress in Polymer Science, 2004. **29**(12): p. 1173-1222.

91. Zhou, J., et al., *Reversible Immobilization and Direct Electron Transfer of Cytochrome c on a pH-Sensitive Polymer Interface.* Chemistry – A European Journal, 2007. **13**(10): p. 2847-2853.

92. Czeslik, C., O. Hollmann, and T. Gutberlet, *Structure and protein binding capacity of a planar PAA brush.* Langmuir, 2007. **23**(3): p. 1347-1353.

93. Qin, W.S., et al., *Cellulase activities in biomass conversion: measurement methods and comparison.* Critical Reviews in Biotechnology, 2010. **30**(4): p. 302-309.

94. Parnell, A.J., et al., *Synthesis, characterization and swelling behaviour of poly(methacrylic acid) brushes synthesized using atom transfer radical polymerization.* Polymer, 2009. **50**(4): p. 1005-1014.

95. Chibowski, S., M. WiÅ“niewska, and E. Opala Mazur, *The effect of temperature on the adsorption and conformation of polyacrylic acid macromolecules at the ZrO2â€“polymer solution interface.* Powder Technology, 2004. **141**(1â€“2): p. 12-19.

96. WiÅ›niewska, M., S. Chibowski, and T. Urban, *Adsorption and thermodynamic properties of the aluminaâ€“polyacrylic acid solution system.* Journal of Colloid and Interface Science, 2009. **334**(2): p. 146-152.

97. Lee, Y.M., S.H. Kim, and C.S. Cho, *Synthesis and swelling characteristics of pH and thermoresponsive interpenetrating polymer network hydrogel composed of poly(vinyl alcohol) and poly(acrylic acid).* Journal of Applied Polymer Science, 1996. **62**(2): p. 301-311.

Chapter 4: Conductive oxygen barrier films using supramolecular assembly of graphene embedded polyelectrolyte multilayers

(This chapter is reproduced with permission from Journal of colloid and interface science, 409(2013), 219-226.)

4.0 Abstract

In this work, we show the development of synergistic graphene embedded polyelectrolyte multilayer assembly. Three types of films were developed by exploiting the change in the macromolecular structure of two polyelectrolytes namely branched polyethylenimine and polyacrylic acid as a result of pH triggered dissociation. The films differ in thickness and morphology and clear evidence of these differences are presented here. We also examined the effect of these films on two properties namely oxygen permeability and sheet resistance. Depending on the fabrication conditions, these films can provide an impressive three orders of magnitude improvement in oxygen barrier property and close to five orders of magnitude reduction in sheet resistance.

4.1 Introduction

In recent years there is a growing trend towards using flexible plastic as packaging material due to its low cost, easy formability, light weight and reasonably good durability. Glass has been traditionally used in the food packaging industry and fabrication of display panels on account of its transparency, heat tolerance and gas shielding capability[1]. However today, flexible plastics are making rapid inroads in replacing glass in most of these applications. In order to truly compete as an alternative packaging material, flexible plastic needs to fulfill an important requirement of preserving the product from environmental degradation. Dust, oxidation and moisture are principal forces in nature that can have a deleterious effect on

perishable food products and sensitive electronic components[2]. Unfortunately, flexible plastics despite their numerous advantages suffer from poor gas barrier properties[3]. Efforts have been directed to overcome this problem by depositing inorganic coatings and thin films of polymer blends to improve the gas shielding capability. Among the inorganic materials, aluminum and silicon oxide coatings are excellent candidates to limit the permeation of gas molecules. However, inorganic coatings especially pure SiO_2 thin films require high temperature for effective deposition[4]. Most flexible plastics have low glass transition temperatures (T_g) imposing a limitation on the use of inorganic coatings.

Flexible plastics are positioned to make key contributions to the electronics industry in the near future. Devices such as organic light emitting diodes (OLED) expected to corner a 40% share of the mobile phone display market by 2015 present exciting growth prospects for the plastics industry[5]. With the world rapidly moving towards miniaturization, researchers have sought to make electronic components more compact by designing new prototypes that promote improved electrical conductivity and gas barrier properties. This would be particularly useful in the fabrication of certain semiconductor materials such as the dielectric constant oxides that are frequently used in the construction of large capacitors. These devices are liable to fail in the presence of non-conducting oxide coatings[6, 7]. Other devices with similar conductive gas barrier requirements include solar cells grown on flexible supports and flat panel displays[8-10]. Silicon oxide though available ubiquitously, acts as an electrical insulator[11]. So it cannot be directly applied for the above applications. In recent years, there has been a growing interest in the use of nanomaterials to supplement the gas barrier properties of thin polymer films. A number of theoretical models have been used to examine the critical role played by the aspect ratio of nano/colloidal materials dispersed in polymer matrix in improving the gas barrier

properties[12-14]. Upon encountering a nanofiller, gas molecules are forced to adopt a tortuous pathway producing a significant lag in the transmission. Therefore, high aspect ratio nanomaterials such as clay platelets[15-17], mica sheets[18, 19], cellulose[20, 21] and graphene oxide[22] have been used to build gas resistant thin films. Inspite of their high gas/moisture barrier properties, these nanomaterials provide little advantage in the preparation of conductive films. On the other hand, graphene with its sp^2 hybridized 2D structure has unique physical and electronic properties[23]. Thin graphene layers are impermeable to most gases and could serve as excellent nanofillers in the polymer matrix[24]. High charge mobility and ballistic transport at room temperature endow graphene with superior electrical conductivity making it a promising candidate for applications such as electrochemical sensing, field effect transistors (FET) and supercapacitors[25].

Layer-by-layer (LbL) assembly is a versatile technique that can be used to add multiple functionalities to a host of substrates. The success of the LbL technique lies in its ubiquity and simple operation. The extension of Iler's work[26] to the polyelectrolyte multilayer assembly by Decher and co-workers[27, 28] has given rise to a large number of nanoscopic functional materials. The non-covalent functionalization of nanomaterials using polyelectrolytes followed by sequential assembly is a form of LbL that has successfully demonstrated its utility. A number of interactions such as electrostatic, hydrophobic, hydrogen bonding, are ascribed to the formation of multilayered polyelectrolyte LbL assembly.[29] Multifunctional tailor-made substrates fabricated using this route have found several applications such as in catalysis[30], [31, 32], membrane science[33, 34], biosensors[35-38] and drug delivery[39-42]. Ionic strength and pH of the solution can influence the adsorption process producing films of distinct morphology and properties[43-46].

With an estimated theoretical elastic modulus of single-layered graphene projected to be 1 TPa, and surface conductivity about 50×10^6 S/cm, GNPs enjoy superior mechanical and electrical properties[47]. In recent years, methods such as thermal expansion, dielectric heating and acid intercalation have facilitated exfoliation of graphitic flakes enabling the production of high surface area single layered graphene nanoplatelets[48]. In this study we report the LbL assembly of GNP embedded polyelectrolyte multilayers. Unlike inorganic coatings prepared under high temperature conditions, the GNP/PEM LbL assembly can be processed at room temperature. Similarly, compared to the recently developed fabrication methods for free standing graphite papers[49] and graphene nanoplatelet-high density polyethylene (GNP-HDPE) nanocomposite[50], the LbL process can be accomplished under milder process conditions using lower energy input. The GNP embedded polyelectrolyte films serve two purposes. Firstly, they serve as barriers to gas permeation. Secondly, graphene with its unique electronic configuration is positioned to deliver improved electrical conductance. The combination of gas barrier properties and electrical conductance make these films attractive candidates for applications in the semiconductor and electronics industry. Graphene dispersion in polyelectrolytes followed by its LbL assembly has been a subject of extensive examination[51, 52]. Both strong and weak polyelectrolytes have been utilized for this purpose with varying degrees of success. While strong polyelectrolytes are fairly stable over a wide range of pH, weak polyelectrolytes are known to exhibit a remarkable variation in the charge distribution when subjected to a pH change[53]. This can affect the film thickness, the mechanism of interaction, the adsorption kinetics and the quality of adhesion of the films to the base substrate. Unlike other studies that utilized graphene oxide followed by its reduction[54, 55], our process did not use any oxidation or reduction steps. Instead we chose two weak polyelectrolytes namely branched

polyethylenimine (BPEI) and polyacrylic acid (PAA) for LbL deposition. BPEI is rich in amino pendant groups giving it a cationic character. The abundant availability of primary, secondary and tertiary amino residues provides ample opportunities to use BPEI to complement the anionic carboxylic group rich PAA in a multilayered assembly. Using different process conditions three sets of GNP embedded LbL assemblies were developed. They comprised of hydrogen bonding, electrostatic and composite interactions (combination of hydrogen bonding and electrostatic interactions).

4.2 Experimental Procedures

4.2.1 Materials

Polyacrylic acid (PAA) sodium salt (35 wt% solution in water) and branched polyethylenimine (BPEI) average M_w ~25,000 were purchased from Sigma Aldrich. Poly (ethylene terephthalate) (PET) films (Mylar A: thickness approximately 76.2 μm) produced by Dupont-Teijin were obtained from Tekra (New Berlin, WI). Exfoliated graphene nanoplatelets (GNP) (BET surface area: 300 m^2/gm and size 1μm, and average thickness of 2-4 nm) were purchased from XG Sciences, Lansing, MI. All aqueous solutions were prepared using deionized (DI) water (>18.1 MΩ) supplied by a Barnstead Nanopure Diamond-UV purification unit equipped with a UV source and final 0.2 μm filter. Unless specified otherwise, all procedures were carried out at room temperature.

4.2.2 Layer-by-layer (LbL) assembly of polyelectrolyte modified GNP

For the hydrogen bonded assembly, the concentration of PAA and BPEI was adjusted to 2 mg/ml and 1 mg/ml respectively. GNP platelets were dispersed in BPEI solution (now called BPEI-GNP) using a Fisher Scientific Ultrasonic probe (16 W) by sonicating for 1 hour. GNP-BPEI

solution was stirred overnight before use. The pH of the PAA and BPEI-GNP solution was adjusted to 4.0 and 7.5 respectively. For the deposition of the electrostatic layers, GNP were dispersed in 2 mg/ml BPEI solution using ultrasonication followed by magnetic stirring for at least 8 hours. The excess polyelectrolyte is removed by passing the BPEI modified graphene solution through a 0.22 μm cellulose-acetate membrane-filter systems from Nalgene. The BPEI modified graphene platelets collected on the filter membrane were washed with copious quantity of DI water and subjected to another cycle of filtration. They are finally suspended in DI water and the pH is adjusted to 3.5-3.8. The PAA solution used for electrostatic deposition (concentration: 2mg/ml) was adjusted to a pH of 6.0. For the preparation of composite films, the desired number of hydrogen bonded bilayers was initially deposited. This was followed by the required number of electrostatic layers.

The LbL assembly was carried out using a customized Carl-Zeiss slide-stainer. Before depositing the multilayers, the surface of the polyester films was cleaned using a Harrick plasma cleaner (Harrick Scientific Corporation, Broading Ossining, NY). The films were subjected to air plasma for a period of 15 minutes. Air plasma helps in surface activation by producing hydrophilic moieties on the surface of the films. The immersion time was fixed to 15 minutes followed by a DI water rinse cycle of 2 minutes. After the deposition of each layer, the films were allowed to dry naturally for 5 minutes. After the LbL process was complete, the films were heated in an oven maintained at 65^0C for 2 hours to promote thermal crosslinking.

4.2.3 Multilayers Characterizations

Multilayer films of GNP films on PET surface were characterized using scanning electron microscopy (SEM, JEOL 6610LV). The samples were cross-sectioned to reveal the thickness of the deposited films using a single edged razor blade that was cleaned with ethanol

prior to use. The samples were coated with a thin layer of osmium for enhanced conductivity before SEM measurements. The surface resistance of multilayer films was measured with a Gamry Instruments Femtostat Station with frequency ranging from 1-10000 Hz.

4.2.4 Oxygen Transmission Measurements

Oxygen barrier properties of films were tested in accordance using a MOCON 2/21 ML instrument (Mocon Inc., Minneapolis, MN, USA). The samples were tested at 0% relative humidity (RH) at a temperature of 23^0C.

4.3 Results and Discussion

Hydrophilic polymers with numerous polar groups typically exhibit low specific free volume[56]. The polar groups can undergo hydrogen bonding producing a compact polymer structure that can prevent the permeation of gas molecules. The LbL assembly of BPEI and PAA is a pH driven process. These polymers form interpenetrating hydrogen bonded network when the terminal groups of the polymer chains exist in uncharged state[57]. The presence of impermeable material in the polymer matrix can further add to the gas barrier properties. Materials with high aspect ratio are generally preferred as fillers because of their ability to significantly increase the lag time for gas permeation through the polymer. Commercially available GNPs used in this study were prepared by using a unique non-oxidizing technology that enabled the platelets to retain their sp^2 configuration[58]. With an individual platelet thickness averaging 2 nm, and particle diameter of about 1-2 microns, the graphene nanoplatelets used in this study exhibit a significantly high aspect ratio increasing the chances of providing strong resistance to gas permeation. The elongated sheet-like geometry of graphene combined with high aspect ratio is also expected to achieve low percolation threshold value due to its

ability to form a conducting network as compared to spherical or elliptical fillers[59]. However, the platelets have a tendency of stacking up reducing the effectiveness of using graphene as a high aspect ratio material. However ultrasonication of graphene followed by continuous overnight stirring helps in improved dispersion of the nanoplatelets. The ultrasonication disrupts the stacking of the graphene platelets exposing individual platelets to BPEI functionalization. BPEI adsorbs on the graphene platelets due to hydrophobic interactions[52]. In case of negatively charged substrates, BPEI can assume a flat 'pancake-like' structure as the cationic polymer segments in BPEI compensate the surface charges[60]. However in this case, the interaction between the neutral GNP and BPEI results in an optimized structure with bulky globular BPEI adsorbing on the surface of GNP. The polyelectrolyte modification minimizes graphene-graphene interaction improving the exfoliation of the platelets within the BPEI matrix. In our study we tested three different LbL configurations of graphene embedded polyelectrolyte multilayers. The effect of these configurations on oxygen barrier properties and electrical sheet resistance has been shown in the subsequent sections. Mylar PET film about 76 μm thick was used as a base substrate in all cases.

4.3.1 Types of LbL deposited GnP/PEM films

The schematic diagram shown in Figure 4.1 shows the three types of LbL assembly namely hydrogen bonded, electrostatic and composite films. This section highlights the role played by adsorption conditions to produce GNP/PEM films with specific type of interactions.

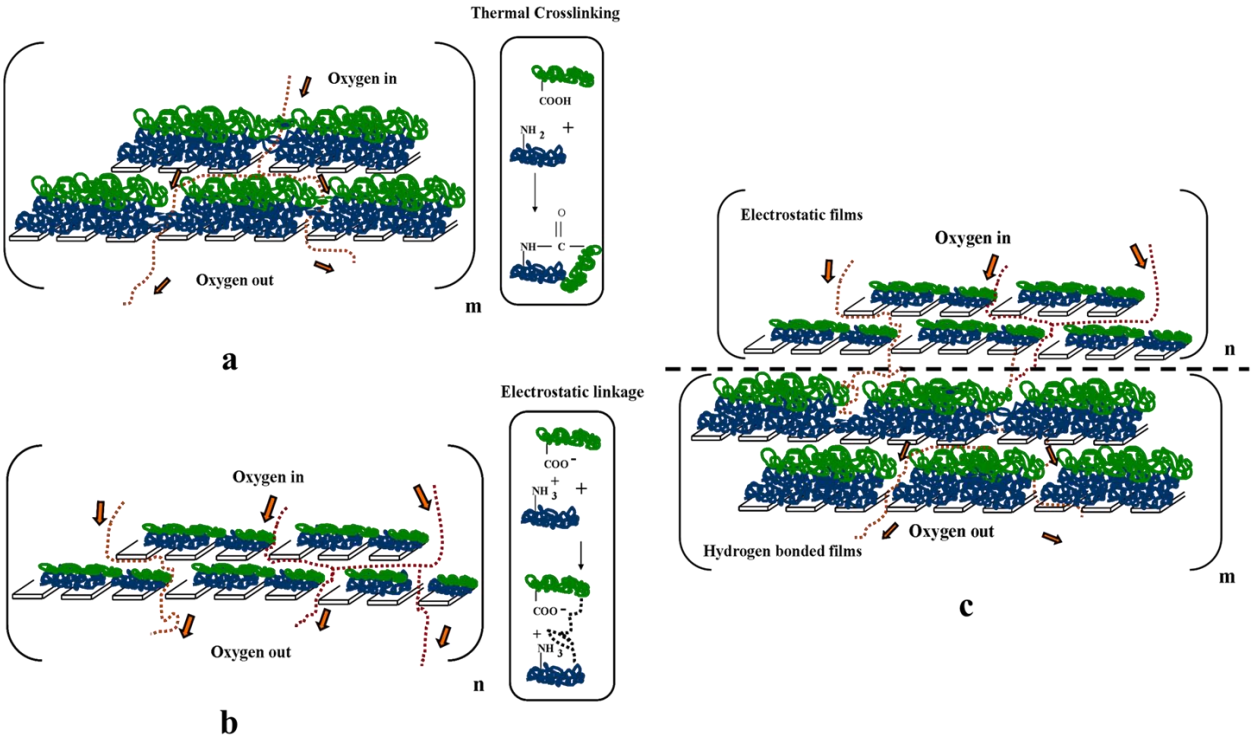

Figure 4.1. Supramolecular assembly of graphene embedded polyelectrolyte multilayers. (a)Multilayers assembled using hydrogen bonded assembly. m denotes number of bilayers deposited. (b) Multilayers deposited using electrostatic interactions. n denotes the number of electrostatic bilayers deposited. (c) Composite film consisting of 'm' number of hydrogen bonded bilayers followed by 'n' number of electrostatic bilayers.

4.3.1.1 Hydrogen bonded films

Figure 4.1a shows a schematic representation of the hydrogen bonded multilayers. *m* indicates the number of bilayers of hydrogen bonded graphene films deposited on the PET substrate. In this configuration, a multilayer assembly of BPEI-GNP and PAA was assembled on PET. The pH of the BPEI-GNP solution was adjusted to 7.5 whereas PAA was adjusted to 4.0. The native pH of BPEI-graphene is between 9.5-10.2. We observed that the BPEI-graphene solution when used in the LbL assembly without pH adjustment resulted in non-uniform coatings. We believe that the large difference between the pH values of BPEI-graphene and PAA solution can induce precipitation of certain charged groups in both the polyelectrolyte solutions leading to poor quality of LbL deposited film. The pK_a value for the primary and secondary amines in BPEI is

approximately 4.5 and 6.7 respectively[61]. At a pH 7.5, most of the amine residues in BPEI should exist in uncharged state. The pK_a value of PAA is close to 4.8[62]. Hence, at a pH 4.0, most of the terminal groups in PAA exist in uncharged state (carboxylic acid groups –COOH) rather than as carboxylate ion $-COO^-$. The presence of neutral terminal groups for both PAA and BPEI results in the deposition of highly coiled, loopy polyelectrolyte network. The interdiffusion of the polyelectrolyte segments followed by thermal crosslinking for 2 hours at 65 ^{0}C gives rise to compact film architecture.

4.3.1.2 Electrostatically assembled films

Another type of LbL configuration was tested by retaining the same polyelectrolytes as before, except for two changes. The schematic representation of the same is shown in Figure 4.1b. *n* denotes the number of electrostatic bilayers deposited. The deposition of BPEI-graphene solution during the LbL process represents a unique situation where both BPEI and polyelectrolyte modified graphene are competing for adsorption on the negatively charged PAA chains. Lu and co-workers[52] addressed this issue by subjecting the polyelectrolyte-graphene solution to vacuum filtration. By filtering the polyelectrolyte-graphene solution through 0.22 µm filter, Lu and co-workers removed the excess unbound polyelectrolyte minimizing the ill-effects of competitive adsorption. The removal of non-conducting polyelectrolyte solution should also help in improved interconnection between individual graphene platelets. To counter the dense nature of the films produced in the earlier configuration, we implemented another change that targeted the interactions between the cationic and anionic components of the LbL assembly. The BPEI functionalized graphene after vacuum filtration was dispersed in DI water and the pH was adjusted to 3.5-3.8. This pH value is lower than the pK_a value of the primary amines in BPEI (usually around 4.5). At this pH condition, the BPEI modified graphene platelets are positively

charged. The BPEI chains that are functionalized on graphene platelets occur in protonated state ($-NH_3^+$). Meanwhile, the pH of PAA solution was adjusted to 6.0. This value is higher than the pK_a value of PAA. Thus at this pH, PAA chains mostly exist in the ionized form. Though ionic crosslinks are possible, the overall LbL assembly is governed by electrostatics.

4.3.1.3 Composite film

The synergistic combination of the above two systems is expected to deliver a result that includes contributions due to both hydrogen bonding and electrostatics, as shown in Figure 4.1c. Using the same pH conditions as described before, a composite film consisting of the desired number of hydrogen bonded layers followed by electrostatic layers were deposited. The composite film is depicted as *m*H+ *n*E where H and E stand for hydrogen bonded and electrostatic films respectively.

4.3.2 Morphology and Thickness of GNP embedded PEM films

The three types of LbL configurations listed above have distinct impact on the morphology and the thickness of the deposited films. Previous research has established that hydrogen bonded and electrostatically assembled PEMs can exhibit differences in morphology such as thickness and surface roughness[63, 64]. Some of the hydrogen bonded multilayers are reported to exhibit an exponential growth pattern[65, 66]. After a certain number of bilayers are deposited these films may show linear increase in thickness[67]. Most electrostatic assemblies grow linearly[68] enabling easy estimation of thickness of individual bilayer. However for exponential or hybrid (exponential+linear) growth regimes, the task is harder and requires more detailed analysis. In our case, the presence of graphene in the multilayer assembly can add complexity to the deposition process and influence the growth of these films. Though

establishing the growth pattern of GNP embedded multilayers is not within the scope of this work, the morphology and thickness information about these films can provide useful insight into understanding the gas barrier and sheet resistance properties.

Figure 4.2 shows SEM micrographs of the three LbL configurations for a 20 bilayer sample. The cross-sectional images (Figures 4.2 a,c,e) give an idea of the thickness of the multilayers whereas Figures 4.2 (b,d,f) establish the surface morphology of these films. For the 20 bilayer sample under consideration, the thickness is highest for the hydrogen bonded assembly (about 5.5 μm). Electrostatic assembly results in thinner film (See Figures 4.2c). With a thickness of around 705 nm, the electrostatic film is substantially thinner than the hydrogen bonded film. The composite film (Figure 4.2e) has a thickness of 3.77 μm (lower than hydrogen bonded film but higher than electrostatically assembled multilayers). The effect of the interactive forces associated with these configurations is evident from Figures 4.2 b,d,f. Figure 4.2b shows surface morphology of 20 bilayer hydrogen bonded assembly. The surface is relatively smooth and free of graphene agglomerations. On the other hand, Figure 4.2d shows the agglomerations of GNPs as a result of the electrostatic assembly. We suspect that the formation of aggregates is due to poor adhesion of BPEI functionalized graphene on the PET substrate. Hydrogen bonded films generally have good adhesive properties due to the presence of polar groups. A lower share of hydrogen bonding interactions in case of electrostatic films can reduce

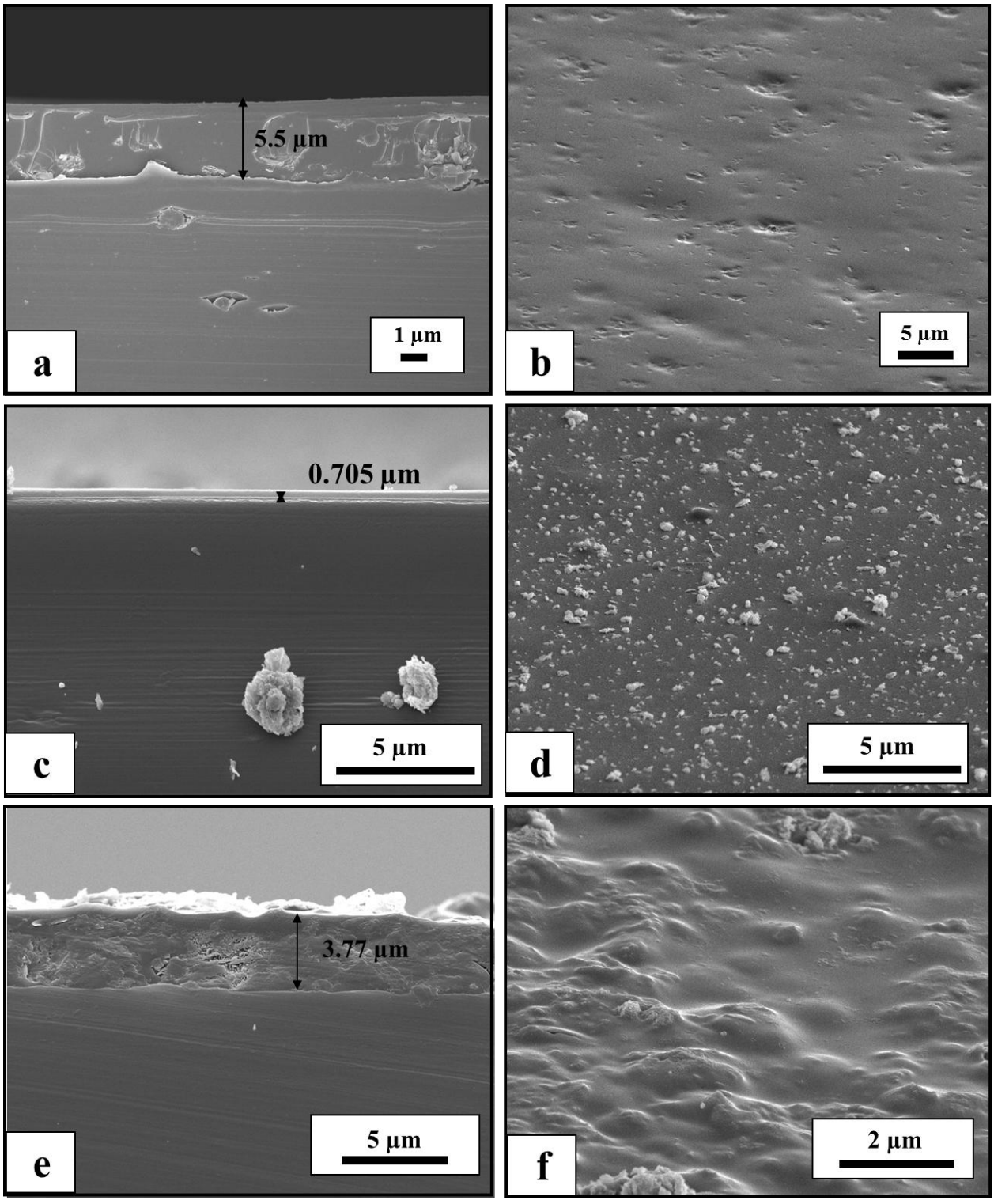

Figure 4.2 SEM micrographs of 20 bilayer GNP embedded PEM assembly. a, c, e show sectional view of hydrogen bonded, electrostatic and composite (10H + 10E) multilayers respectively. Thickness of the coating is 5.5 µm, 0.705 µm, 3.77 µm respectively. b, d, f show surface morphology of hydrogen bonded, electrostatic and composite films respectively.

the adhesive capacity of the multilayers to hold the GNPs together. Figure 2f shows the surface morphology of a composite film. As expected, the surface morphology is a synergistic combination of the two assemblies shown previously. The surface has a certain texture resembling the hydrogen bonded films along with some degree of graphene agglomeration associated with electrostatic films. The adhesion provided by the underlying hydrogen bonded films facilitates good surface coverage by the electrostatic films. The improved interconnection between individual GNPs in the electrostatic layers promotes reduction in sheet resistance. The other cases (4, 10, 15 and 30 bilayers samples) show similar thickness trend (See Figures. 4.3,4.4,4.5)

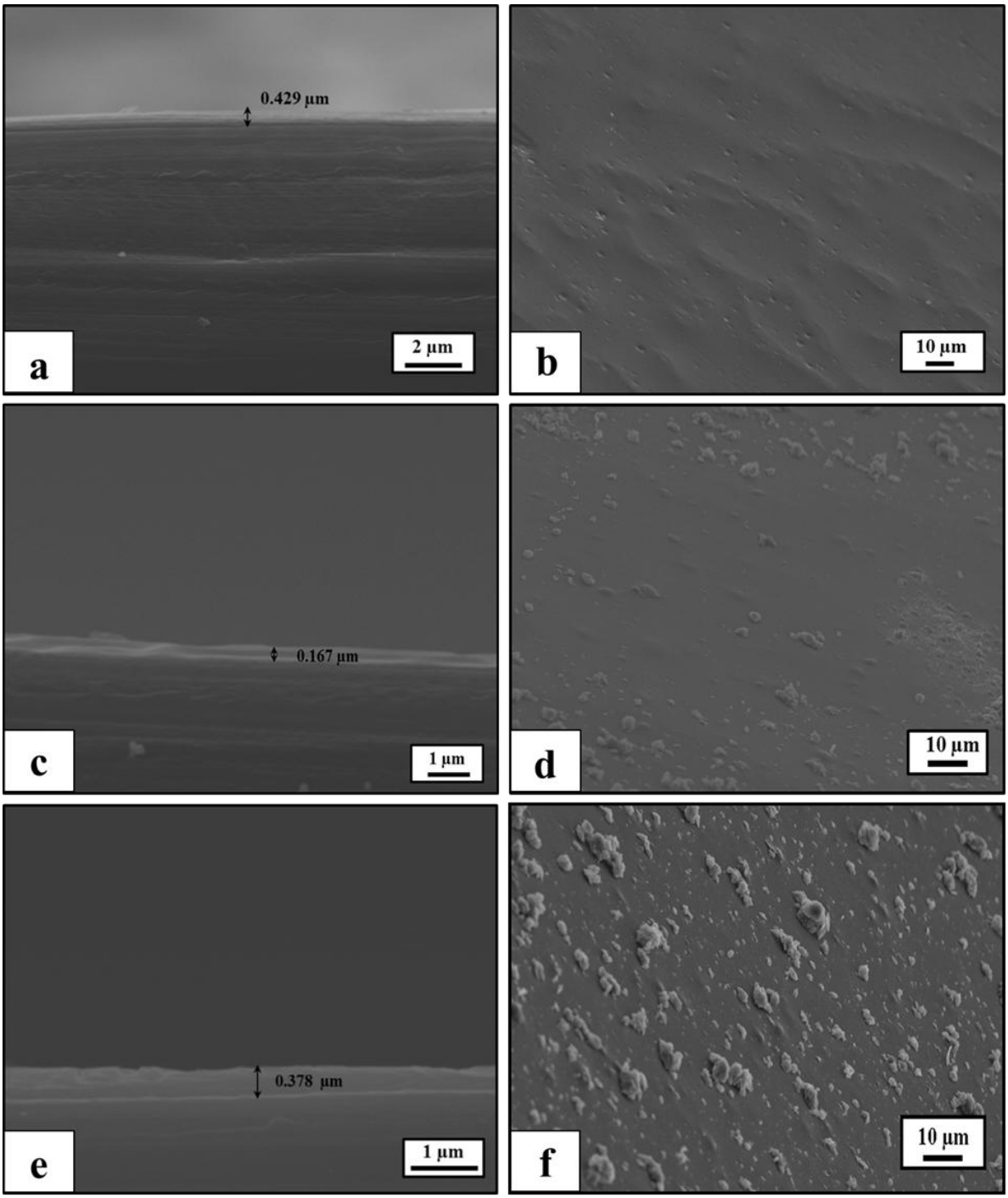

Figure 4.3 SEM micrographs of 4 bilayer GNP embedded PEM assembly. a, c, e show sectional view of hydrogen bonded, electrostatic and composite (2H + 2E) multilayers respectively. Thickness of the coating is 0.429 µm, 0.167 µm, 0.378 µm respectively. b, d, f show surface morphology of hydrogen bonded, electrostatic and composite films respectively.

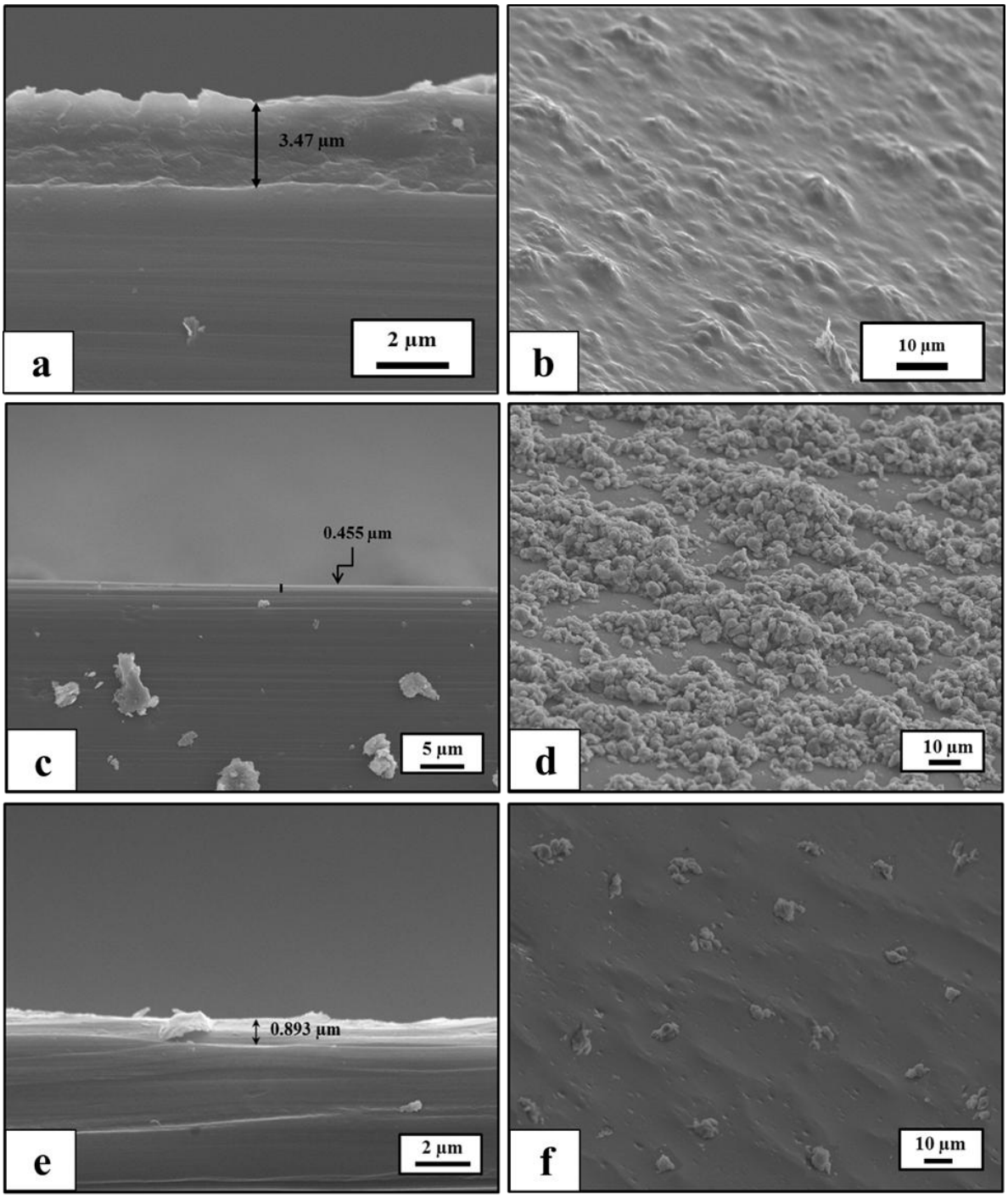

Figure 4.4 SEM micrographs of 10 bilayer GNP embedded PEM assembly. a, c, e show sectional view of hydrogen bonded, electrostatic and composite (5H + 5E) multilayers respectively. Thickness of the coating is 3.47 µm, 0.455 µm, 0.893 µm respectively. b, d, f show surface morphology of hydrogen bonded, electrostatic and composite films respectively.

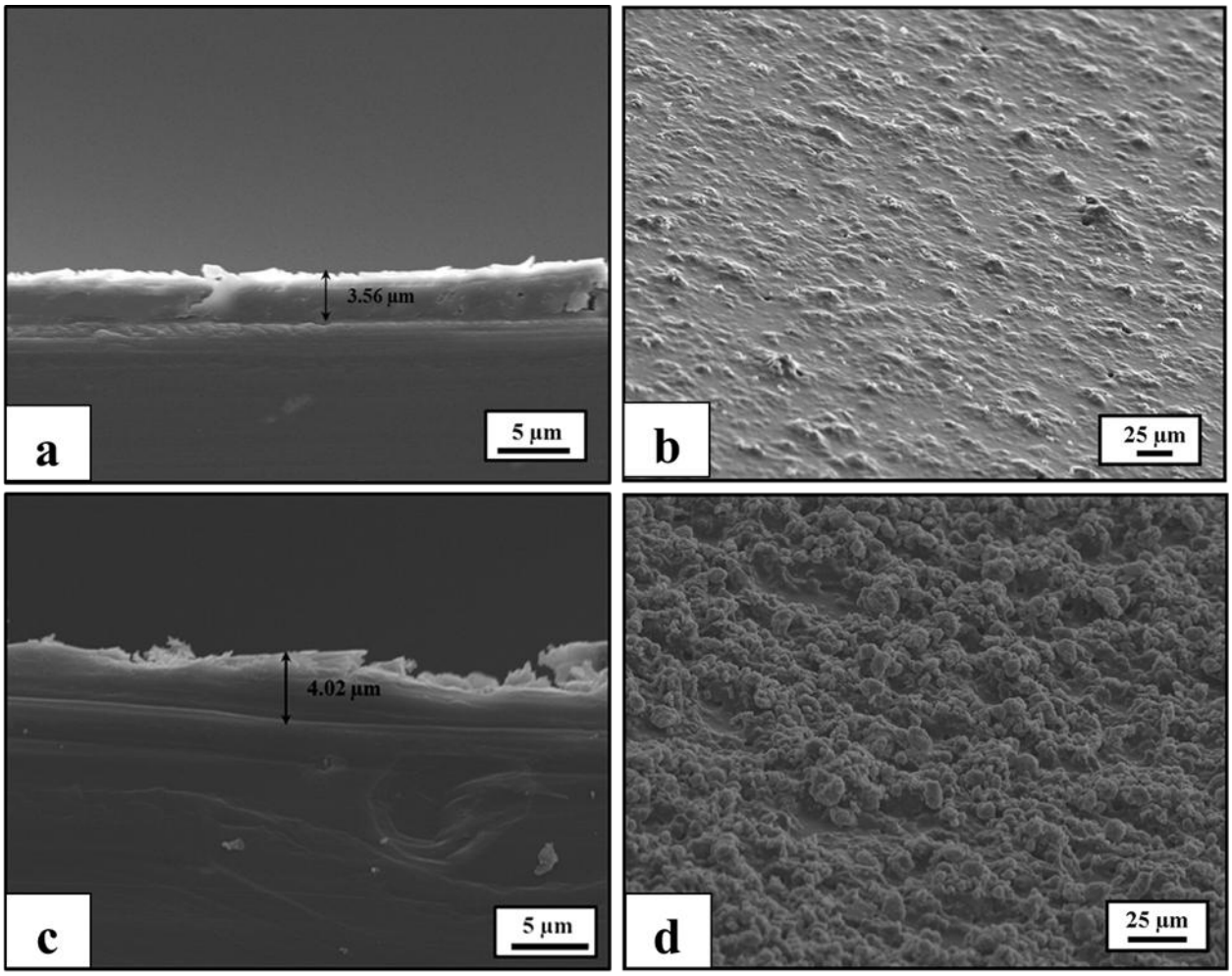

Figure 4.5 SEM micrographs of composite films with fixed number of hydrogen bonded multilayers (10 bilayers) and variable number of electrostatic layers a and c show sectional view of composite films with (10H + 5E) and 10H +20 E) multilayers respectively. Thickness of the coating is 3.56µm and 4.02 µm respectively. b and d show surface morphology of the composite films (10H +5E) and (10H + 20E) respectively.

4.3.3 Oxygen barrier properties of GNP/PEM multilayers

Figures 4.6 a-d help us compare the effect of hydrogen bonding, electrostatic and composite interactions on the barrier properties of PET films. A bare PET film has an oxygen transmission rate (OTR) of 30.3 cc O_2/m^2.day atm. Deposition of just 4 bilayers of hydrogen bonded BPEI-graphene/PAA reduces the OTR by 90.07% (Figure 4.6a). Measurements were also done after depositing 10 and 20 bilayers (See Figures 4.6b and 4.6c). The OTR decreases as the number of bilayers increase. A 20 bilayer film (Fig. 4.6c) shows an impressive 98.6% reduction in the OTR value. The electrostatically assembled GNP/PEM films present a completely different result. Lack of hydrogen bonding can cause little or no significant reduction in the specific free volume greatly diminishing the ability of the graphene embedded film to function as effective oxygen barrier. A 20 bilayer electrostatic film exhibits a mere 14% reduction in OTR (Figure 4.6c). Compared to electrostatic films, composite films display improved gas barrier properties (Figures 4 a-d). These films show a decreasing trend in OTR as the number of bilayers increased. When the deposition of hydrogen bonded layers reached 10, the OTR reduced by 98%. Increasing the number of electrostatic layers alone on hydrogen bonded films has little effect on the OTR values. This can be inferred from Figure 4.6d where increasing the number of electrostatic layers (from 5 to 20) on fixed number of hydrogen bonded films results in a very small decrease in the OTR.

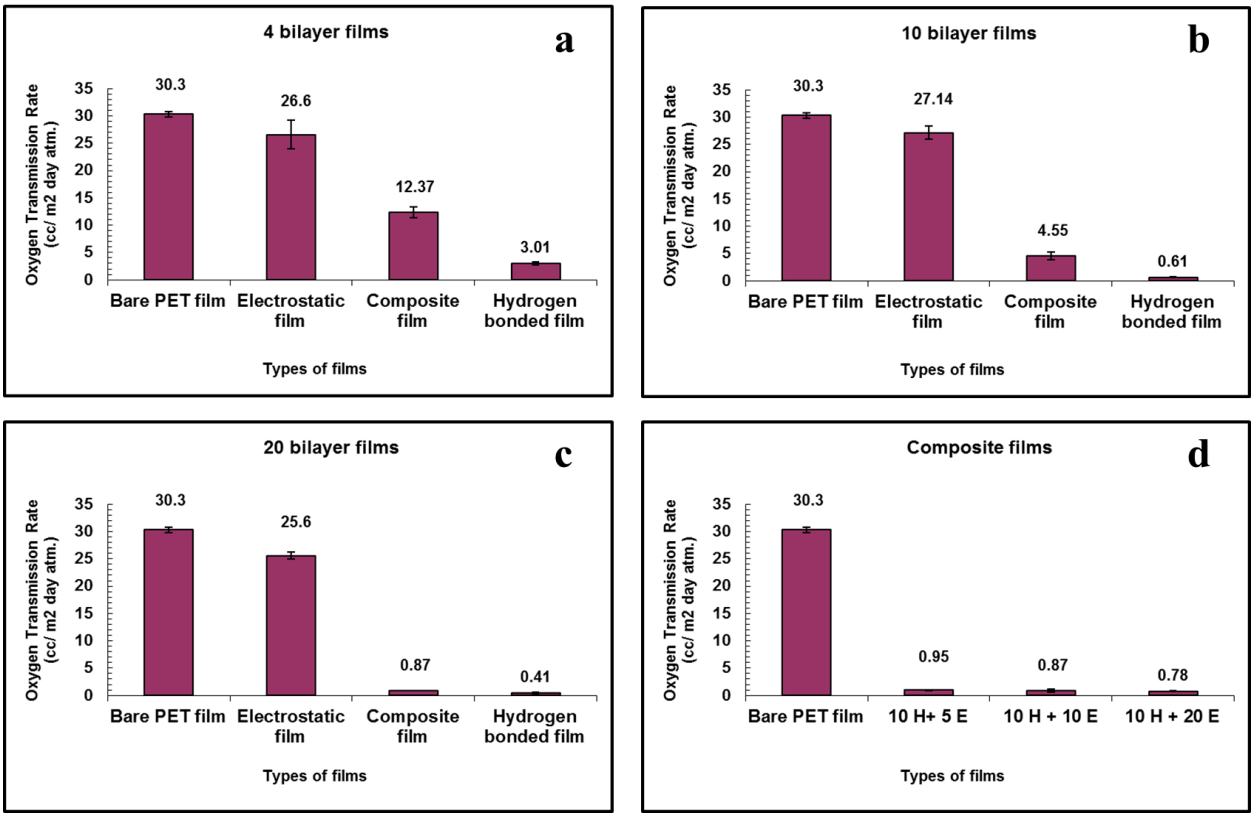

Figure 4.6 Oxygen transmission rate (OTR) for different types of configurations. (a) 4 bilayer system. The composite film consists of 2 hydrogen bonded and 2 electrostatic bilayers. (b) 10 bilayer system. Composite film consists of 5 hydrogen bonded and 5 electrostatic bilayers. (c) 20 bilayer system. Composite film consists of 10 hydrogen bonded and 10 electrostatic bilayers. (d) Composite films consisting of 10 hydrogen bonded (H) followed by varying number of electrostatic (E) bilayers.

Table 4.1 Oxygen permeability coefficient of hydrogen bonded films on PET substrate at STP conditions

Number of bilayers	**Thickness of the coating µm**	**Permeability coefficient (10^{-18} cc. cm/cm^2.s.Pa)**	
		Film (P_f)	Total (P_t)
4 bilayers	0.439	3.02	244.5
10 bilayers	3.47	4.55	53.45
20 bilayers	5.5	4.82	37.68

Table 4.2 Oxygen permeability coefficient of electrostatic films on PET substrate at STP conditions

Number of bilayers	**Thickness of the coating µm**	**Permeability coefficient (10^{-18} cc. cm/cm^2.s.Pa)**	
		Film (P_f)	Total (P_t)
4 bilayers	0.167	76.7	2146
10 bilayers	0.455	25.2	2205
20 bilayers	0.705	24.2	2094

Table 4.3. Oxygen permeability coefficient of composite films on PET substrate at STP conditions

Number of bilayers	**Thickness of the coating µm**	**Permeability coefficient (10^{-18} cc. cm/cm^2.s.Pa)**	
		Film (P_f)	Total (P_t)
4 bilayers	0.379	16.6	1003.4
10 bilayers	0.893	10.1	374.03
20 bilayers	3.77	7.12	76.79

Table 4.4. Oxygen permeability coefficient of composite films (variable electrostatic layers) on PET substrate at STP conditions

Number of bilayers	**Thickness of the coating µm**	**Permeability coefficient (10^{-18} cc. cm/cm^2.s.Pa)**	
		Film (P_f)	Total (P_t)
10 H+ 5E	3.56	7.36	83.43
10 H+ 10E	3.77	7.12	76.70
10H + 20E	4.02	6.78	69.26

The SEM data from the previous section also provides critical information about film thickness that can be used for the estimation of the oxygen permeability coefficient. Unlike the OTR, the permeability coefficient takes into account the contribution of the thickness of the film and can provide useful information to compare different systems. For the calculation of film permeability coefficient, its contribution to the total permeability coefficient (inclusive of both the film as well as the PET substrate) was decoupled using a method described elsewhere[69]. Tables 4.1-4.4 show oxygen permeability coefficients for different LbL configurations at STP conditions. With thickness ranging from nanometers to few microns, the GNP/PEM films

developed in this study show superior oxygen barrier properties compared to a 76.2 µm thick PET film. The graphene embedded PEM films show low permeability coefficients almost three orders of magnitude lower than the uncoated PET substrate (2433×10^{-18} cc.cm/cm^2.s.Pa). Since hydrogen bonded systems display the best oxygen barrier properties, a 20 bilayer hydrogen bonded BPEI/PAA system (without GNP) was assembled under the same pH conditions and its permeability coefficient was estimated to be 3.05×10^{-18} cc.cm/cm^2.s.Pa . However, the same result can be achieved by using just 4 bilayers of hydrogen bonded GNP/PEM multilayers assembled under similar deposition conditions. Among polymers, ethylene vinyl alcohol (EVOH) finds great application in the packaging industry on account of its low oxygen permeability. EVOH films with ethylene concentration ranging from 25-45 mol% are reported to exhibit enhanced gas barrier properties[70]. However, the GNP embedded hydrogen bonded and composite PEM films developed in this study have oxygen permeability coefficients that are at least 10 times lower than the permeability coefficient of a 15 µm thick EVOH film containing 44 mol% ethylene and about 1.4-3 times lower than the similarly sized EVOH film with 32 mol% ethylene[70]. The GNP/PEM films also show vastly superior oxygen barrier properties as compared to other graphene based nanocomposites reported in literature[49, 71]. With permeability coefficient in the range of 10^{-18} cc.cm/cm^2.s.Pa, these coatings (hydrogen bonded and composite films) are comparable to SiO_2 thin films deposited on commercial gas barrier foils using plasma enhanced chemical vapor deposition (PECVD) technique[72]. Some important observations can be made from the data presented in Tables 4.1-4.4. Table 4.1 shows the effect of increasing number of hydrogen bonded GNP multilayers on oxygen permeability. While the total permeability coefficient (P_t) continues to register a drop, the permeability coefficient of the deposited film (P_f) increases slightly. This could be because the increase in the thickness of the

coating negates the corresponding small drop in OTR. The data shown in Table 4.2 reinforces the poor barrier properties of electrostatic films. With increase in the number of bilayers, the data shows no clear trend partly because of poor adhesion of the GNP multilayers in absence of uncharged polar groups. Table 4.3 shows a healthy decrease in P_f and P_t. The increasing number of hydrogen bonded multilayers facilitates a decrease in the permeability coefficient. Table 4.4 shows the effect of increasing number of electrostatic films deposited on fixed number of hydrogen bonded films. Both P_t and P_f do not register a significant decrease which is consistent with our hypothesis that electrostatic films do not contribute to barrier properties.

4.3.4 Electrical resistance of the GNP/PEM multilayers

The electrical sheet resistance was also tested as a function of the number of bilayers. As seen from Figure 4.7a, at 1 Hz, the electrical sheet resistance of the bare PET film is about 111.1 GΩ. The high value of resistance indicates that the film is highly resistive. The deposition of hydrogen bonded BPEI-graphene/PAA films reduces the resistance. The PET substrate shows a successive reduction in the resistance value for 4, 10 and 20 bilayers. For 20 bilayers, the value reduces to about 142 GΩ. Though there is a substantial reduction in the electrical resistance of the PET film, the values still end up in GΩ. We suspect that the high values of sheet resistance are a result of the dense network of hydrogen bonded polyelectrolytes surrounding the graphene platelets. The polymer wrapping of GNPs is known to reduce their conductivity.

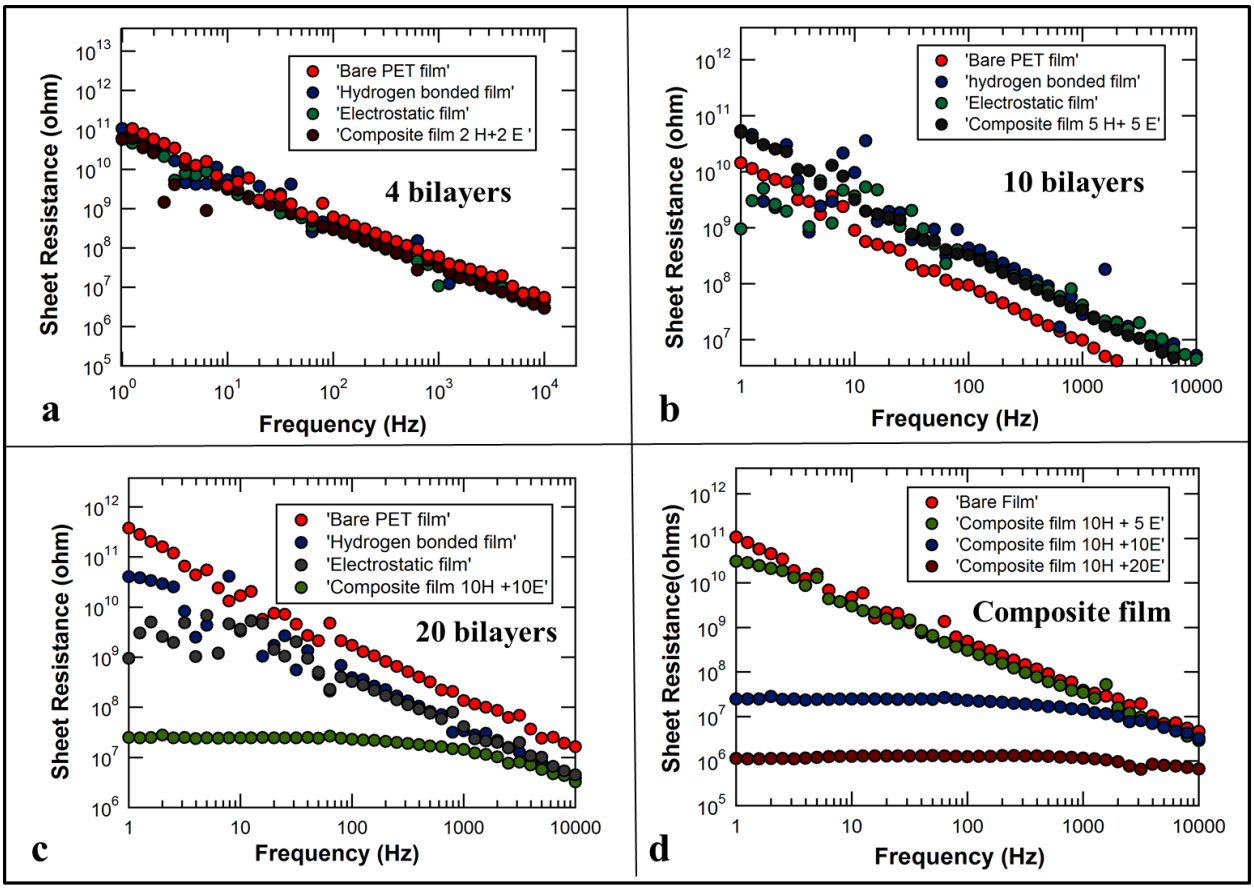

Figure 4.7. Sheet resistance for different configurations of LbL assembled graphene embedded multilayers. Sheet resistance at 1 Hz for various samples is as follows:
(a) Bare PET film: 111.1 GΩ, hydrogen bonded film: 108.2 GΩ, electrostatic film: 61.3 GΩ, composite film: 57.6 GΩ.
(b) Bare PET film: 115.2 GΩ, hydrogen bonded film: 90.9 GΩ, electrostatic film: 54.3 GΩ , composite film: 50.2 GΩ.
(c) Bare PET film: 110.2 GΩ, hydrogen bonded film: 40.8 GΩ, electrostatic film: 0.949 GΩ, composite film: 24.8 MΩ.
(d) Bare PET film: 112.3 GΩ, composite film (10H + 5 E): 31.2 GΩ, (10H + 10 E): 24.8 MΩ, (10H+20 E): 1.14 MΩ

Further, the loopy, coiled conformation of the polyelectrolytes prevents the interconnection between the individual graphene units limiting the electrical conductance of the film. As inferred from the SEM images, unlike the dense hydrogen bonded films, electrostatically assembled BPEI modified graphene/PAA films are substantially thinner. The combined effect of elimination of excess polyelectrolyte and thin film structure promotes further

reduction in the electrical sheet resistance. As seen from Fig. 4.7c, a 20 bilayer electrostatic film exhibits a sheet resistance of 0.95 GΩ. However, we suspect that further reduction in electrical resistance is hard to achieve due to poor adhesion of the multilayers to the substrate PET film. For the composite films, the electrical resistance drops further. Figure 7d shows substantial reduction in the sheet resistance as the number of electrostatic layers is increased. The sheet resistance for a composite film consisting of 10 hydrogen bonded bilayers followed by 20 electrostatic bilayers drops to about 1.14 MΩ (Figure 4.7d). This represents a five orders of magnitude reduction in sheet resistance. We believe that the composite film shows improved performance due to the synergistic effect of hydrogen bonded and electrostatic multilayers. Hydrogen bonded films have good adhesive properties due to presence of polar groups. The presence of hydrogen bonded films provides the adhesion to the electrostatic layers.

4.4 Conclusion

In summary, we showed the effect of three configuration types of graphene embedded polyelectrolyte systems. Hydrogen bonded graphene films showed good oxygen barrier property. Electrostatic films given their thin morphology and absence of excessive non-conducting polyelectrolyte exhibit lower sheet resistance. A composite film comprising of graphene embedded hydrogen bonded and electrostatic coatings satisfied both these requirements. The composite film showed oxygen permeability coefficient that is comparable to SiO_2 coatings with electrical sheet resistance five orders of magnitude lower than the base substrate. Besides the configurations described here, there is certainly more scope for improvement especially with respect to the electrostatic layers. The deposition process for the electrostatic layers comprising of BPEI modified graphene/PAA multilayers needs to be monitored for precipitation of charged groups. Being a pH sensitive system makes the solutions prone to sedimentation. This problem

can be overcome by sonicating the BPEI modified graphene frequently (every 2 hours) and adjusting the pH of the solutions in case of change. A more robust reproducible design can be obtained by casting films made from polystyrene sulfonate (PSS) functionalized graphene and a conjugate polycation such as poly(diallydimethylammonium chloride) (PDAC) which are less sensitive to pH changes. These modifications may entail making suitable changes in the hydrogen bonded layers. Another parameter that significantly alters the morphology and potentially the conductivity of the coatings is the annealing temperature. The glass transition temperature (T_g) of PET is reported to be about 70^0C[73]. This has restricted the annealing temperature in our experiments to 65^0C. Higher temperatures generally contribute to increased crosslinking (improves gas barrier properties) and evaporation of moisture from the multilayers (facilitates improved conductivity). Using a polymer substrate with increased temperature tolerance can help achieve these objectives.

REFERENCES

REFERENCES

1. Ebina, T. and F. Mizukami, *Flexible transparent clay films with heat-resistant and high gas-barrier properties.* Advanced Materials, 2007. **19**(18): p. 2450-+.

2. Charton, C., et al., *Development of high barrier films on flexible polymer substrates.* Thin Solid Films, 2006. **502**(1-2): p. 99-103.

3. Shirakura, A., et al., *Diamond-like carbon films for PET bottles and medical applications.* Thin Solid Films, 2006. **494**(1-2): p. 84-91.

4. Teshima, K., et al., *Gas barrier properties of silicon oxide films prepared by plasma-enhanced CVD using tetramethoxysilane.* Vacuum, 2002. **66**(3-4): p. 353-357.

5. Laaperi, A., *Disruptive factors in the OLED business ecosystem.* Information Display, 2009. **9**(09): p. 09.

6. Grill, A., et al., *Base Electrodes for High Dielectric-Constant Oxide Materials in Silicon Technology.* Journal of Materials Research, 1992. **7**(12): p. 3260-3265.

7. Grill, A., C. Jahnes, and C. Cabral, *Layered TaSiN as an oxidation resistant electrically conductive barrier.* Journal of Materials Research, 1999. **14**(4): p. 1604-1609.

8. Dennler, G., et al., *Flexible, conjugated polymer-fullerene-based bulk-heterojunction solar cells: Basics, encapsulation, and integration.* Journal of Materials Research, 2005. **20**(12): p. 3224-3233.

9. Jorgensen, M., K. Norrman, and F.C. Krebs, *Stability/degradation of polymer solar cells.* Solar Energy Materials and Solar Cells, 2008. **92**(7): p. 686-714.

10. Chou, C.-T., et al., *Transparent Conductive Gas-Permeation Barriers on Plastics by Atomic Layer Deposition.* Advanced Materials, 2013. **25**(12): p. 1750-1754.

11. Inagaki, N., S. Tasaka, and M. Makino, *Plasma polymer deposition from mixture of tetramethoxysilane and oxygen on PET films and their oxygen gas barrier properties.* Journal of Applied Polymer Science, 1997. **64**(6): p. 1031-1039.

12. Lape, N.K., E.E. Nuxoll, and E.L. Cussler, *Polydisperse flakes in barrier films.* Journal of Membrane Science, 2004. **236**(1): p. 29-37.

13. DeRocher, J.P., et al., *Barrier membranes with different sizes of aligned flakes.* Journal of Membrane Science, 2005. **254**(1-2): p. 21-30.

14. Nielsen, L.E., *Models for the permeability of filled polymer systems.* Journal of Macromolecular Science-Chemistry, 1967. **1**(5): p. 929-942.

15. Gain, O., et al., *Gas barrier properties of poly(ε-caprolactone)/clay nanocomposites: Influence of the morphology and polymer/clay interactions.* Journal of Polymer Science Part B: Polymer Physics, 2005. **43**(2): p. 205-214.

16. Priolo, M.A., et al., *Super Gas Barrier of Transparent Polymer-Clay Multilayer Ultrathin Films.* Nano Letters, 2010. **10**(12): p. 4970-4974.

17. Grunlan, J.C., et al., *Effect of clay concentration on the oxygen permeability and optical properties of a modified poly(vinyl alcohol).* Journal of Applied Polymer Science, 2004. **93**(3): p. 1102-1109.

18. Alves, V.D., N. Costa, and I.M. Coelhoso, *Barrier properties of biodegradable composite films based on kappa-carrageenan/pectin blends and mica flakes.* Carbohydrate Polymers, 2010. **79**(2): p. 269-276.

19. Sanchez-Garcia, M.D., L. Hilliou, and J.M. Lagaron, *Nanobiocomposites of Carrageenan, Zein, and Mica of Interest in Food Packaging and Coating Applications.* Journal of Agricultural and Food Chemistry, 2010. **58**(11): p. 6884-6894.

20. Yang, Q., et al., *Transparent cellulose films with high gas barrier properties fabricated from aqueous alkali/urea solutions.* Biomacromolecules, 2011. **12**(7): p. 2766-2771.

21. Aulin, C., M. Gallstedt, and T. Lindstrom, *Oxygen and oil barrier properties of microfibrillated cellulose films and coatings.* Cellulose, 2010. **17**(3): p. 559-574.

22. Huang, H.-D., et al., *High barrier graphene oxide nanosheet/poly(vinyl alcohol) nanocomposite films.* Journal of Membrane Science, 2012. **409-410**(0): p. 156-163.

23. Gokhale, A.A., J. Lu, and I. Lee, *Immobilization of cellulase on magnetoresponsive graphene nano-supports.* Journal of Molecular Catalysis B: Enzymatic, 2013. **90**(0): p. 76-86.

24. Kim, H., Y. Miura, and C.W. Macosko, *Graphene/Polyurethane Nanocomposites for Improved Gas Barrier and Electrical Conductivity*. Chemistry of Materials, 2010. **22**(11): p. 3441-3450.

25. Geim, A.K., *Graphene: Status and Prospects.* Science, 2009. **324**(5934): p. 1530-1534.

26. Iler, R.K., *Multilayers of Colloidal Particles.* Journal of Colloid and Interface Science, 1966. **21**(6): p. 569-&.

27. Decher, G. and J.D. Hong, *Buildup of Ultrathin Multilayer Films by a Self-Assembly Process .1. Consecutive Adsorption of Anionic and Cationic Bipolar Amphiphiles on*

Charged Surfaces. Makromolekulare Chemie-Macromolecular Symposia, 1991. **46**: p. 321-327.

28. Decher, G. and J.D. Hong, *Buildup of Ultrathin Multilayer Films by a Self-Assembly Process .2. Consecutive Adsorption of Anionic and Cationic Bipolar Amphiphiles and Polyelectrolytes on Charged Surfaces.* Berichte Der Bunsen-Gesellschaft-Physical Chemistry Chemical Physics, 1991. **95**(11): p. 1430-1434.

29. Lee, I., *Molecular Self-Assembly: Smart Design of Surface and Interface via Secondary Molecular Interactions.* Langmuir, 2013. **29**(8): p. 2476-2489.

30. Hendricks, T.R., et al., *Effects of catalyst introduction methods using PAMAM dendrimers on selective electroless nickel deposition on polyelectrolyte multilayers.* Langmuir, 2007. **23**(13): p. 7404-7410.

31. Yu, A.M., et al., *Mesoporous silica particles as templates for preparing enzyme-loaded biocompatible microcapsules.* Advanced Materials, 2005. **17**(14): p. 1737-+.

32. Lvov, Y. and F. Caruso, *Biocolloids with ordered urease multilayer shells as enzymatic reactors.* Analytical Chemistry, 2001. **73**(17): p. 4212-4217.

33. Shan, W.Q., et al., *Polyelectrolyte multilayer films as backflushable nanofiltration membranes with tunable hydrophilicity and surface charge.* Journal of Membrane Science, 2010. **349**(1-2): p. 268-278.

34. Dotzauer, D.M., et al., *Catalytic membranes prepared using layer-by-layer adsorption of polyelectrolyte/metal nanoparticle films in porous supports.* Nano Letters, 2006. **6**(10): p. 2268-2272.

35. Hassler, B.L., et al., *Renewable dehydrogenase-based interfaces for bioelectronic applications.* Langmuir, 2007. **23**(13): p. 7127-7133.

36. Devesh, S., et al., *Neuropathy Target Esterase Biosensor in* , 2010: INTECH: Intelligent and Biosensors edited by Vernon S. Somerset. 386.

37. Lu, J., et al., *Simple fabrication of a highly sensitive glucose biosensor using enzymes immobilized in exfoliated graphite nanoplatelets Nafion membrane.* Chemistry of Materials, 2007. **19**(25): p. 6240-6246.

38. Lu, J., et al., *Nanometal-decorated exfoliated graphite nanoplatelet based glucose biosensors with high sensitivity and fast response.* Acs Nano, 2008. **2**(9): p. 1825-1832.

39. Sambanthamoorthy, K., et al., *Identification of a Novel Benzimidazole That Inhibits Bacterial Biofilm Formation in a Broad-Spectrum Manner.* Antimicrobial Agents and Chemotherapy, 2011. **55**(9): p. 4369-4378.

40. Mehrotra, S., et al., *Time Controlled Protein Release from Layer by-Layer Assembled Multilayer Functionalized Agarose Hydrogels (vol 20, pg 247, 2010).* Advanced Functional Materials, 2010. **20**(6): p. 878-878.

41. Mehrotra, S., I. Lee, and C. Chan, *Multilayer mediated forward and patterned siRNA transfection using linear-PEI at extended N/P ratios.* Acta Biomaterialia, 2009. **5**(5): p. 1474-1488.

42. Mehrotra, S., et al., *Time Controlled Release of Arabinofuranosylcytosine (Ara-C) from Agarose Hydrogels using Layer-by-Layer Assembly: An In Vitro Study.* Journal of Biomaterials Science-Polymer Edition, 2012. **23**(1-4): p. 439-463.

43. Clark, S.L., M.F. Montague, and P.T. Hammond, *Ionic effects of sodium chloride on the templated deposition of polyelectrolytes using layer-by-layer ionic assembly.* Macromolecules, 1997. **30**(23): p. 7237-7244.

44. Yang, S.Y. and M.F. Rubner, *Micropatterning of polymer thin films with pH-sensitive and cross-linkable hydrogen-bonded polyelectrolyte multilayers.* Journal of the American Chemical Society, 2002. **124**(10): p. 2100-2101.

45. Hendricks, T.R., W. Wang, and I. Lee, *Buckling in nanomechanical films.* Soft Matter, 2010. **6**(16): p. 3701-3706.

46. Hendricks, T.R. and I. Lee, *Wrinkle-free nanomechanical film: Control and prevention of polymer film buckling.* Nano Letters, 2007. **7**(2): p. 372-379.

47. Biswas, S., H. Fukushima, and L.T. Drzal, *Mechanical and electrical property enhancement in exfoliated graphene nanoplatelet/liquid crystalline polymer nanocomposites.* Composites Part a-Applied Science and Manufacturing, 2011. **42**(4): p. 371-375.

48. Fukushima, H., *Graphite nanoreinforcements in polymer nanocomposites,Department of Chemical Engineering and Materials Science, Michigan State University, East Lansing, MI, USA*, 2003.

49. Wu, H. and L.T. Drzal, *Graphene nanoplatelet paper as a light-weight composite with excellent electrical and thermal conductivity and good gas barrier properties.* Carbon, 2012. **50**(3): p. 1135-1145.

50. Jiang, X. and L.T. Drzal, *Reduction in percolation threshold of injection molded high-density polyethylene/exfoliated graphene nanoplatelets composites by solid state ball milling and solid state shear pulverization.* Journal of Applied Polymer Science, 2012. **124**(1): p. 525-535.

51. Hendricks, T.R., et al., *Intact pattern transfer of conductive exfoliated graphite nanoplatelet composite films to polyelectrolyte multilayer platforms.* Advanced Materials, 2008. **20**(10): p. 2008-+.

52. Lu, J., et al., *Stable aqueous suspension and self-assembly of graphite nanoplatelets coated with various polyelectrolytes.* Journal of Nanomaterials, 2010. **2010**: p. 2.

53. Shiratori, S.S. and M.F. Rubner, *pH-dependent thickness behavior of sequentially adsorbed layers of weak polyelectrolytes.* Macromolecules, 2000. **33**(11): p. 4213-4219.

54. Kim, H.M., J.K. Lee, and H.S. Lee, *Transparent and high gas barrier films based on poly(vinyl alcohol)/graphene oxide composites.* Thin Solid Films, 2011. **519**(22): p. 7766-7771.

55. Yu, L., et al., *A graphene oxide oxygen barrier film deposited via a self-assembly coating method.* Synthetic Metals, 2012. **162**(7-8): p. 710-714.

56. Nagel, C., et al., *Free volume and transport properties in highly selective polymer membranes.* Macromolecules, 2002. **35**(6): p. 2071-2077.

57. Yang, Y.H., et al., *Super Gas Barrier of All-Polymer Multilayer Thin Films.* Macromolecules, 2011. **44**(6): p. 1450-1459.

58. http://xgsciences.com/wp-content/uploads/2012/09/About-xGnP.pdf.

59. Kim, S., I. Do, and L.T. Drzal, *Multifunctional xGnP/LLDPE Nanocomposites Prepared by Solution Compounding Using Various Screw Rotating Systems.* Macromolecular Materials and Engineering, 2009. **294**(3): p. 196-205.

60. Schneider, M., M. Brinkmann, and H. Mohwald, *Adsorption of polyethylenimine on graphite: An atomic force microscopy study.* Macromolecules, 2003. **36**(25): p. 9510-9518.

61. Willner, I., et al., *Photoinduced Electron-Transfer Processes Using Organized Redox-Functionalized Bipyridinium Polyethylenimine Tio2 Colloids and Particulate Assemblies.* Journal of Physical Chemistry, 1993. **97**(28): p. 7264-7271.

62. Bequet, S., et al., *New composite membrane for water softening.* Desalination, 2000. **131**(1-3): p. 299-305.

63. Quinn, J.F., et al., *Next generation, sequentially assembled ultrathin films: beyond electrostatics.* Chemical Society Reviews, 2007. **36**(5): p. 707-718.

64. Lavalle, P., et al., *Comparison of the structure of polyelectrolyte multilayer films exhibiting a linear and an exponential growth regime: An in situ atomic force microscopy study.* Macromolecules, 2002. **35**(11): p. 4458-4465.

65. DeLongchamp, D.M. and P.T. Hammond, *Highly ion conductive poly(ethylene oxide)-based solid polymer electrolytes from hydrogen bonding layer-by-layer assembly.* Langmuir, 2004. **20**(13): p. 5403-5411.

66. Picart, C., et al., *Buildup mechanism for poly (L-lysine)/hyaluronic acid films onto a solid surface.* Langmuir, 2001. **17**(23): p. 7414-7424.

67. Laachachi, A., et al., *Diffusion of Polyphosphates into (Poly(allylamine)-montmorillonite) Multilayer Films: Flame Retardant-Intumescent Films with Improved Oxygen Barrier.* Langmuir, 2011. **27**(22): p. 13879-13887.

68. He, J.-A., et al., *Oriented Bacteriorhodopsin/Polycation Multilayers by Electrostatic Layer-by-Layer Assembly.* Langmuir, 1998. **14**(7): p. 1674-1679.

69. Chatham, H., *Oxygen diffusion barrier properties of transparent oxide coatings on polymeric substrates.* Surface and Coatings Technology, 1996. **78**(1): p. 1-9.

70. Zhang, Z.B., I.J. Britt, and M.A. Tung, *Permeation of oxygen and water vapor through EVOH films as influenced by relative humidity.* Journal of Applied Polymer Science, 2001. **82**(8): p. 1866-1872.

71. Kalaitzidou, K., H. Fukushima, and L.T. Drzal, *Multifunctional polypropylene composites produced by incorporation of exfoliated graphite nanoplatelets.* Carbon, 2007. **45**(7): p. 1446-1452.

72. Jiang, J., et al., *Oxygen Barrier Coating Deposited by Novel Plasma-enhanced Chemical Vapor Deposition.* Journal of Applied Polymer Science, 2010. **115**(5): p. 2767-2772.

73. Fielding-Russell, G.S. and P.S. Pillai, *A study of the crystallization of polyethylene terephthalate using differential scanning calorimetry and X-ray techniques.* Die Makromolekulare Chemie, 1970. **135**(1): p. 263-274.

Chapter 5: Amperometric detection and quantification of nitrate ions using a highly sensitive nanostructured PEDOT biosensor

(This chapter is submitted to a peer-reviewed journal and is currently undergoing revisions)

5.0 Abstract

In this work, we developed a novel one-step electropolymerized nitrate biosensor with detection limit as low as 0.1 ppm. In our work, we exploit the unidirectional flow of electrical signal in 1D conductive polyethylenedioxythiophene (PEDOT) nanowires to produce a fast acting, highly sensitive biosensor. Nitrate reductase, an enzyme responsible for conversion of nitrate species to nitrite is entrapped during the electropolymerization of PEDOT. Our work shows that the polymerization conditions such as polymerization time and potential can play a major role in the performance of the sensor. The sensor developed here has high resilience against interfering species. Based on kinetic and operational parameters, we show that the nitrate biosensor developed in this study shows impressive sensing and quantification capabilities as compared to other electrochemical sensors.

5.1 Introduction

Human activities have contributed to as much as 30% increase in nitrogen and nitrogen based compounds in the environment as compared to natural modes of fixation[1]. The increasing use of fertilizers with nitrogen precursors and automobiles emitting nitrogen oxides have put immense burden on the existing nitrogen cycle. The inability of natural sources to recycle the excess nitrogen based materials makes nitrogen a major contributor to eutrophication. A cascading set of events due to elevated nitrogen levels leading to ‘algal bloom’, formation of ‘dead zones’ because of depletion of dissolved oxygen and consequently loss of marine

biodiversity is well-documented[2, 3]. Various natural and biological processes are responsible for transformation of nitrogen based compounds into nitrate. The presence of nitrate in water supplies presents major health risks. To limit the consumption of nitrate, the U.S. Environmental Protection Agency (EPA) and the World Health Organization (WHO) set the maximum limit of nitrate in drinking water supplies as 10 ppm nitrate-nitrogen (equivalent to 45 ppm nitrate) and 11 ppm nitrate-nitrogen (same as 50 ppm nitrate), respectively[4]. Numerous studies have been conducted in the past regarding determination of nitrate or nitrogen based compounds in water supplies[5-7]. Using the data collected by the U.S. Geological Survey National Water-Quality Assessment Program, Rupert[8] studied the general trend of nitrate concentration in ground-water supplies by evaluating data from a 24 well-network spread all over the US. Close to 30% of the well network showed an increase in nitrate concentrations. Half of these wells recorded nitrate concentration above the maximum limit prescribed by the regulatory agencies.

One of the most prominent ill effects of increased nitrate consumption in humans is the low oxygen carrying capacity of the blood. The conversion of ingested nitrate to nitrite followed by incorporation of nitrite with hemoglobin leads to the formation of a complex called methemoglobin (MetHb)[9]. In infants there is greater incidence of nitrite because of the lower gastric acidity[10]. Cellular anoxia is a likely consequence of lower oxygen transport throughout the body. This disorder is commonly referred to as methemoglobinemia. Besides this, nitrate is also responsible for the formation of several N-nitroso compounds (NOC) which in turn increase the risk of cancer. Studies regarding the impact of nitrate uptake on occurrence of gastric and abdominal cancers have been carried out[11-13]. Consumption of nitrate is also linked to growth of cancerous lesions in the human thyroid gland[14]. Nitrate is also suspected to disrupt the

endocrine functioning of the thyroid gland by blocking the iodide symporter independently or in conjugation with potent inhibitors such as perchlorate and thiocyanate[15].

Previous methods for detection and quantification of anions include ion chromatography (IC), complexation electrospray mass spectrometry (cESI-MS) and Raman spectroscopy[16-18]. However, these methods require extensive instrumentation and are not particularly attractive for instant field tests. Biosensors on the other hand have demonstrated a great potential for the development of simple portable systems capable of detection and quantification even at minute concentrations. Several examples of biosensors capable of accurate and sensitive analysis are found in literature[19-21]. Detection of nitrate using an enzymatic biosensor has been extensively studied in the past few decades. Nitrate reductase, an enzyme capable of facilitating reduction of nitrate species has been used as the biorecognition element for the fabrication of nitrate detecting biosensor. This enzyme also plays a significant role in the 'denitrification cycle' by participating in the nitrogen acquisition mechanism in higher plants[22]. One of the earliest designs for a nitrate biosensor was proposed by Guilbault and co-workers[23]. Low sensitivity and dependence on co-factors reduced the practical applicability of this device. Since then efforts have been dedicated to improve the sensitivity, stability and ruggedness of the biosensor to make it suitable for commercial application. Newer designs include use of metal nanoparticles[24], colloidal clay[25], redox polymers[26, 27] and screen printing technology[28] to improve the performance of the biosensors. The integration of these components helps to improve the microenvironment in which the immobilized enzyme operates and maximizes the output intensity facilitating easy detection of nitrate. However, unlike the biosensor described in this study where we take the full advantage of the nanoscale dimensions by immobilizing the nitrate reductase in upright PEDOT nanoarrays, most of the prior art relies on the incorporation of

nitrate reductase in thin films made from polymeric- nanomaterial matrix. Some of these films may not always retain their nanoscale dimensions during the growth process. The enzyme is likely to be buried deep inside the film blocking its accessibility to the substrate limiting the performance of the sensor.

Conductive polymer nanowire/ nanotubes are attractive candidates to serve as supports for enzyme immobilization. Nanostructures made from conductive polymers (CP) are known to exhibit much higher conductivities than bulk materials. In some cases it can be as high as 15 orders of magnitude depending on the parameters such as dopant ions or monomer/dopant ratio[29]. Besides the substrate-enzyme accessibility issues observed in thin films as pointed out above, flat 2D films are also prone to lateral current shunting, reducing their signal intensities. On the other hand, nanotubes/nanowires are the smallest dimensions that allow efficient transport of electrons thus enabling detection of single molecules[29]. The use of the enzyme-polymer nanowire matrix as shown in this work is therefore expected to show enhanced electrical performance. This we believe has translated into superior LOD and instantaneous response (2-5 seconds) making the sensor one of the frontrunners in the class of electrochemical biosensors for detection of nitrate. Among the various techniques used to grow nanotubular/wire structure, the templated route is a convenient approach to growth polymeric nanostructures of well-defined morphology. Typically, template assisted polymerization enables the growth of polymer nanostructures with enhanced molecular and supramolecular morphology[30]. Use of hard templates such as track-etched polycarbonate (PC) and nanoporous anodic alumina membrane is very common[31]. Templates allow highly oriented growth of polymers[32]. The morphology of the polymer nanostructures is dictated by the shape and size of the pore in the hard template and hence polymeric nanostructures of desired aspect ratio can be easily grown in

the pores. In our work, regulated growth of polymer/enzyme nanowire structures enabled precise control over growth of nanostructures enabling improved operational stability and superior signal to noise ratio. Using the standard CMOS processes and techniques such as dielectrophoretic assembly, large arrays of nanowires made from conducting polymers can be easily aligned on silicon chips. This readily available technology can be easily extended to our biosensor application to produce commercial sensors in the near future. [33].

Compared to other heterocycles, PEDOT is a conducting polymer that retains its conductivity and structural stability over a wide range of temperature[34]. The oxidation of EDOT produces a transparent conductive polymer with high electrochemical stability and low band-gap[35, 36]. EDOT also affords easy functionalization with redox active groups to improve the overall solubility and processibility[37]. Because of the many advantages, PEDOT can serve as an attractive candidate for applications such as optoelectronics[38, 39], electrochromics[40, 41], and supercapacitators[42, 43].

In this work, using a fast one-step electropolymerization process, PEDOT/enzyme nanowires were grown in the pores of PC membrane. The insolubility of EDOT in aqueous solution and high polymerization potential were overcome by adding sufficient quantity of surfactant. This study shows that PEDOT serves an excellent matrix to entrap nitrate reductase. PEDOT/enzyme biosensor was fabricated at specific process conditions such as applied potential and polymerization times. By meticulously optimizing the process conditions we establish a strong link between the performance of the biosensor and the morphology of the PEDOT/enzyme nanowires. As compared to other electrochemical nitrate reductase based sensors in literature (comparison shown in subsequent section), the electropolymerized nanobiosensor developed in this study shows several superior attributes: low limit of detection

(LOD) of about 0.108 ppm, fast fabrication (about 300 seconds), a very quick response time and low background noise. The sensor developed in this study also showed a significant resilience against interfering species. The kinetic parameters of nitrate reduction were estimated from the initial rate data and compared with similar data obtained by replacing nitrate species with other interfering substrates. Substrate binding affinity with nitrate was estimated to be several orders of magnitude higher than other interfering ions such as perchlorate and carbonate.

5.2 Experimental

5.2.1 Materials

Sodium chloride (NaCl), sodium dodecyl sulfate (SDS), methyl viologen, potassium perchlorate, potassium nitrate, sodium carbonate and ethylene dioxythiophene (EDOT) were purchased from Sigma Aldrich. Conductive copper tape (adhesive on one side) was purchased from Mcmaster-Carr, GA. Nucleopore track-etched polycarbonate (PC) membrane with pore size 200 nm was purchased from Fisher Scientific. Nitrate reductase (Y-NaR) was purchased from Nitrate elimination Co., MI.

5.2.2 Preparation of template assisted PEDOT/enzyme nanowire electrode

Templated growth of PEDOT nanostructures is described elsewhere[42, 44] [45] In our work, we extend the templated growth of PEDOT nanostructures to coimmobilize nitrate reductase using a one-step electropolymerization process. Based on our knowledge, this is the first attempt to grow PEDOT/enzyme nanowire structures using single step process while still retaining the integrity of the 1D nanowire structure. Unlike other biosensor fabrication techniques where a film of the conducting polymer and enzyme is co-immobilized, in this work we retain the upright 1D

nanowire structure synthesized in the PC membrane to take full advantage of the electrical conductivity of 1D nanowire structure as explained in the previous section.

The one step electropolymerization of PEDOT/nitrate reductase is summarized briefly as given below. Commercially available 13 mm polycarbonate membrane was sputter-coated with a 15 nm thick gold layer using a Denton Vacuum sputter coater. A conductive copper tape was attached to the other side of the PC membrane. This was covered with a circular insulating tape. The sputter-coated side of the membrane was covered with a partial insulating disc such that the effective electroactive area available for polymerization is about 0.2 cm^2. The commercial nitrate reductase is available in freeze-dried form. The nitrate reductase is added to the electropolymerization bath consisting of 0.05 M EDOT, 0.07 M SDS and 0.1 M NaCl. About 1 ml of the electropolymerization bath solution is added to one vial of the freeze-dried enzyme sample (protein concentration about 120-125 µg/ml) and the mixture is allowed to equilibrate at room temperature for at least 15 minutes.

Electrochemical polymerization of EDOT/Enzyme complex is carried out using a 3-electrode system. The working electrode comprised on the Au- coated PC membrane as prepared earlier. Saturated calomel electrode (SCE in saturated KCl) served as the reference electrode whereas a thin platinum wire was used as a counter electrode. Electrochemical polymerization was carried out at desired oxidation potential and time. The polymerization of EDOT/enzyme in the pores of the PC membrane was confirmed by the formation of bluish-black composite on the exposed portion of the membrane. To check the electroactivity of the working electrode, the working electrode was immersed in 10 ml, 10 mM stirred phosphate buffer saline (PBS).1 mM MV was added as a redox mediator to the PBS buffer. Prior to immersion of the electrode, the buffer solution was deoxygenated by bubbling argon for 30 minutes.

5.2.3 Characterization of PEDOT/enzyme nanowires

The scanning electron microscopy (SEM) investigation for high-resolution imaging was carried out using a JEOL 7500F with field emission. Transmission electron microscopy (TEM) studies were carried out using a JEOL 100CX. After the electrochemical polymerization of PEDOT/enzyme nanostructures, the PC membrane was dissolved using methylene chloride and mild sonication. A few drops of the solution were put on a lacey carbon coated TEM grid and dried overnight. The grids were then observed under SEM and TEM.

5.3 Results and Discussion

The growth of conductive polymers using a templated approach offers attractive opportunities to fabricate electronic interfaces of desired aspect ratio. In this study, using a one-step electropolymerization process we developed a highly sensitive PEDOT based nanostructured biosensor with a LOD close to 108 ppb (0.108 ppm) nitrate. A schematic diagram depicting the growth of PEDOT in a polycarbonate (PC) membrane is shown in Figure 5.1

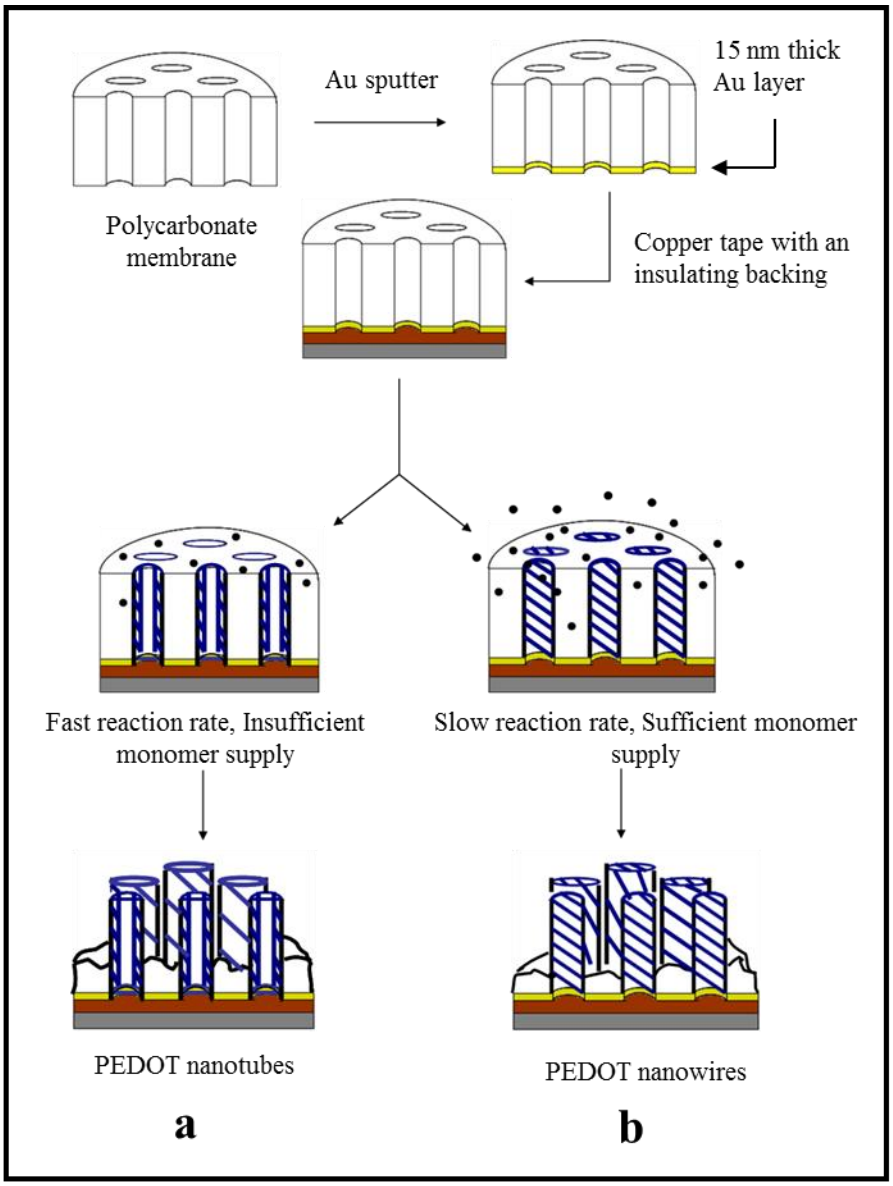

Figure 5.1 Electrochemical polymerization of EDOT using a templated approach. (a) Formation of polymer nanotubes (b) Formation of polymer nanowires

Along with the monomer, the electropolymerization bath consists of SDS (surfactant), supporting electrolyte (NaCl) and nitrate reductase. Though two different types of structures (hollow nanotubular (a) and filled nanowire (b) structure) are feasible depending on the process conditions, in this paper we will be focusing on the growth of a filled nanowire structure. A completely filled nanowire structure is a result of high concentration of monomer and relatively

longer polymerization time. High concentration of monomer ensures steady supply of EDOT to the active sites in the pores of the PC membrane. A long polymerization time allows the polymer to grow along the wall of the pore and then fill the pore cavity resulting in a well-formed nanowire structure. Detailed discussion regarding the mechanism of growth of PEDOT nanotubes vs. nanowire structure is available elsewhere[42, 44, 46].

Under oxidizing potential, most conducting polymers undergo p-doping followed by entry of counter-ions from the supporting electrolyte solution to maintain electroneutrality[47]. In this case, the Cl^- ions from the supporting electrolyte solution diffuse into the PEDOT structure during the electropolymerization process. To overcome the issue of EDOT insolubility in aqueous medium, sodium dodecyl sulfate (SDS) is added to the supporting electrolyte solution. The anionic DS^- ions of SDS bind with the $EDOT^+$ radical to form a pseudo-complex which is stable in aqueous medium[48]. The hydrophilic ends of SDS also wet the electrode surface and allow the subsequent deposition of PEDOT. The addition of SDS also serves another important purpose. It lowers the oxidation potential at which EDOT polymerizes [48, 49]. This is particularly important in biological systems which are known to deteriorate when subjected to higher oxidation potential. Unlike electropolymerization of some conducting polymers such as polyaniline[50] and polypyrrole[51] that need an acidic environment, the electropolymerization of PEDOT aided by addition of SDS can be carried out in DI water without pH adjustment. Acidic environment usually spurs the preferential complexation of H_3O^+ ions which can reduce the nucleophilicity of water [52]. The use of surfactants for synthesis of PEDOT can avoid this problem. The use of neutral aqueous medium can largely preserve the biomolecule structure and function. Once synthesized, PEDOT largely retains its stability and

conductivity as opposed to polypyrrole which is likely to develop defects due to multiple α, β and β,β-linkages [36].

The addition of nitrate reductase to the electropolymerization bath solution and the subsequent one step electrochemical synthesis of polymer entraps the enzyme within the PEDOT nanowires grown in the pores of the PC membrane. With the isoelectric point of nitrate reductase close to 6.1, the enzyme attains a weak negative charge when added to the neutral aqueous electrochemical bath solution. Weak electrostatic interactions are likely to exist between the cationic $EDOT^{+}$ radical and the enzyme. The hybrid electrochemical adsorptive process involving electrophoretic migration of charged species located in the close vicinity of the bioelectronic interface leads to the deposition of nitrate reductase in amounts exceeding that obtained by regular adsorption [47]. Other advantages of one step electrochemical adsorptive process include precise control over the growth of the PEDOT/enzyme nanostructure by monitoring the charge build-up during the process, limited structural damage to the enzyme due to lack of harsh chemical reactions and ability to electrogenerate the PEDOT/enzyme coating on different types of electrodes with complex geometry [53].

5.3.1 Anodic polymerization of EDOT

Oxidation onset potential ($E_{ox\ onset}$) of EDOT depends on the components of the electropolymerization bath solution more particularly the concentration of the surfactant used for polymerization[52, 54]. The $E_{ox\ onset}$ was determined from linear sweep voltametry curves as shown in Figure 5.2. The magnitude of current density is plotted as a function of potential. At lower potential, EDOT polymerization is mostly subdued. However at a potential of 0.82V, the current starts rising and a slight bulge-shaped profile can been seen. With further increase in the applied potential, the current starts increasing rapidly as more and more EDOT starts getting

polymerized. The LSV profile for EDOT polymerized in presence of 0.07 M SDS and 0.1 M NaCl is indicated by curve a. A qualitative confirmation of the participation of nitrate reductase in the EDOT polymerization process can be obtained from curve b. Curve b shows the LSV profile when nitrate reductase was added to the electropolymerization bath solution. The addition of enzyme delays the onset polymerization of EDOT. $E_{ox\ onset}$ for this curve is close to 0.90-0.92 V. Also the magnitude of the current density of the EDOT polymerization in presence of nitrate reductase is much lower. This could be because the $EDOT^{+}$ cations can form weak electrostatic complexes with negatively charged nitrate reductase. The polymerization of $EDOT^{+}$/nitrate reductase (in presence of DS^{-} ions) can differ from traditional $EDOT^{+}/DS^{-}$ complexes and the same needs to be probed in detail using more quantitative tools.

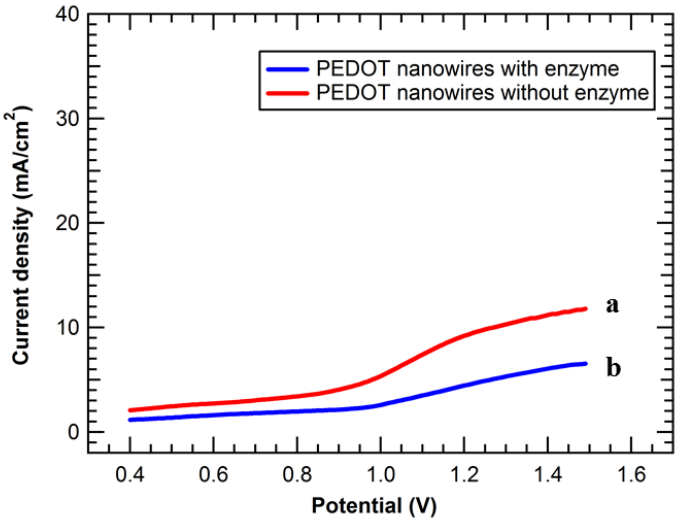

Figure 5.2 Linear sweep voltammetry (LSV) profile of EDOT polymerization (a) in absence of enzyme (b) in presence of enzyme.

5.3.2 Chronoamperometric growth of PEDOT/enzyme nanowires

Chronoamperometry is a potentiostatic technique that has been frequently used for oxidative growth of conducting polymers[55, 56]. Unlike cyclic voltammetry, chronoamperometry allows the polymerization to occur at user defined fixed potential thus preventing the system from

reaching an overoxidation state. The one step electropolymerization of EDOT/nitrate reductase was carried out at three different potentials namely 0.85 V, 1.1 V and 1.4 V respectively. The electropolymerization time was fixed at 300 seconds in each case. For comparison, the electrodes were subjected to EDOT polymerization in absence of nitrate reductase using the same conditions as before. Six systems were subjected to polymerization and the variation of current density w.r.t time is shown in Figure 5.3. All the six cases show a common trend.

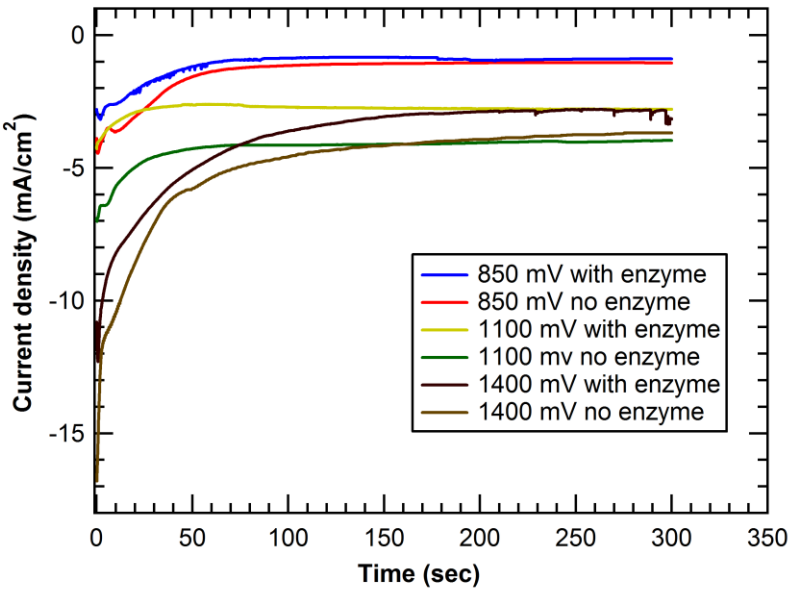

Figure 5.3 Chronoamperometric plot of current density as a function of electropolymerization time. Inclusion of enzyme reduces the creation of active sites for polymerization evidenced by lower current density during the initial phase of polymerization.

The chronoamperometric graphs can be divided into three separate regions. The first region lasts for a few seconds but shows a sharp increase in the current. In this region, active sites within the pores of the membrane (along the walls and on the gold electrode) where the EDOT monomer is likely to polymerize are created. Zeng and co-workers[57] found similar behavior when choline oxidase was added to the electropolymerization bath solution consisting of EDOT monomer. Region II shows a gentle decrease in the current as the system tries to stabilize. It is reported that it is in this region that the diffusion and deposition of monomer units occurs [57]. In the process,

the active sites within the pores of the membrane are used up. Region III shows the current reaching a steady plateau value indicating no further creation of active sites. Linear growth of the polymer/enzyme nanowire is expected to occur to occur in this region. The addition of enzyme to the electropolymerization bath solution is expected to slow down the polymerization process. As seen earlier, the slight increase in the E_{ox} onset potential confirms this. Addition of enzyme reduces the number of active sites available for polymerization. Hence the three cases that include incorporation of the enzyme in the PEDOT matrix show lower current in region I.

5.3.3 Morphology of PEDOT /enzyme nanostructures

In the previous section, we observed from the chronoamperometric plots that application of varied potentials can lead to differential creation of active sites. Initially at low potentials, the degree of polymerization is very low. However as the potential crosses the $E_{ox\ onset}$, the degree of polymerization increases and this is represented by increase in current density. Since 0.85 V is less than $E_{ox\ onset}$ (for enzyme incorporated system), the driving force for creation of active sites in the pores of the membrane is subdued. The morphology of PEDOT/enzyme nanowires formed at this potential is therefore not very distinct. At 0.85 V, the nanowires are short, clustered with loss in form especially at the ends. This is evident from the SEM and TEM images of PEDOT/enzyme nanowires synthesized at 0.85 V shown in Figures 5.4 (a) and (b) respectively. However, as the potential is raised beyond the $E_{ox\ onset}$, the nanowires appear more distinct and their morphology at the ends is well-formed. The SEM and TEM images shown in Figure 5.4 (c) and (d) confirm this. As the potential is raised further to 1.4 mV, more and more polymer gets deposited in the pores of the membrane. As seen from Figure 5.4 (e) and (f) , irregularly shaped nanowires are commonly produced at this potential. At higher potential, overoxidation of PEDOT becomes the dominating factor. In case of most polythiophenes, increasing oxidation

potential results in ‘overoxidation’ that results in rapid degradation and irreversible loss in polymer conductivity[58]. Du and Wang[59] have established that effects of over-oxidation cannot be neglected when the electropolymerization potential exceeds 1.1 V. Another possible impediment in carrying out EDOT polymerization at higher potential is the possible breakdown of water. The decomposition of water at 1.23 V allows only a limited potential window for the polymerization of EDOT [60, 61].

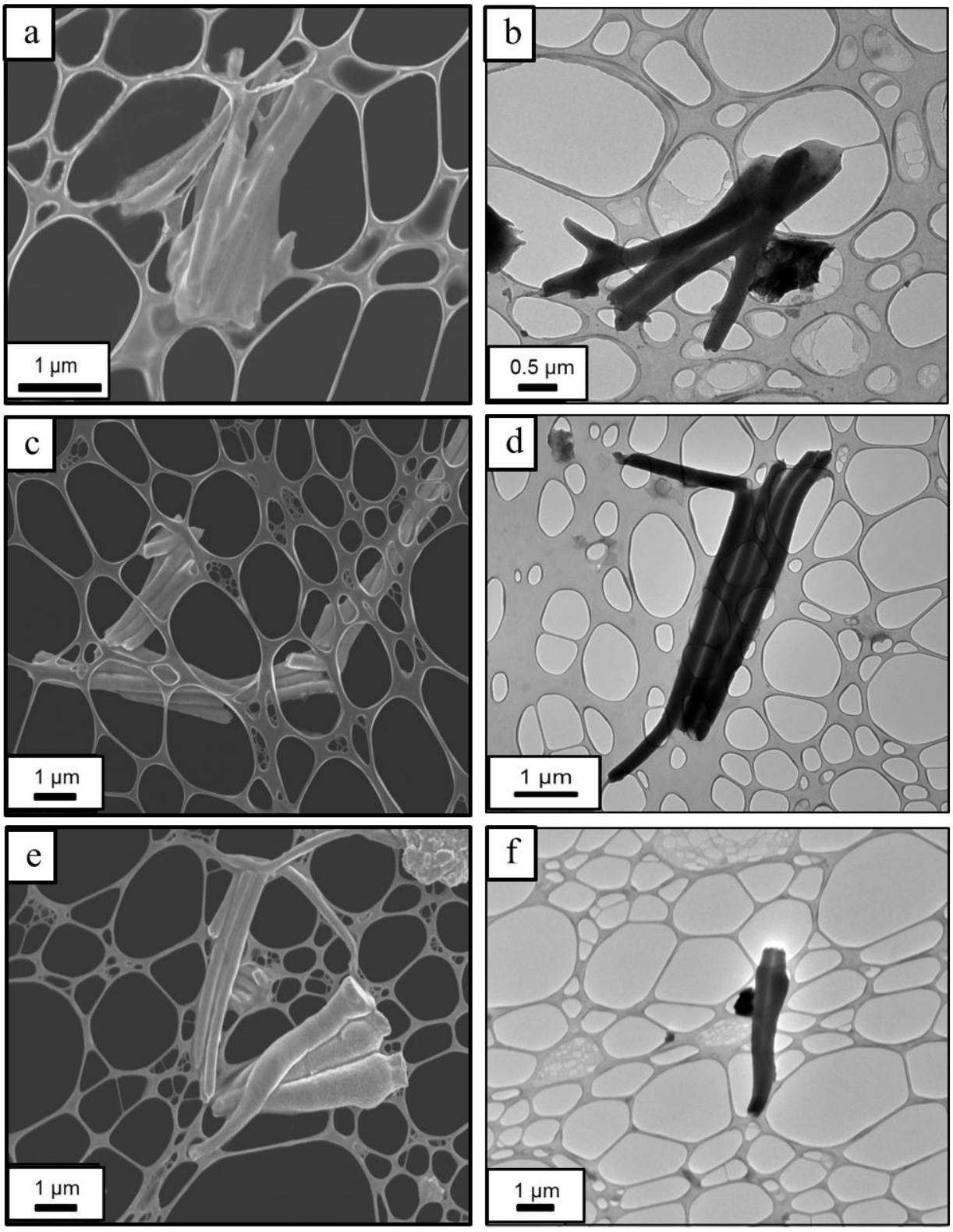

Figure 5.4 Microscopy images of PEDOT nanowires at different oxidation potential. SEM images of nanowires polymerized at (a) 0.85 V (c) 1.1 V (e) 1.4 V. Corresponding TEM images (b) 0.85 V (d) 1.1 V (f) 1.4 V.

Digital images of the polymer suspension in dichloromethane following the dissolution for PC membrane (for preparation of SEM/TEM samples) shown in Figure 5.5 give us a qualitative idea of the degree of polymerization at different potentials. PEDOT has a characteristic bluish-black color. Upon dissolution of the PC membrane, the polymer/enzyme nanowires get dispersed in the organic solvent. At 0.85 V, the extent of polymerization is low, so very little polymer is formed. Hence the solution is mostly clear. The formation of the polymer at higher potential namely 1.1 V and 1.4 V is confirmed by the characteristic bluish-black color of PEDOT as seen from Figure 5.5. Upon visual inspection, the bluish-black color of the PEDOT solution obtained at 1.4 V appears to be more intense than the one at 1.1 V.

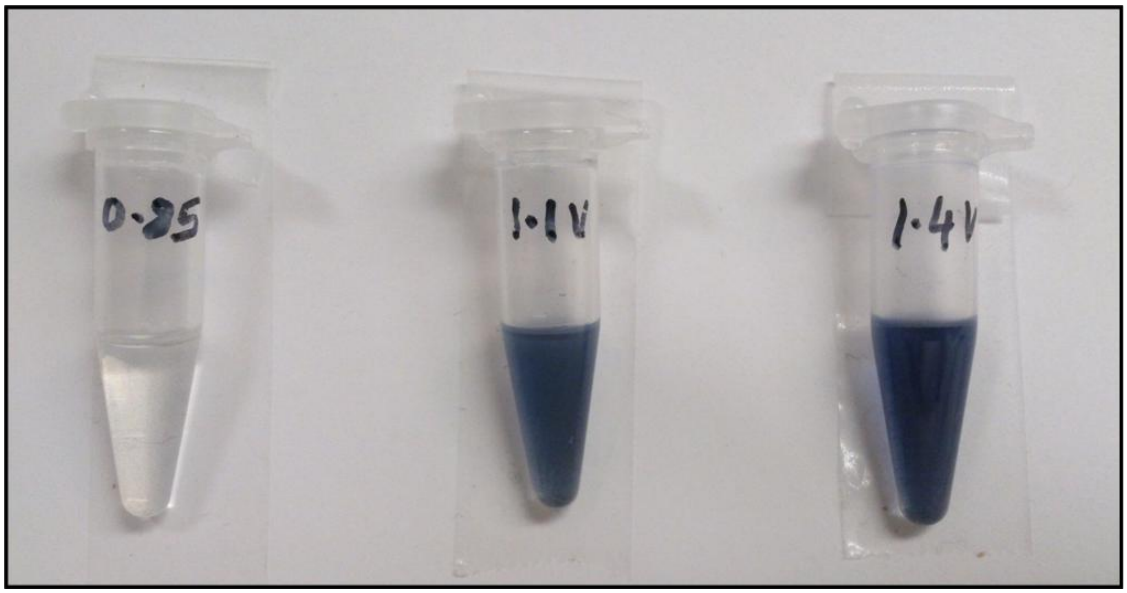

Figure 5.5 Digital images of PEDOT in dichloromethane solution. EDOT polymerized at 0.85 V yields clear solution indicative of low degree of polymerization. At 1.1 and 1.4 V, bluish-black PEDOT is formed.

5.3.4 Amperometric detection of nitrate ions

The electropolymerized biosensor developed in the previous section was subjected to addition of potassium nitrate. With each successive addition of potassium nitrate, the cumulative nitrate concentration was evaluated. As mentioned before, nitrate reductase is an enzyme that operates

under anaerobic conditions. Therefore prior to the test, the PBS buffer was thoroughly purged with argon gas for about 30 minutes. Besides argon purging, other methods include using oxygen scavengers such as sodium sulfite [62]. However, we avoided using external scavengers since their effect on the electropolymerized PEDOT sensor is relatively unknown. However in future, use of oxygen scavengers prior to the amperometric test seems to be a viable option for carrying out instant field tests. 1mM MV was added to the PBS buffer prior to argon purging. Methyl viologen is a well-known redox mediator that can aid shuttling of electrons between the bioelectronics interface and the active site of the enzyme. The addition of MV proves to be useful particularly in case of nitrate reductase based biosensors because the active site catalyzing the reduction of nitrate to nitrite is buried deep within the enzyme[22, 27]. The presence of MV in the buffer solution helps in efficient transmission of electrical signal enhancing the chances of achieving a quick response.

Biosensors fabricated at three different potentials namely 0.85 V, 1.1 V and 1.4 V were subjected to amperometric test. The sensor polymerized at 0.85 V comprises of polymer/enzyme nanowires with morphological defects (especially at the ends). The polymer/emzymes nanowires are also short and mostly buried within the pores of the membrane. The nitrate ions suffer from accessibility issues since they need to diffuse through the pores of the membrane and reach the polymer/enzyme nanowires. Hence the biosensor developed at this potential fails to give a measurable response. However, detection of nitrate ions is still possible. This is seen from Figure 5.6. Addition of nitrate leads to spike in the current. However, the poorly formed nanostructures are unable to sustain the increase in the current. Within a few seconds the current starts tailing off. The inability of the biosensor to achieve steady state current after successive addition of nitrate ions makes it difficult to quantify the analyte content in the solution.

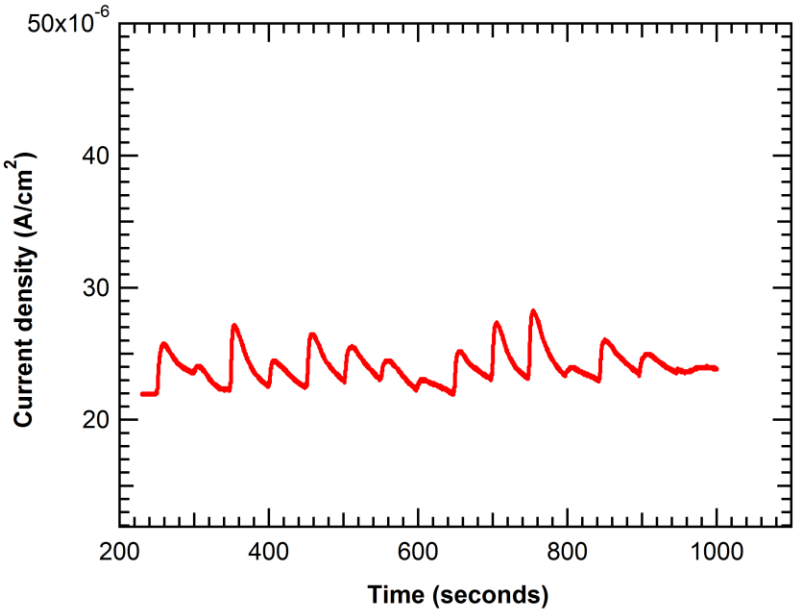

Figure 5.6. Amperometric profile of nitrate biosensor fabricated at polymerization potential of 0.85 V. Detection of nitrate species is possible but quantification information is hard to establish.

Similarly, the sensor fabricated using a polymerization potential of 1.4 V suffers from quantification issues. (See Figure 5.7)

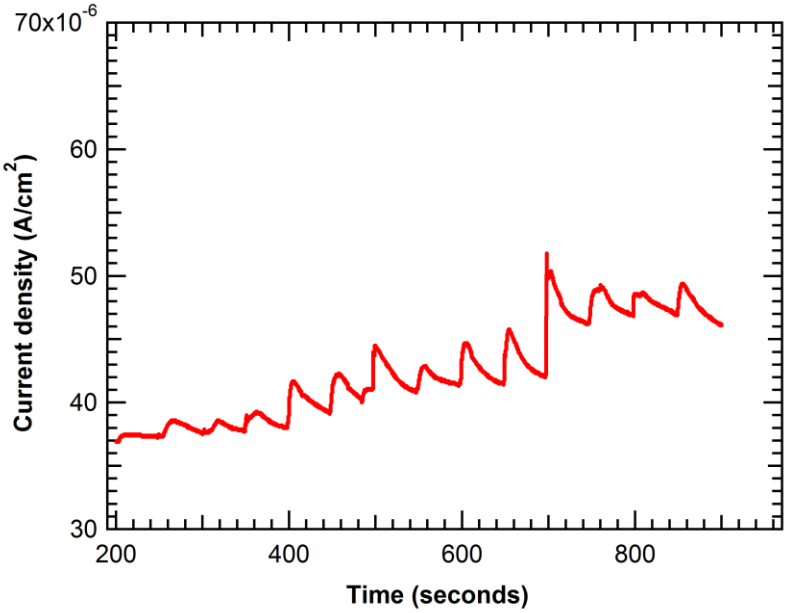

Figure 5.7 Amperometric profile of nitrate biosensor fabricated at polymerization potential of 1.4 V. Detection of nitrate species is possible but no quantification information is hard to establish.

However, unlike the poor/incomplete oxidation of EDOT as observed at 0.85 V, the polymerization at 1.4 V suffers from overoxidation. This means that though the polymer/enzyme nanowires are formed in the pores of the membrane, a loss of conductivity due to overoxidation can result in poor signal transmission. Also higher potential can also result in some nanowires outgrowing the pores. The outgrown nanowires can combine and form polymer/enzyme thin film on the surface of the membrane. This can damage the advantages afforded by 1D nanowire structure. We found higher incidence of nanowires growing up to 9 microns in length at this polymerization condition. (See Figure 5.8). Such long nanowires were not observed routinely observed at other conditions.

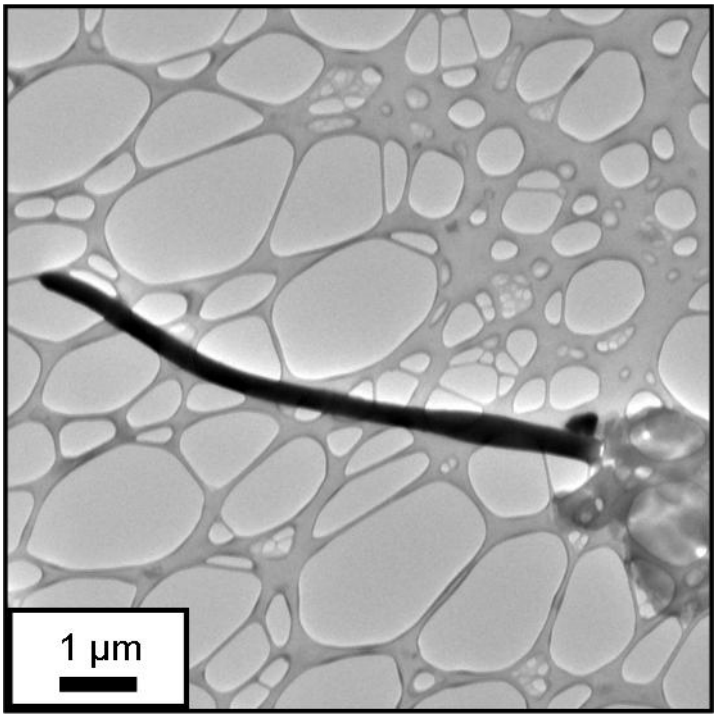

(a)

Figure 5.8. TEM micrographs of PEDOT nanowires fabricated at polymerization potential of 1.4 V. (a) length of nanowire close to 6.5 microns (b) length of nanowire close to 9 microns. Growth is irregular.

Figure 5.8 (cont'd)

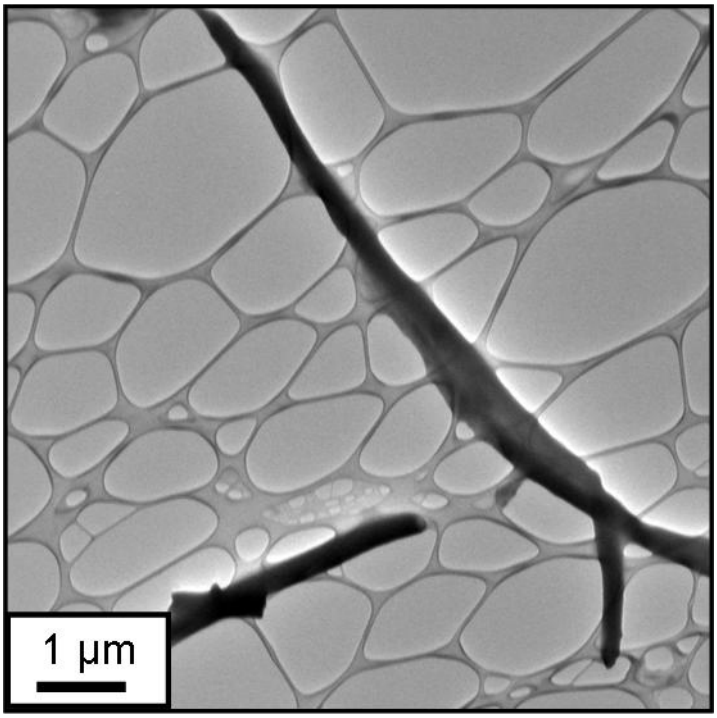

(b)

Another configuration of PEDOT/enzyme biosensor was tested by polymerization at 1.1 V. The selection of 1.1 V was made keeping in mind that the $E_{ox\ onset}$ for the enzyme incorporated system is close to 0.9-0.92 V. Fabrication of the biosensor at 1.1 V should eliminate morphological defects resulting from incomplete polymerization and/or overoxidation. Also 1.1 V is also lower than the theoretical potential at which water undergoes decomposition. The biosensor showed improved performance when fabricated at this condition. The step-wise increase in current (see Figure 5.9a) occurs as a result of successive addition of KNO_3 solution. This facilitates easy quantification of the added analyte. Since 1.1 V also lies in the small potential window where the oxidation of EDOT yields a highly conductive polymer, we observed a quick response of the biosensor to the addition of nitrate solution. The sensor records

a rise in current with 2-5 seconds on addition of the analyte solution. The sensor also enjoys very low detection limit (LOD: 108 ppb). As seen from Figure 5.9b, the sensor shows a linear response to nitrate addition in the range 200 ppb-1100 ppb.

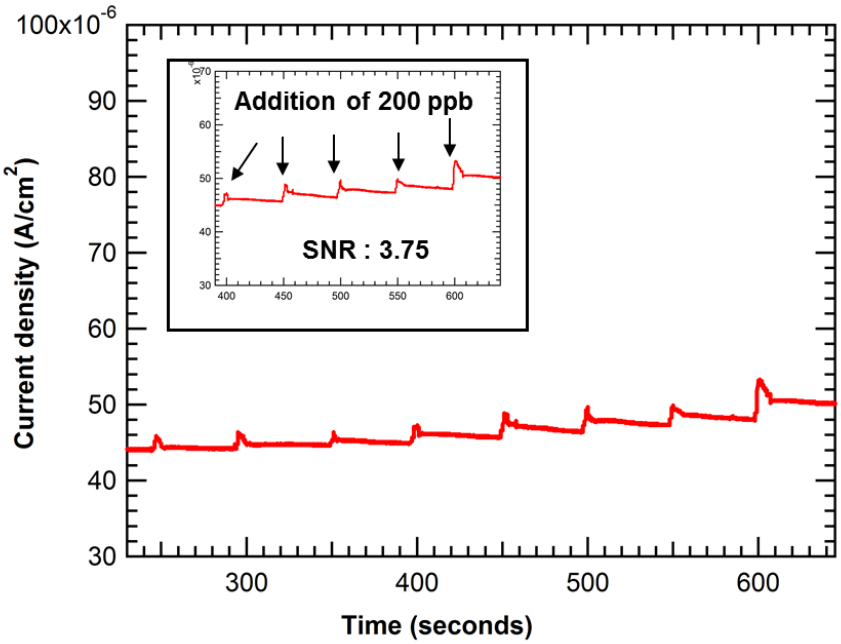

(a)

Figure 5.9 (a) Amperometric profile of nitrate biosensor fabricated at 1.1 V, 300 sec. in presence of nitrate species. Inset image shows step-wise increase in current after addition of 200 ppb nitrate after every 50 seconds (b) Linear range of operation of the sensor.

Figure 5.9 (cont'd)

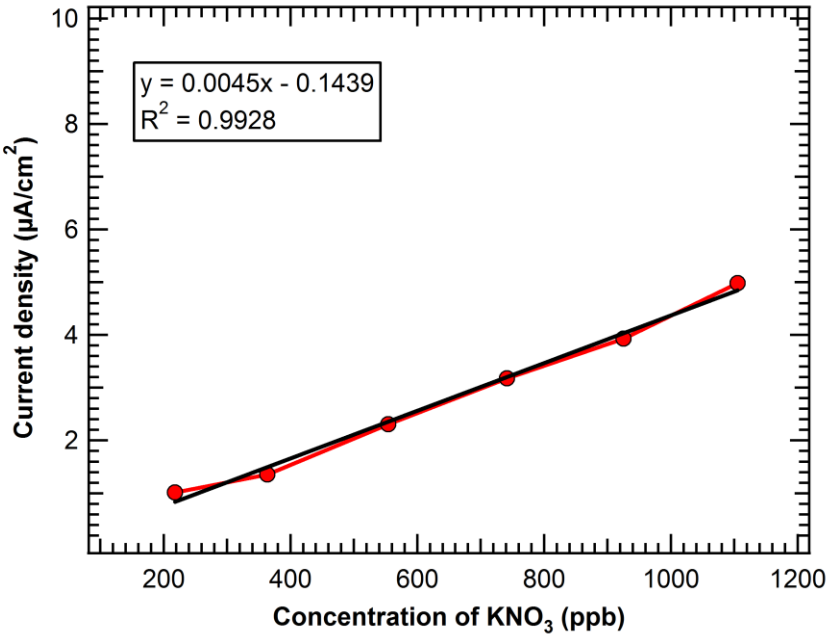

(b)

In order to understand the effect of the polymerization time on the performance of the biosensor, we fabricated a sensor using a polymerization potential of 0.95 V (just enough to ensure optimum polymerization of EDOT) and polymerization times of 300 seconds and 600 seconds respectively. At 300 sec, just like before detection of nitrate species was observed but quantification trend was hard to establish. (See Figure 5.10).

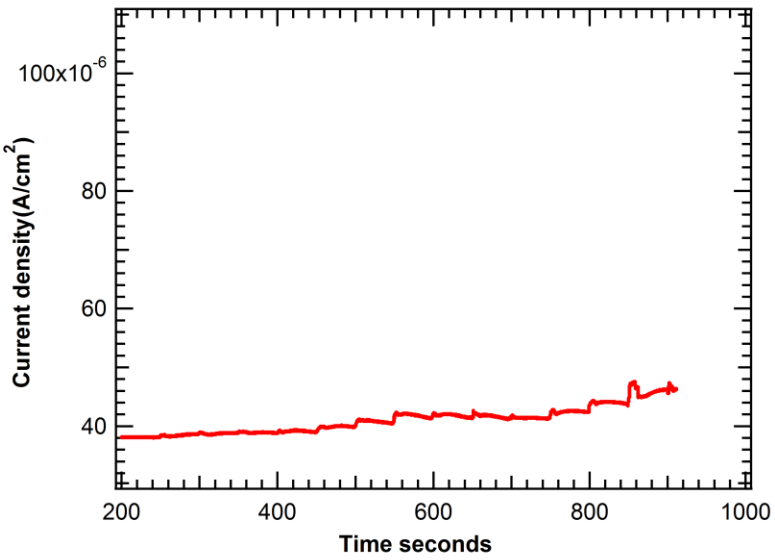

Figure 5.10. Amperometric profile of nitrate biosensor fabricated at polymerization potential of 0.95 V (300 sec.). The nitrate species are detected but quantitative trend difficult to establish.

But on increasing the polymerization time to 600 sec, a step-wise increase in current with fast response was observed (See Figure 5.11a). The biosensor fabricated at this condition shows a LOD of around 363 ppb. The linear range is from 550 ppb-1600 ppb (Refer Figure 5.11b). Increasing the polymerization time to 600 seconds allows higher degree of EDOT polymerization. Also longer time allows more enzyme to get entrapped within the PEDOT matrix thus improving the response of the sensor. However SNR for this sensor is low. Thus by increasing the polymerization time, a quantifiable set of data can be obtained. However, high levels of noise in the system can impede the practical applicability of the sensor fabricated at this condition.

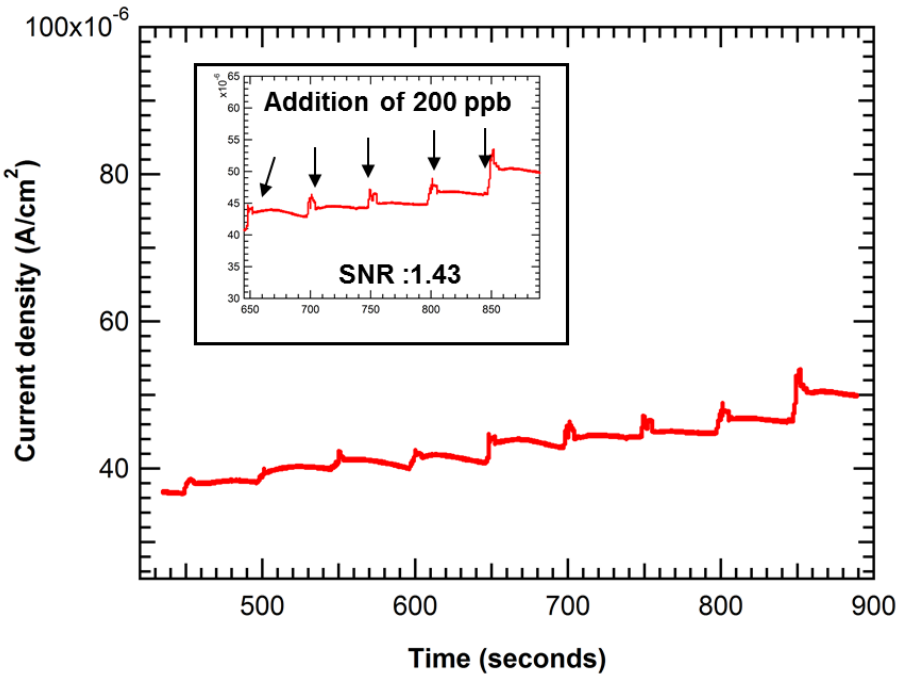

(a)

Figure 5.11 (a) Amperometric profile of nitrate biosensor fabricated at 0.95 V, 600 sec. in presence of nitrate species. Inset image shows step-wise increase in current after addition of 200 ppb nitrate after every 50 seconds (b) Linear range of operation of the sensor.

Figure 5.11 (cont'd)

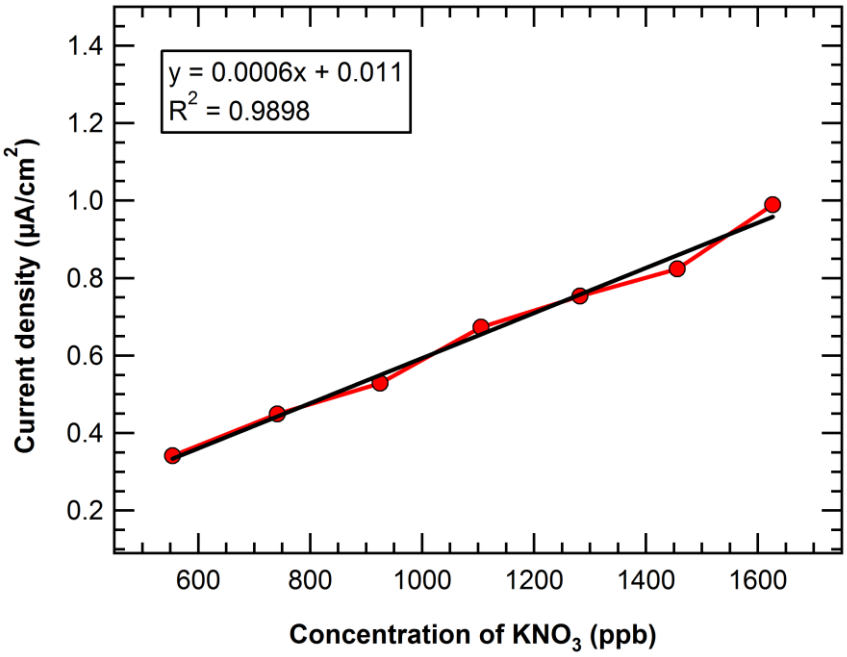

(b)

5.3.5 Effect of other reducible substrates on the nitrate reductase biosensor

Presence of other reducible substrates is likely to affect the performance of the nitrate reductase biosensor. Like all other analytical methods, the nitrate reductase based biosensors are susceptible to interferences due to substrates that share a similar structural affinity. The specificity of nitrate reductase enzyme plays an important role in minimizing the effects of these interferences. The thermodynamics of perchlorate reduction closely matches that of nitrate reduction and this is evident by comparing the Gibb's free energy of both systems (ΔG^0= -801 kJ/mol acetate for perchlorate reduction as compared to ΔG^0=-792 kJ/mol acetate for nitrate reduction) [63]. This makes it a potent interfering ion. Carbonate species (obtained by replacing N in nitrate with C) normally associated with hard water is also a known interfering material largely due to the structural similarity [64]. The kinetic parameter k_{cat} (enzyme turnover number) commonly used in determination of substrate specificity cannot be accurately estimated

due to the lack of information regarding the extent of enzyme loading during the polymerization process. This is one drawback associated with using one-step enzyme/polymer co-immobilization route and has been duly noted in literature [53]. However other kinetic parameters relevant to enzyme kinetics can be obtained by from the Lineweaver Burk plot.

In this work, we carried out studies to ascertain the affinity of the enzymatic biosensor towards the substrates containing nitrate, perchlorate and carbonate species. The biosensor was fabricated at 1.1 V and effect of the above substrates was estimated by adding potassium nitrate, potassium perchlorate and sodium carbonate separately. Refer Figures 5.12 (a) and 5.13 (a) for the amperometric profile obtained after adding perchlorate and carbonate substrates.

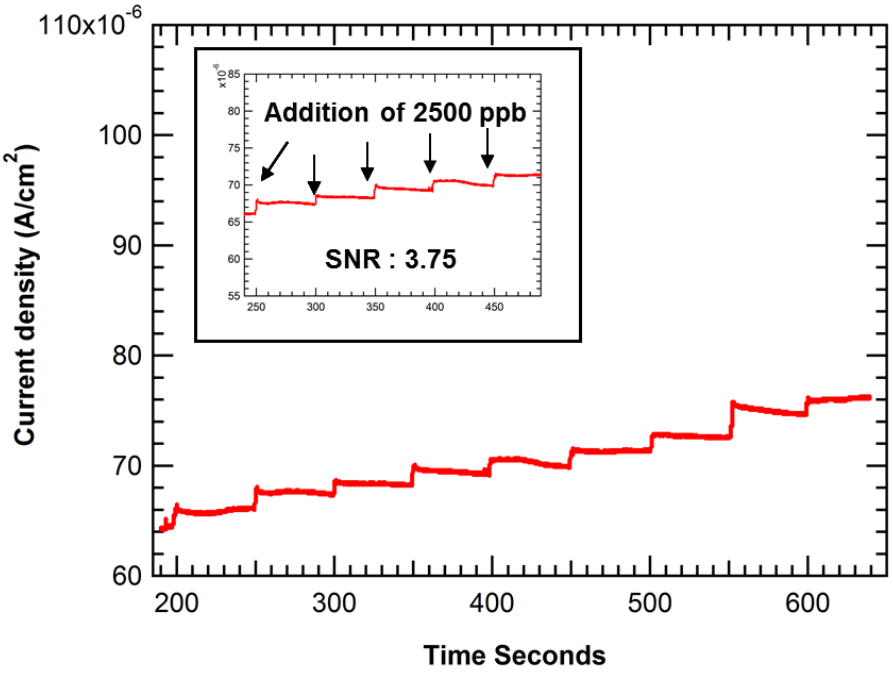

(a)

Figure 5.12. (a) Amperometric profile of nitrate biosensor fabricated at 1.1 V, 300 sec. in presence of perchlorate species. Inset image shows step-wise increase in current after addition of 2.5 ppm perchlorate after every 50 seconds (b) Linear range of operation of the sensor.

Figure 5.12 (cont'd)

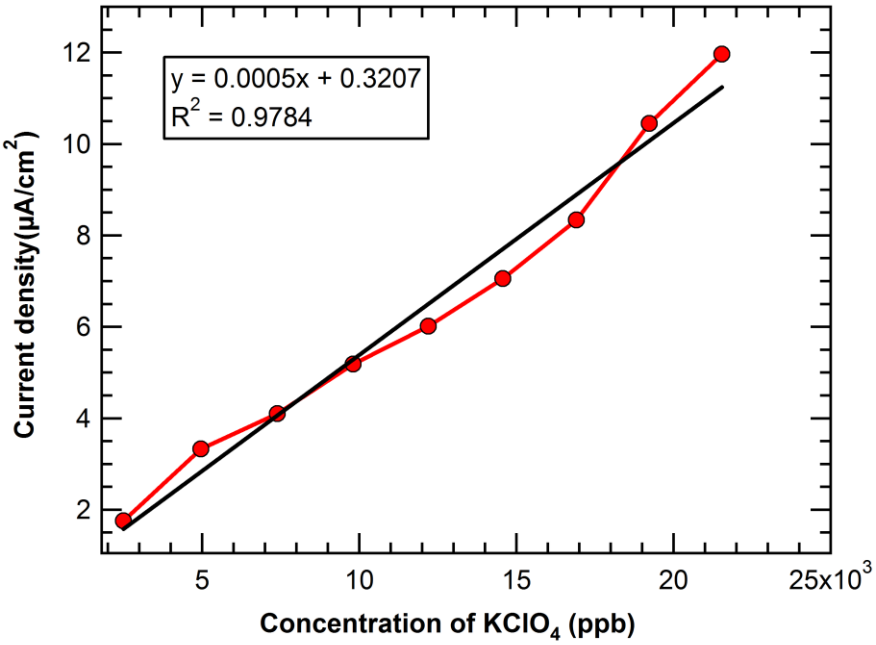

(b)

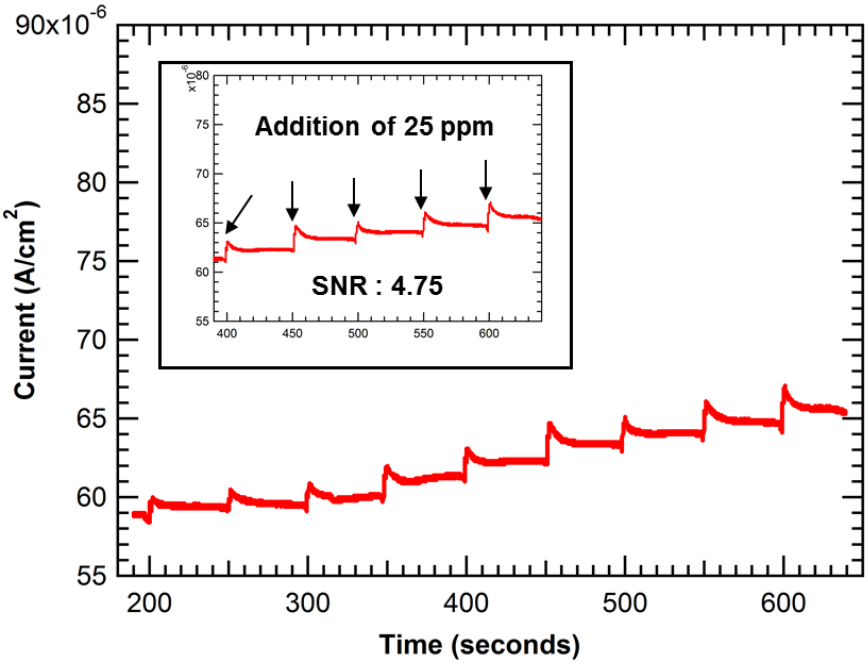

(a)

Figure 5.13. (a) Amperometric profile of nitrate biosensor fabricated at 1.1 V, 300 sec. in presence of carbonate species. Inset image shows step-wise increase in current after addition of 25 ppm nitrate after every 50 seconds (b) Linear range of operation of the sensor.

Figure 5.13 (cont'd)

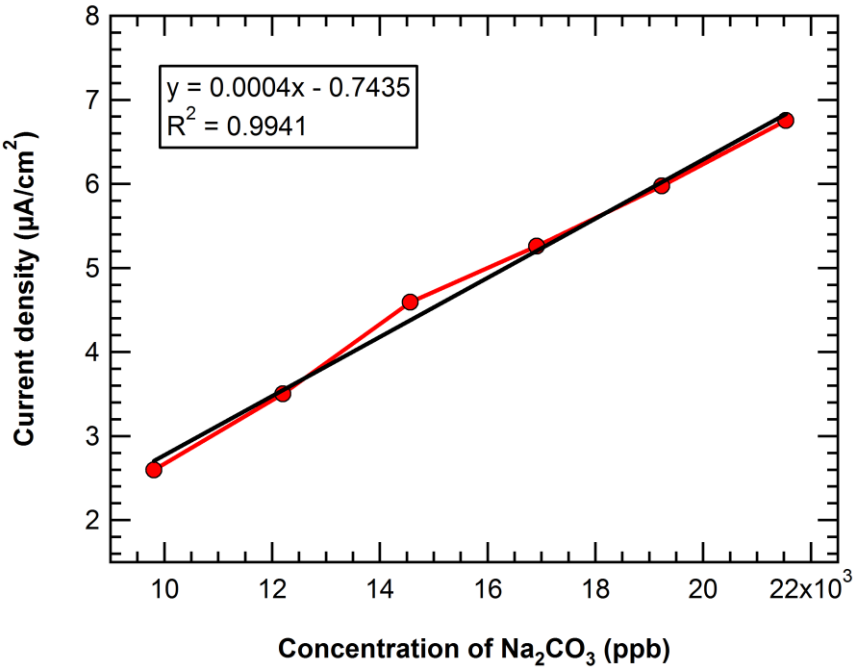

(b)

Adding lower concentrations of perchlorate and carbonate did not yield a quantifiable signal. The sensor shows a linear response in the range from 2.5 ppm- 21.5 ppm for perchlorate (Figure 5.12b) and 9.8 ppm-21.5 ppm for carbonate ions (Figure 5.13b). The biosensor has high sensitivity towards detecting and quantifying nitrate substrates at low concentrations. However, the same electrode requires a much higher concentration of perchlorate and carbonate species to show a quantifiable response. The estimation of the kinetic parameters enables us to make a comparative study of the performance of the biosensor when subjected to different substrates. Figure 5.14 shows the Lineweaver Burk plot for different configurations. The slope of the equation is given by K_m/V_{max}. The y-intercept denotes $1/V_{max}$. While V_{max} denotes the saturation current, K_m denotes the binding affinity shared by the enzyme with the substrate under consideration. Therefore measurement of K_m can provide us with a partial confirmation of the specificity of biosensor towards the substrate under consideration.

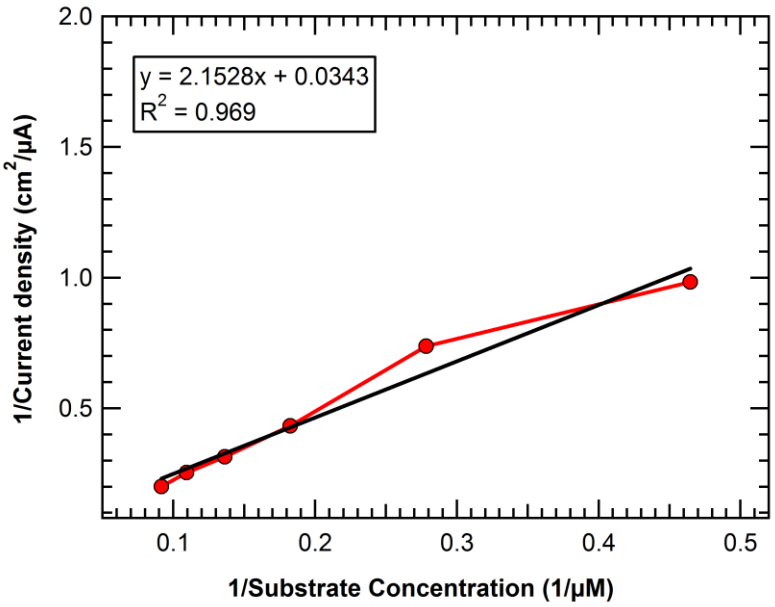

(a)

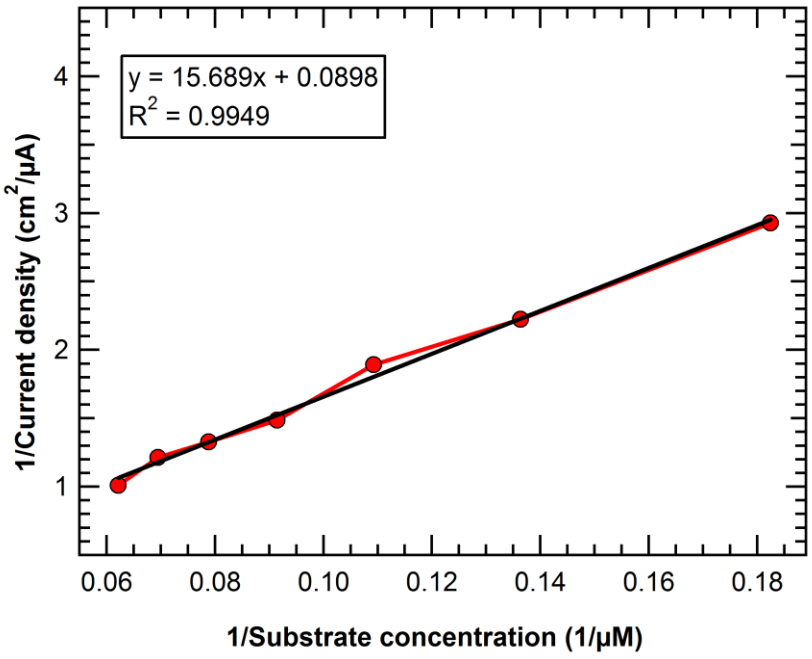

(b)

Figure 5.14 Lineweaver-Burk plots for nitrate biosensor (a) Sensor fabricated at 1.1 V, 300 sec. in presence of nitrate species. (b) Sensor fabricated at 0.95 V, 600 sec. in presence of nitrate species. (c) Sensor fabricated at 1.1 V, 300 sec. in presence of perchlorate species. (d) Sensor fabricated 1.1V, 300 sec. in presence of carbonate species.

Figure 5.14 (cont'd)

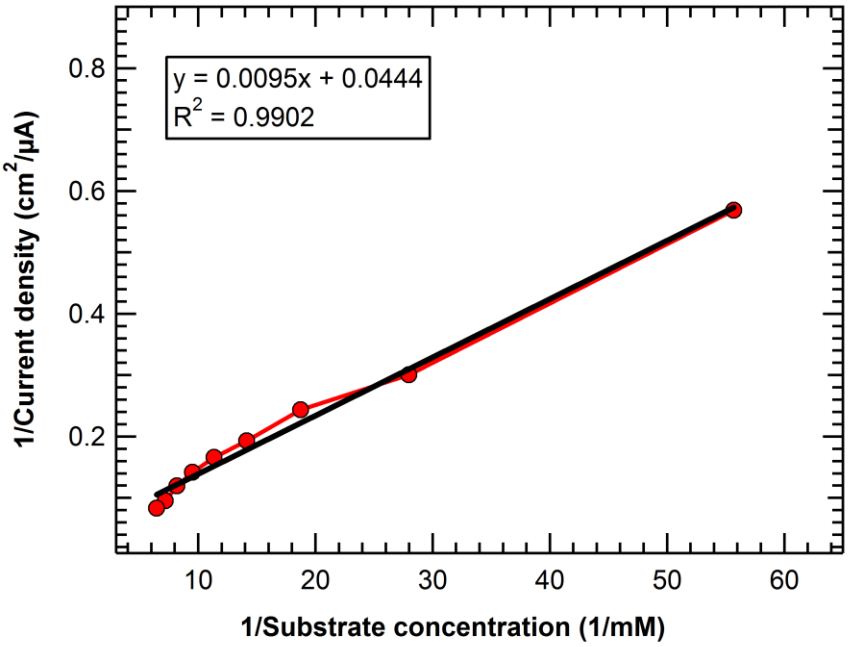

(c)

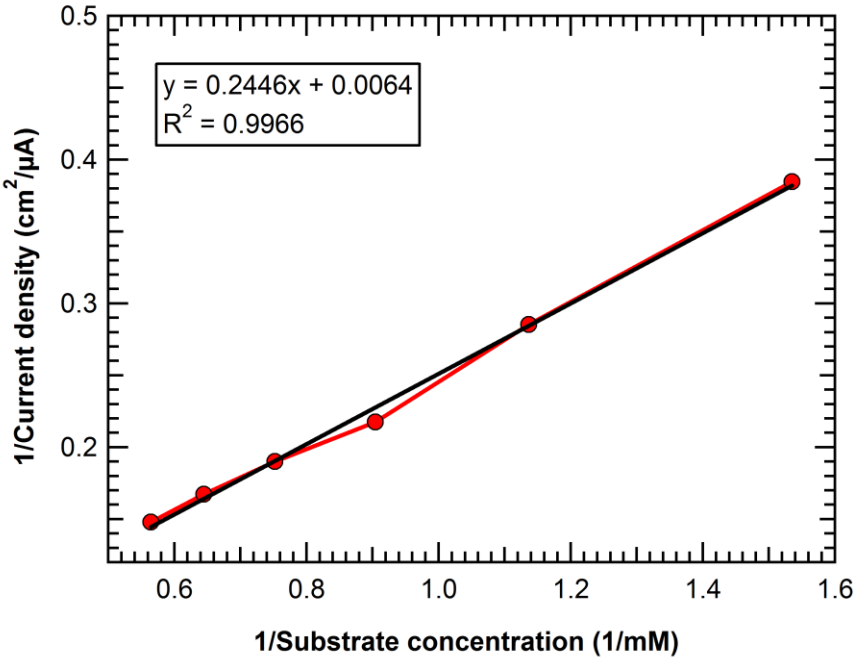

(d)

As seen from Table 1, the K_m value for the biosensor in response to addition of nitrate ions is close to 62.8 µM (sensor fabricated at 1.1V) and around 174.7µM (sensor fabricated at 0.95 V). The value reaches 214.3 µM for perchlorate and 38.2 mM for carbonate species. Lower value of K_m for KNO_3 indicates higher binding affinity towards nitrate ions. The immobilized enzyme requires higher perchlorate and carbonate concentration to catalyze the reduction process. Based on K_m values, the nitrate reductase biosensor (at 1.1V) developed in this work has over three folds affinity for nitrate as compared to perchlorate substrates. The affinity for carbonate species is almost 600 times lower than nitrate ions;

Table 5.1. Estimation of kinetic parameter based on Lineweaver-Burk approximation

Sensor fabrication conditions	**Substrate**	**K_m**	**$V_{max(\mu A/cm^2)}$**
0.95 V, 600 sec	nitrate	174.71 µM	11.136
1.1 V, 300 sec	nitrate	62.74 µM	29.15
1.1 V, 300 sec	perchlorate	214 µM	22.52
1.1 V, 300 sec	Carbonate	38.2 mM	156.25

5.3.6 Operational stability of the biosensor

The operational stability of the biosensor can be determined by successive addition of substrate and monitoring the rise in current (See Inset of figures 6a, 7a, 8a and 9a). In each case equal concentration of substrate was added and the response of the biosensor was measured by estimating the rise in current for each addition. Operational parameters such as signal to noise ratio (SNR) and limit of detection (LOD) were calculated. The SNR was estimated by taking a ratio of mean signal to standard deviation. LOD can be estimated using co-relations described elsewhere[65]. The comparison of these operational parameters for biosensors fabricated at different process conditions in presence of desired substrates is presented in Table 2. Similarly some recent examples of highly sensitive nitrate reductase based biosensors that have low LOD

values are included in Table 2. Table 2 shows that the sensor developed in this study (process conditions: 1.1 V, 300 seconds) has lowest LOD among the tabulated values.

Table 5.2. Operational parameters for different types of biosensors.

Sensor fabrication conditions	**Substrate**	**Limit of Detection (LOD) ppb**	**Signal to Noise Ratio(SNR)**
PEDOT/nitrate reductase nanowire 0.95 V, 600 sec*	Potassium nitrate	363.2	1.43
PEDOT/nitrate reductase nanowire 1.1 V, 300 sec*	Potassium nitrate	108	3.75
PEDOT/nitrate reductase nanowire 1.1 V, 300 sec*	Potassium perchlorate	1113	3.75
PEDOT/nitrate reductase nanowire 1.1 V, 300 sec*	Sodium Carbonate	888	4.75
CNT/Polypyrrole nitrate reductase[66]	Sodium nitrate	14450	3
MV/Nafion nitrate reductase[67]	Sodium nitrate	425	3
Ultrathin film composite membrane(UTFCM)[68]	Potassium nitrate	525	-
MV/Nafion nitrate reductase glassy carbon[64]	Sodium nitrate	<255	-
Polypyrrole-Nitrate reductase-Azure A[26]	Potassium nitrate	1010	-
Polypyrrole-Ag/nitrate reductase[24]	Sodium nitrate	425	-
Nitrate reductase/Glassy carbon[62]	Sodium nitrate	350	3
Screen printed nitrate biosensor[62]		468	3

* Reported in this study

The nitrate reductase based biosensor was tested for long term stability. Sensor stored at 4^0C and tested after 36 hours revealed little or negligible activity towards nitrate species. One possible explanation for this poor performance could be as a result of deterioration of PEDOT at low

temperature. During the electrochemical polymerization, we observed that the EDOT microemulsion becomes unstable at low temperatures. When refrigerated at 4^0C, the microemulsion breaks down with the EDOT /surfactant solution showing high levels of turbidity. We also tested the performance of the sensor stored at room temperature. After 36 hours, the biosensor showed about 58% reduction in current intensity when subjected to the same concentration of nitrate species. This indicates that the enzyme and/or the PEDOT conducting nanowires need additional stabilization. Our future studies are focused in this direction.

5.4 Conclusion

In summary, we showed the development of a highly sensitive PEDOT biosensor capable of detecting and quantifying minute concentrations of nitrate ions. A surfactant assisted templated approach was used to grow hybrid PEDOT/nitrate reductase nanowires. As compared to other nitrate reductase based biosensors, the use of PEDOT/nitrate reductase nanowire structure in this work enabled improved sensitivity, low limit of detection and instantaneous response. The performance of the PEDOT/nitrate reductase biosensor is a function of the fabrication conditions. Parameters like oxidation potential and time influence the degree of EDOT polymerization and may govern the extent of enzyme entrapment within the polymer matrix. Depending on the process conditions, nanowires of different morphologies can be grown. An optimized biosensor with LOD close to 0.108 ppm (108 ppb) and a sensitivity of 2.6 $\mu A/\mu M\ cm^2$ was obtained by fixing the oxidation potential to 1.1 V and polymerization time to 300 seconds. The sensor shows a linear behavior in the range 200 ppb-1100 ppb. The binding efficiency of nitrate reductase incorporated in the PEDOT biosensor is higher than interfering ions such as perchlorate (3.5 times higher) and carbonate (600 times higher) indicating potentially high substrate specificity. Future work will focus on improving the long term stability of the sensor by

investigating effect of temperature on the PEDOT sensor and preventing enzyme leaching using chemical cross-linking agents. Methods such as irreversible entrapment of enzyme obtained by adsorbing a mixture of enzyme and monomer on the electrode surface followed by electropolymerization can provide quantifiable information regarding the degree of enzyme immobilization and help develop robust comparative standards for kinetic characterization and optimization[53, 69].

REFERENCES

REFERENCES

1. Ward, M.H., et al., *Workgroup report: Drinking-water nitrate and health-recent findings and research needs.* Environmental Health Perspectives, 2005. **113**(11): p. 1607-1614.

2. Conley, D.J., et al., *ECOLOGY Controlling Eutrophication: Nitrogen and Phosphorus.* Science, 2009. **323**(5917): p. 1014-1015.

3. Anderson, D., P. Glibert, and J. Burkholder, *Harmful algal blooms and eutrophication: Nutrient sources, composition, and consequences.* Estuaries, 2002. **25**(4): p. 704-726.

4. World Health, O., *Guidelines for Drinking-water Quality: First Addendum to Third Edition, Volume 1, Recommendations*2006: World Health Organization.

5. Binghui, Z., Z. Zhixiong, and Y. Jing, *Ion chromatographic determination of trace iodate, chlorite, chlorate, bromide, bromate and nitrite in drinking water using suppressed conductivity detection and visible detection.* Journal of Chromatography A, 2006. **1118**(1): p. 106-110.

6. Daniel, W.L., et al., *Colorimetric Nitrite and Nitrate Detection with Gold Nanoparticle Probes and Kinetic End Points.* Journal of the American Chemical Society, 2009. **131**(18): p. 6362-6363.

7. Dasary, S.S.R., et al., *Gold Nanoparticle Based Label-Free SERS Probe for Ultrasensitive and Selective Detection of Trinitrotoluene.* Journal of the American Chemical Society, 2009. **131**(38): p. 13806-13812.

8. Rupert, M.G., *Decadal-scale changes of nitrate in ground water of the United States, 1988-2004.* Journal of Environmental Quality, 2008. **37**(5): p. S240-S248.

9. Avery, A.A., *Infantile methemoglobinemia: reexamining the role of drinking water nitrates.* Environmental Health Perspectives, 1999. **107**(7): p. 583.

10. Fraser, P. and C. Chilvers, *Health-Aspects of Nitrate in Drinking-Water.* Science of the Total Environment, 1981. **18**(Apr): p. 103-116.

11. Gulis, G., M. Czompolyova, and J.R. Cerhan, *An ecologic study of nitrate in municipal drinking water and cancer incidence in Trnava District, Slovakia.* Environmental Research, 2002. **88**(3): p. 182-187.

12. Moralessuarezvarela, M.M., A. Llopisgonzalez, and M.L. Tejerizoperez, *Impact of Nitrates in Drinking-Water on Cancer Mortality in Valencia, Spain.* European Journal of Epidemiology, 1995. **11**(1): p. 15-21.

13. Sandor, J., et al., *Association between gastric cancer mortality and nitrate content of drinking water: Ecological study on small area inequalities.* European Journal of Epidemiology, 2001. **17**(5): p. 443-447.

14. Ward, M.H., et al., *Nitrate Intake and the Risk of Thyroid Cancer and Thyroid Disease.* Epidemiology, 2010. **21**(3): p. 389-395.

15. Braverman, L.E., et al., *The effect of perchlorate, thiocyanate, and nitrate on thyroid function in workers exposed to perchlorate long-term.* Journal of Clinical Endocrinology & Metabolism, 2005. **90**(2): p. 700-706.

16. Blount, B.C. and L. Valentin-Blasini, *Analysis of perchlorate, thiocyanate, nitrate and iodide in human amniotic fluid using ion chromatography and electrospray tandem mass spectrometry.* Analytica chimica acta, 2006. **567**(1): p. 87-93.

17. Niedzielski, P., I. Kurzyca, and J. Siepak, *A new tool for inorganic nitrogen speciation study: Simultaneous determination of ammonium ion, nitrite and nitrate by ion chromatography with post-column ammonium derivatization by Nessler reagent and diode-array detection in rain water samples.* Analytica chimica acta, 2006. **577**(2): p. 220-224.

18. Senapati, D., et al., *A Label-Free Gold-Nanoparticle-Based SERS Assay for Direct Cyanide Detection at the Parts-per-Trillion Level.* Chemistry-A European Journal, 2011. **17**(30): p. 8445-8451.

19. Lu, J., et al., *Nanometal-decorated exfoliated graphite nanoplatelet based glucose biosensors with high sensitivity and fast response.* ACS nano, 2008. **2**(9): p. 1825-1832.

20. Lu, J., et al., *Simple fabrication of a highly sensitive glucose biosensor using enzymes immobilized in exfoliated graphite nanoplatelets nafion membrane.* Chemistry of Materials, 2007. **19**(25): p. 6240-6246.

21. Kohli, N., et al., *Nanostructured biosensor for measuring neuropathy target esterase activity.* Analytical Chemistry, 2007. **79**(14): p. 5196-5203.

22. Campbell, W.H., *Nitrate reductase structure, function and regulation: bridging the gap between biochemistry and physiology.* Annual review of plant biology, 1999. **50**(1): p. 277-303.

23. Kiang, C.-H., S.S. Kuan, and G.G. Guilbault, *Enzymic determination of nitrate: electrochemical detection after reduction with nitrate reductase and nitrite reductase.* Analytical Chemistry, 1978. **50**(9): p. 1319-1322.

24. Atmeh, M. and B.E. Alcock-Earley, *A conducting polymer/Ag nanoparticle composite as a nitrate sensor.* Journal of Applied Electrochemistry, 2011. **41**(11): p. 1341-1347.

25. Cosnier, S., et al., *Electrochemical nitrate biosensor based on poly (pyrrole–viologen) film–nitrate reductase–clay composite.* Bioelectrochemistry, 2008. **74**(1): p. 47-51.

26. Sohail, M. and S.B. Adeloju, *Fabrication of Redox-Mediator Supported Potentiometric Nitrate Biosensor with Nitrate Reductase.* Electroanalysis, 2009. **21**(12): p. 1411-1418.

27. Willner, I., A. Riklin, and N. Lapidot, *Electron-transfer communication between a redox polymer matrix and an immobilized enzyme: activity of nitrate reductase in a viologen-acrylamide copolymer.* Journal of the American Chemical Society, 1990. **112**(17): p. 6438-6439.

28. Albanese, D., M. Di Matteo, and C. Alessio, *Screen printed biosensors for detection of nitrates in drinking water.* Computer Aided Chemical Engineering, 2010. **28**: p. 283-288.

29. Wanekaya, A.K., et al., *Nanowire-based electrochemical biosensors.* Electroanalysis, 2006. **18**(6): p. 533-550.

30. Duvail, J.L., et al., *Tuning electrical properties of conjugated polymer nanowires with the diameter.* Applied Physics Letters, 2007. **90**(10).

31. Long, Y.Z., et al., *Recent advances in synthesis, physical properties and applications of conducting polymer nanotubes and nanofibers.* Progress in Polymer Science, 2011. **36**(10): p. 1415-1442.

32. Huang, J.Y., K. Wang, and Z.X. Wei, *Conducting polymer nanowire arrays with enhanced electrochemical performance.* Journal of Materials Chemistry, 2010. **20**(6): p. 1117-1121.

33. Dan, Y.P., et al., *Dielectrophoretically assembled polymer nanowires for gas sensing.* Sensors and Actuators B-Chemical, 2007. **125**(1): p. 55-59.

34. Corradi, R. and S.P. Armes, *Chemical synthesis of poly(3,4-ethylenedioxythiophene).* Synthetic Metals, 1997. **84**(1-3): p. 453-454.

35. Jonas, F. and L. Schrader, *Conductive Modifications of Polymers with Polypyrroles and Polythiophenes.* Synthetic Metals, 1991. **41**(3): p. 831-836.

36. Kros, A., N.A.J.M. Sommerdijk, and R.J.M. Nolte, *Poly(pyrrole) versus poly (3,4-ethylenedioxythiophene): implications for biosensor applications.* Sensors and Actuators B-Chemical, 2005. **106**(1): p. 289-295.

37. Kros, A., R.J.M. Nolte, and N.A.J.M. Sommerdijk, *Poly (3,4-ethylenedioxythiophene)-based copolymers for biosensor applications.* Journal of Polymer Science Part a-Polymer Chemistry, 2002. **40**(6): p. 738-747.

38. Dobbelin, M., et al., *Innovative materials and applications based on poly(3,4-ethylenedioxythiophene) and ionic liquids.* Journal of Materials Chemistry, 2010. **20**(36): p. 7613-7622.

39. Perepichka, I.F. and D.F. Perepichka, *Handbook of thiophene-based materials: applications in organic electronics and photonics*2009: Wiley Online Library.

40. Il Cho, S. and S.B. Lee, *Fast electrochemistry of conductive polymer nanotubes: Synthesis, mechanism, and application.* Accounts of Chemical Research, 2008. **41**(6): p. 699-707.

41. Poverenov, E., et al., *Major Effect of Electropolymerization Solvent on Morphology and Electrochromic Properties of PEDOT Films.* Chemistry of Materials, 2010. **22**(13): p. 4019-4025.

42. Liu, R., S. Il Cho, and S.B. Lee, *Poly(3,4-ethylenedioxythiophene) nanotubes as electrode materials for a high-powered supercapacitor.* Nanotechnology, 2008. **19**(21).

43. Ryu, K.S., et al., *Poly(ethylenedioxythiophene) (PEDOT) as polymer electrode in redox supercapacitor.* Electrochimica Acta, 2004. **50**(2-3): p. 843-847.

44. Xiao, R., et al., *Controlled electrochemical synthesis of conductive polymer nanotube structures.* Journal of the American Chemical Society, 2007. **129**(14): p. 4483-4489.

45. Cho, S.I., et al., *Electrochemical synthesis and fast electrochromics of poly(3,4-ethylenedioxythiophene) nanotubes in flexible substrate.* Chemistry of Materials, 2005. **17**(18): p. 4564-4566.

46. Cho, S.I., et al., *Nanotube-Based Ultrafast Electrochromic Display.* Advanced materials, 2005. **17**(2): p. 171-175.

47. Vidal, J.C., E. Garcia-Ruiz, and J.R. Castillo, *Recent advances in electropolymerized conducting polymers in amperometric biosensors.* Microchimica Acta, 2003. **143**(2-3): p. 93-111.

48. Sakmeche, N., et al., *Improvement of the electrosynthesis and physicochemical properties of poly(3,4-ethylenedioxythiophene) using a sodium dodecyl sulfate micellar aqueous medium.* Langmuir, 1999. **15**(7): p. 2566-2574.

49. Sakmeche, N., et al., *Application of sodium dodecylsulfate (SDS) micellar solution as an organized medium for electropolymerization of thiophene derivatives in water.* Synthetic Metals, 1997. **84**(1-3): p. 191-192.

50. Bhadra, S., et al., *Progress in preparation, processing and applications of polyaniline.* Progress in Polymer Science, 2009. **34**(8): p. 783-810.

51. Zhou, M. and J. Heinze, *Electropolymerization of pyrrole and electrochemical study of polypyrrole. 2. Influence of acidity on the formation of polypyrrole and the multipathway mechanism.* Journal of Physical Chemistry B, 1999. **103**(40): p. 8443-8450.

52. Zhang, S.S., et al., *Electrochemical polymerization of 3,4-ethylenedioxythiophene in aqueous solution containing N-dodecyl-beta-D-maltoside.* European Polymer Journal, 2006. **42**(1): p. 149-160.

53. Cosnier, S., *Biomolecule immobilization on electrode surfaces by entrapment or attachment to electrochemically polymerized films. A review.* Biosensors & Bioelectronics, 1999. **14**(5): p. 443-456.

54. Wen, Y.P., et al., *Electrochemical polymerization of 3,4-ethylenedioxythiophene in aqueous micellar solution containing biocompatible amino acid-based surfactant.* Journal of Electroanalytical Chemistry, 2009. **634**(1): p. 49-58.

55. Torres-Gomez, G. and P. Gomez-Romero, *Conducting organic polymers with electroactive dopants. Synthesis and electrochemical properties of hexacyanoferrate-doped polypyrrole.* Synthetic Metals, 1998. **98**(2): p. 95-102.

56. Kim, Y., et al., *Photoelectrochemical oxidative polymerization of aniline and its application to transparent TiO2 solar cells.* Journal of Photochemistry and Photobiology a-Chemistry, 2009. **204**(2-3): p. 110-114.

57. Zeng, H.J., et al., *Choline oxidase immobilized into conductive poly(3,4-ethylenedioxythiophene) film for choline detection.* Applied Surface Science, 2008. **254**(20): p. 6337-6340.

58. Lapkowski, M. and A. Pron, *Electrochemical oxidation of poly(3,4-ethylenedioxythiophene) - "in situ" conductivity and spectroscopic investigations.* Synthetic Metals, 2000. **110**(1): p. 79-83.

59. Du, X. and Z. Wang, *Effects of polymerization potential on the properties of electrosynthesized PEDOT films.* Electrochimica Acta, 2003. **48**(12): p. 1713-1717.

60. Fic, K., E. Frackowiak, and F. Beguin, *Unusual energy enhancement in carbon-based electrochemical capacitors.* Journal of Materials Chemistry, 2012. **22**(46): p. 24213-24223.

61. Wen, Y.P., et al., *Poly(3,4-ethylenedioxythiophene methanol)/ascorbate oxidase/nafion-single-walled carbon nanotubes biosensor for voltammetric detection of Vitamin C.* Chinese Journal of Polymer Science, 2012. **30**(3): p. 460-469.

62. Quan, D., et al., *Electrochemical determination of nitrate with nitrate reductase-immobilized electrodes under ambient air.* Analytical Chemistry, 2005. **77**(14): p. 4467-4473.

63. Bardiya, N. and J.H. Bae, *Dissimilatory perchlorate reduction: A review.* Microbiological Research, 2011. **166**(4): p. 237-254.

64. Glazier, S.A., E.R. Campbell, and W.H. Campbell, *Construction and characterization of nitrate reductase-based amperometric electrode and nitrate assay of fertilizers and drinking water.* Analytical Chemistry, 1998. **70**(8): p. 1511-1515.

65. Borgmann, S., et al., *Amperometric Biosensors,* in *Advances in Electrochemical Science and Engineering*, D.M.K. R. C. Alkire, J. Lipkowski, Editor 2011, Wiley-VCH Verlag GmbH & Co. KGaA,Weinheim, Germany. p. 1-83.

66. Can, F., et al., *Amperometric nitrate biosensor based on Carbon nanotube/Polypyrrole/Nitrate reductase biofilm electrode.* Materials Science and Engineering: C, 2012. **32**(1): p. 18-23.

67. Wang, X., et al., *Development of a conductometric nitrate biosensor based on Methyl viologen/Nafion< sup>®</sup> composite film.* Electrochemistry communications, 2006. **8**(2): p. 201-205.

68. Moretto, L.M., et al., *Nitrate biosensor based on the ultrathin-film composite membrane concept.* Analytical Chemistry, 1998. **70**(10): p. 2163-2166.

69. Cosnier, S. and C. Innocent, *A novel biosensor elaboration by electropolymerization of an adsorbed amphiphilic pyrrole-tyrosinase enzyme layer.* Journal of Electroanalytical Chemistry, 1992. **328**(1–2): p. 361-366.

Chapter 6: Conclusions and future work

6.1 Conclusions

The supramolecular assembly of different components opens up exciting opportunities for the development of novel materials. In the preceding chapters, detailed descriptions regarding design of an improved biocatalyst (for cellulosic ethanol production) and development of nanostructured synergistic interfaces (conductive gas barrier films and bioelectronic enzymatic interface for nitration detection and quantification) using supramolecular techniques have been presented. The versatility of the applications presented here is an indication in itself of the huge potential this field can hold for future research. The subtle manipulations brought about by supramolecular interactions are reminiscent of the pathways evolved by nature over years of perfection. Hence most of these forces operate at ambient process conditions (mild temperature, pressure, pH) inflicting minimum stress on the environment and the same is observed in the development of all the three applications discussed here. However, supramolecular forces are also prone to drastic changes in the microenvironment when subjected to small process changes. From the preceding discussion, this fact is attested by variation in colloidal stability of the biocatalyst as a result of the swelling action of the spacer polyelectrolyte (Chapter 3), change in the film morphology and hence permeation and conductance due to change in deposition pH (Chapter 4) and loss of accurate nitrate quantification capability due to changes in the electropolymerization of polymer/enzyme nanowires (Chapter 5). In view of the several facets observed during the design and development of the novel materials discussed here, a recapitulation of some important findings for each application is in order. The same are presented in this final chapter.

The first project involved development of a novel nanobiocatalyst that is capable of overcoming the geometric limitation (due to 2D geometry) and steric hindrance as a result of enzyme immobilization to deliver improved catalytic activity. The biocatalyst uses a supramolecular bottom-up approach that incorporates a plethora of charged components such as polyelectrolytes, nanoparticles and cellulase enzymes. The incorporation of each component imparts additional functionality to the biocatalyst architecture and the same has been discussed in chapter 3. Salient features of these nanobiocatalyst are improved dispersion of high surface area graphene platelets stabilized by supramolecular assembly of strong polylelectrolytes, inclusion of iron-oxide nanoparticles to facilitate recycle and recuse of the immobilized enzyme and pH tunable swelling of polyacrylic acid brushes to manipulate colloidal stability and hence enzymatic activity. The immobilized enzymes developed in this study show an activity as high as 80% compared to free enzymes with retention in specific enzyme activity up to 55% after four cycles of reuse.

In Chapter 4, the supramolecular assembly of cationic polyelectrolyte functionalized graphene platelets along with anionic polyelectrolyte was discussed and the material properties of these films wrt oxygen barrier and conductance were reported. Three separate types of assemblies were identified by making subtle changes in the deposition conditions to produce predominantly (a) hydrogen bonded films (b) electrostatic films (c) composite films. In all the three cases, the same cationic and anionic polyelectrolytes were used. However, a variation in the pH condition during the film deposition process resulted in change in the charge density of these polyelectrolytes. As a result, films of different types of interactions were fabricated. The composite films developed in this work have oxygen barrier properties comparable to commercial grade silicon oxide coatings and resistance that decreased by high orders of magnitude. With more modifications, a further decrease in electrical sheet resistance is possible

which would improve the chances of these films to be used in the semiconductor/electronics industry.

In Chapter 5, an electropolymerized PEDOT/nitrate reductase nanobiosensor was developed from a surfactant stabilized supramolecular matrix. The sensor enjoys low LOD (close to 0.1 ppm nitrate) and shares a high binding affinity towards nitrate species as compared to other interfering anions. Manipulating the electropolymerization time and potential causes a change in the morphology of the PEDOT/nitrate reductase nanowires. It is expected that the level of enzyme entrapment with the polymer matrix can be tweaked by proper optimization of these two parameters. Another important feature of this sensor is the retention of 1D nanowire dimension. Because of the templated approach used to grow the nanowire, the PEDOT/enzyme nanowires return their upright nanowire dimensions contributing to increased signal efficiency and hence better detection and quantification.

6.2 Future outlook

The design of the supramolecular nanostructures discussed in the preceding chapters holds immense promise to expand the existing work to several new applications. For example, in Chapter 3, iron-oxide doped graphene platelets were used as nanocarriers for immobilization of cellulase in the saccharification reaction. However, because of the sheer robustness and simplicity of assembly, it is possible to substitute cellulase with other enzymes. This means that the same graphene based support can be used in a number of biocatalytic reactions. Besides this, a very novel extension of using this nanostructured support can be in the field of targeted drug delivery applications. Several variations of magnetic carbonaceous composites for biomedical applications such as cancer treatment and magnetic resonance imaging (MRI) are already available in literature [1-4]. While the ferrous component of the composite helps in guiding or

tracking the flow of the drug/tracer in the body, the carbonaceous component provides an excellent contrast for imaging[5]. Other than the biobased applications, a potential extension of graphene-iron oxide carriers (without the enzyme component) for selective oxidation of secondary alcohols is possible since carbon -iron oxide carriers have been shown to be active in catalytic oxidation reactions with performance comparable to noble-metals[6]. Likewise, the layer-by-layer assembly of polyelectrolyte functionalized graphene platelets also holds immense promise for incorporation of additional components to suit the requirements. Chapter 4 specifically dealt with fabrication of oxygen barrier films. However based on recent research by making minor modifications in these films robust corrosion resistant films can be easily built[7, 8]. Polyelectrolytes are effective in covering several types of substrates shielding the existing defects in their microstructure from direct attack of air and water[8-10]. This property has been shown to provide a comfortable degree of protection to the substrate in presence of a corrosive environment. The LbL assembly also allows for the incorporatation of several non-homogenous components such as cells, nanoparticles charged species within the multilayer structure. This can be exploited to ensure value addition to the supramolecular films. The inclusion of corrosion inhibitors[8] and hydrophobic silica nanoparticles[11, 12] are some excellent options to limit the effect of corrosion and exposure to water respectively. Likewise, the third application discussed in this dissertation namely development of nanostructured biosensor for detection of contaminant ions can be made more user-friendly by use of oxygen scavengers. The nitrate quantification studies shown here used deoxygenated test solution obtained after nitrogen/argon purging for estimation. Further improvements such as addition of oxygen scavenging agents like sodium sulfite or cysteine can prevent the necessity of purging argon/nitrogen through the solution. Similarly, enzymes such as oxyrase or catalase consume oxygen[13]. It has been shown that

supramolecular biocompatible polyelectrolyte films can be used for the controlled release of enzymes, drugs and nanoparticles entrapped within the multilayers by adjusting process condition such as pH and temperature[14-17]. Supramolecular assembly of oxygen scavengers post electropolymerization followed by release in the test solution is another interesting option that can be explored in the future. This should help in the elimination of the inert gas purging step and improve the portability of the sensor.

REFERENCES

REFERENCES

1. Ma, Y., et al., *Plasma synthesis of carbon magnetic nanoparticles and immobilization of doxorubicin for targeted drug delivery.* Journal of Biomaterials Science, Polymer Edition, 2004. **15**(8): p. 1033-1049.

2. Bystrzejewski, M., A. Huczko, and H. Lange, *Arc plasma route to carbon-encapsulated magnetic nanoparticles for biomedical applications.* Sensors and Actuators B: Chemical, 2005. **109**(1): p. 81-85.

3. Rudge, S., et al., *Preparation, characterization, and performance of magnetic iron–carbon composite microparticles for chemotherapy.* Biomaterials, 2000. **21**(14): p. 1411-1420.

4. Leconte, Y., et al., *Continuous production of water dispersible carbon–iron nanocomposites by laser pyrolysis: Application as MRI contrasts.* Journal of colloid and interface science, 2007. **313**(2): p. 511-518.

5. Harrison, B.S. and A. Atala, *Carbon nanotube applications for tissue engineering.* Biomaterials, 2007. **28**(2): p. 344-353.

6. Gao, Y., et al., *Layered-Carbon-Stabilized Iron Oxide Nanostructures as Oxidation Catalysts.* Angewandte Chemie International Edition, 2011. **50**(43): p. 10236-10240.

7. Shchukin, D.G., et al., *Layer-by-Layer Assembled Nanocontainers for Self-Healing Corrosion Protection.* Advanced materials, 2006. **18**(13): p. 1672-1678.

8. Andreeva, D.V., E.V. Skorb, and D.G. Shchukin, *Layer-by-layer polyelectrolyte/inhibitor nanostructures for metal corrosion protection.* Acs Applied Materials & Interfaces, 2010. **2**(7): p. 1954-1962.

9. Farhat, T.R. and J.B. Schlenoff, *Corrosion control using polyelectrolyte multilayers.* Electrochemical and solid-state letters, 2002. **5**(4): p. B13-B15.

10. Andreeva, D.V., et al., *Buffering polyelectrolyte multilayers for active corrosion protection.* Journal of Materials Chemistry, 2008. **18**(15): p. 1738-1740.

11. Zhai, L., et al., *Stable superhydrophobic coatings from polyelectrolyte multilayers.* Nano Letters, 2004. **4**(7): p. 1349-1353.

12. Bravo, J., et al., *Transparent superhydrophobic films based on silica nanoparticles.* Langmuir, 2007. **23**(13): p. 7293-7298.

13. Patel, J., et al., *Comparison of oxygen scavengers for their ability to enhance resuscitation of heat-injured Listeria monocytogenes.* Journal of Food Protection®, 1995. **58**(3): p. 244-250.

14. Chung, A. and M. Rubner, *Methods of loading and releasing low molecular weight cationic molecules in weak polyelectrolyte multilayer films.* Langmuir, 2002. **18**(4): p. 1176-1183.

15. Zhu, Y., et al., *Stimuli-Responsive Controlled Drug Release from a Hollow Mesoporous Silica Sphere/Polyelectrolyte Multilayer Core–Shell Structure.* Angewandte Chemie, 2005. **117**(32): p. 5213-5217.

16. Qiu, X., et al., *Studies on the drug release properties of polysaccharide multilayers encapsulated ibuprofen microparticles.* Langmuir, 2001. **17**(17): p. 5375-5380.

17. Shi, X. and F. Caruso, *Release behavior of thin-walled microcapsules composed of polyelectrolyte multilayers.* Langmuir, 2001. **17**(6): p. 2036-2042.